

AFWAL-TR-80-3101
Volume I

6
LEVEL



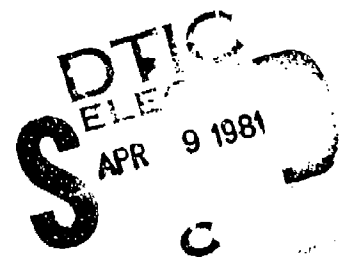
**MULTI-RATE DIGITAL CONTROL SYSTEMS WITH
SIMULATION APPLICATIONS
Volume I: Technical Report**

*RICHARD F. WHITBECK
SYSTEMS TECHNOLOGY, INC.
HAWTHORNE, CA 90250*

*DENNIS G. J. DIDALEUSKY
FLIGHT DYNAMICS LABORATORY
WRIGHT-PATTERSON AIR FORCE BASE, OH 45433*

SEPTEMBER 1980

TECHNICAL REPORT AFWAL-TR-80-3101 VOL I
Final Report — January 1979-May 1980



Approved for public release; distribution unlimited.

FLIGHT DYNAMICS LABORATORY
AIR FORCE WRIGHT AERONAUTICAL LABORATORIES
AIR FORCE SYSTEMS COMMAND
WRIGHT-PATTERSON AIR FORCE BASE, OH 45433

81 4

8 037

AD A 097549

DTIC FILE COPY

NOTICE

When Government drawings, specifications, or other data are used for any purpose other than in connection with a definitely related Government procurement operation, the United States Government thereby incurs no responsibility nor any obligation whatsoever; and the fact that the government may have formulated, furnished, or in any way supplied the said drawings, specifications, or other data, is not to be regarded by implication or otherwise as in any manner licensing the holder or any other person or corporation, or conveying any rights or permission to manufacture use, or sell any patented invention that may in any way be related thereto.

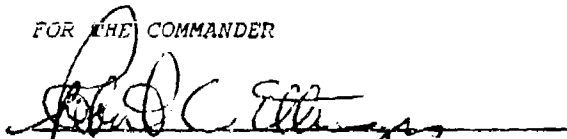
This report has been reviewed by the Office of Public Affairs (ASD/PA) and is releasable to the National Technical Information Service (NTIS). At NTIS, it will be available to the general public, including foreign nations.

This technical report has been reviewed and is approved for publication.



DENNIS G. J. DIDALEUSKY, Captain, USAF
Project Engineer
Control Dynamics Branch
Flight Control Division

FOR THE COMMANDER



ROBERT C. ETTINGER, Colonel, USAF
Chief, Flight Control Division



R. O. ANDERSON, Chief
Control Dynamics Branch
Flight Control Division

"If your address has changed, if you wish to be removed from our mailing list, or if the addressee is no longer employed by your organization please notify AFWAL/FIGC, W-PAFB, OH 45433 to help us maintain a current mailing list".

Copies of this report should not be returned unless return is required by security considerations, contractual obligations, or notice on a specific document.

Unclassified

SECURITY CLASSIFICATION OF THIS PAGE (When Data Entered)

19 REPORT DOCUMENTATION PAGE		READ INSTRUCTIONS BEFORE COMPLETING FORM	
1. REPORT NUMBER AFWAL-TR-80-3101-Vol-1	2. GOVT ACCESSION NO. AD-A097549	3. RECIPIENT'S CATALOG NUMBER	
4. TITLE (and Subtitle) MULTI-RATE DIGITAL CONTROL SYSTEMS WITH SIMULATION APPLICATIONS. Volume I. Technical Report,		5. TYPE OF REPORT & PERIOD COVERED Final Report. 29 Jan 79 - 29 May 80	
6. AUTHOR(s) R. F. Whitbeck D. A. Didaleusky		7. PERFORMING ORG. REPORT NUMBER STI-TR-1142-11	
8. CONTRACT OR GRANT NUMBER(s) F33615-79-C-3601		9. PROGRAM ELEMENT, PROJECT, TASK AREA & WORK UNIT NUMBERS Program Element 61102F, Project 2304 Mathematics, Task N3, Math. of Flt. Control	
10. CONTROLLING OFFICE NAME AND ADDRESS Systems Technology, Inc. 13766 South Hawthorne Boulevard Hawthorne, California 90250		11. REPORT DATE September 1980	
12. CONTROLLING OFFICE NAME AND ADDRESS Flight Dynamics Laboratory Air Force Wright Aeronautical Laboratories Air Force Systems Command Wright-Patterson Air Force Base, Ohio 45433		13. NUMBER OF PAGES 12/146	
14. MONITORING AGENCY NAME & ADDRESS (if different from Controlling Office)		15. SECURITY CLASS. (of this report) Unclassified	
16. DISTRIBUTION STATEMENT (of this Report) Approved for public release; distribution unlimited.		15a. DECLASSIFICATION/DOWNGRADING SCHEDULE	
17. DISTRIBUTION STATEMENT (of the abstract entered in Block 20, if different from Report)			
18. SUPPLEMENTARY NOTES			
19. KEY WORDS (Continue on reverse side if necessary and identify by block number) Digital Control Systems Frequency Response Computational Delays Servo Analysis Sampled Data Switch Decomposition Tustin Transform sis z-Transforms Closed-Loop Systems Simulation Error Closed-Loop w-Domain Linear Systems Analysis Analysis Multi-Rate Sampling Root Locus			
20. ABSTRACT (Continue on reverse side if necessary and identify by block number) Many current digital design procedures attempt only to approach the characteristics of existing analog designs. No explicit methodology exists which can exploit the unique characteristics of multi-rate or multiple-order digital computation and filtering. The objective of this research effort is to develop a multi-rate/multiple-order theory for the design of closed-loop digital control systems with characteristics and attributes that are either difficult or impossible to attain with analog or single-rate controllers. The key idea in this (continued)			

DD FORM 1 JAN 73 1473

EDITION OF 1 NOV 65 IS OBSOLETE

Unclassified

SECURITY CLASSIFICATION OF THIS PAGE (When Data Entered)

A

34040-5

Unclassified

SECURITY CLASSIFICATION OF THIS PAGE(When Data Entered)

20. ABSTRACT (Continued)

methodology is to use the logic of the computer to take a scalar continuous output signal, sample it at a relatively high rate, and then sort out the various samples into a vector of pseudo measurements. The potential of such a scheme is significant, since it offers, among other things, the possibility of using fewer sensors and the potential for providing gracefully degrading system performance in the face of sensor failure.

The pseudo measurement concept may be likened to the observer concept of linear system theory. An "observer" is a dynamic subsystem which processes the available measurements and control inputs to obtain asymptotic estimates of those states which are not measured. The distinction between the observer and pseudo measurement concept is as follows. Additional pseudo states required for proper control action are obtained via design of a multi-rate or multiple-order sampling sequence in the pseudo measurement approach, while the estimate of system states not measured is attained by design of a dynamic subsystem in the observer approach. The pseudo measurement concept is based on using information contained in a scalar measurement, sampled at a high rate, to generate a lower rate measurement vector. This vector is likened to pseudo states since it effectively provides distinctively different information in the form of separate sampling sequences shifted in time.

The report is organized in three volumes. Volume I contains the theoretical developments as well as illustrative examples and case studies. The basic tools needed to assess the pseudo measurement concept are reviewed and extended. The concept of the frequency response of the continuous variables of single-rate digitally controlled system is then given sufficient generality to treat multi-rate systems (including the pseudo measurement concept). A YF-16 case study is used to compare pseudo measurement gains against conventional YF-16 analog controller gains. The pseudo measurement gains are found to be comparable with the conventional gains, indicating the approach does not require control authority more excessive than an analog controller design.

As a "byproduct," an important relationship is deduced which made it feasible to apply the switch decomposition/frequency response technique to the error analysis of simulations of continuous systems and/or discretely controlled continuous systems. An illustrative example demonstrates the significant spectral differences between a closed-loop system (employing an analog or digital controller) and an all-digital simulation of the closed-loop system. The example also treats problems encountered when simulation software is implemented on two different computers, each working in a slightly different frame time (the so-called independent processor problem). This provides a tool which can be profitably applied to the "error" analysis of simulations; perhaps to predict expected differences between actual flight test and man-in-the-loop moving-base simulations.

Volume II describes two algorithms useful in the analysis of multi-rate systems, while Volume III gives FORTRAN listings for these algorithms. The first algorithm converts a continuous transfer function in the s-domain into alternate descriptions in the z-, w-, and w'-domains. The second algorithm calculates a low data rate discrete transform given a high data rate discrete transfer function. This algorithm is presented in Section IV of Volume I and later derived in Section IV of Volume II.

Unclassified

SECURITY CLASSIFICATION OF THIS PAGE(When Data Entered)

FOREWORD

The research described in this report was performed by Systems Technology, Inc., Hawthorne, California, under Air Force Contract F33615-79-C-3601. The Task Number N3, Mathematics of Flight Control, was under Project Number 2304, Mathematics. This work was directed by the Control Dynamics Branch, Flight Control Division, Flight Dynamics Laboratory, Air Force Wright Aeronautical Laboratories, Air Force Systems Command, Wright-Patterson Air Force Base, Ohio. The work was administered by Captain Dennis G. J. Didaleusky.

Richard F. Whitbeck was the Systems Technology, Inc., Project Engineer under the direction of Duane McRuer.

The authors wish to express their appreciation to the Systems Technology publication staff for their efforts in preparing this three-volume report.

The authors also wish to express their thanks to Ms. Susan Riedel at Systems Technology, Inc., and to Captain Stanley Larimer and Dr. Robert Schwanz at the Flight Dynamics Laboratory for their appreciable efforts in reviewing the technical report.

This report is organized in three volumes. Volume I contains the theoretical developments as well as illustrative examples and case studies. Volume II describes two algorithms useful in the analysis of multi-rate systems, the DISCRET and TXCONV computer programs. Volume III contains the FORTRAN listings for these computer programs.

This report covers work performed from January 1979 through May 1980. The report was submitted by the authors in August 1980.

Accession For	
NTIS GRA&I	<input checked="checked" type="checkbox"/>
DTIC TAB	<input type="checkbox"/>
Unannounced	<input type="checkbox"/>
Justification	
By	
Distribution/	
Availability Codes	
Dist	Avail and/or Special
A	

TABLE OF CONTENTS

	<u>Page</u>
I. INTRODUCTION.....	1
II. VECTOR SWITCH DECOMPOSITION: CONSTRUCTION OF THE PSEUDO MEASUREMENT VECTOR.....	4
A. Introduction.....	4
B. Review of the Multi-Rate Transform Domain.....	5
C. Vector Switch Decomposition and Multi-Rate Sampling.....	10
D. Multiple-Order Sampling.....	13
E. Non-Synchronous Sampling.....	15
F. The Pseudo Measurement Concept.....	17
G. An Illustrative Example.....	21
H. Some Properties of the Pseudo Measurement Concept.....	31
III. FREQUENCY RESPONSE OF SINGLE-RATE SYSTEMS.....	34
A. Introduction.....	34
B. Continuous System Frequency Response.....	35
C. Mathematical Preliminaries.....	36
D. Open-Loop Frequency Response: Continuous Output Sampled.....	38
E. Open-Loop Frequency Response: Continuous Output.....	44
F. Single-Rate Closed-Loop Frequency Response.....	47
G. Section Summary.....	51
IV. FREQUENCY RESPONSE OF MULTI-RATE SYSTEMS.....	54
A. Introduction.....	54
B. A Basic Result.....	54
C. A Closed-Loop Application.....	64
D. General Results.....	76
E. Application to Simulation Error Analysis.....	81
F. An Important Algorithm.....	94
G. Computation of $(W_{GW})^T$, G^T/N Given.....	97
H. Section Summary.....	102

	<u>Page</u>
V. A PSEUDO MEASUREMENT EXERCISE.....	103
A. Analog Controller — YF-16.....	103
B. Frequency Response.....	106
C. A Comment on a Simulation Artifact.....	107
D. The Pseudo Measurement Design.....	108
E. Section Summary.....	112
VI. SUMMARY AND CONCLUSIONS.....	114
REFERENCES.....	116
APPENDIX A. FREQUENCY RESPONSE OF FAST-INPUT/SLOW-OUTPUT CLOSED-LOOP SYSTEM USING MULTI-RATE THEORY.....	A-1
APPENDIX B. COMPUTATION OF $(W_{*}M_2W_2)^T$ AND $(W_2M_3W_3)^T$	B-1
APPENDIX C. NUMERICAL DETAILS FOR AN ILLUSTRATIVE EXAMPLE.....	C-1
APPENDIX D. LISTING OF TRANSFER FUNCTIONS.....	D-1

LIST OF FIGURES

	<u>Page</u>
1. Multi-Rate System	5
2. Closed-Loop Multi-Rate System.....	9
3. Decomposition of a Sample Sequence.....	11
4. Multiple-Order Sampling.....	13
5. Components of Decomposed Signal.....	15
6. A Set of Non-Synchronously Sampled Signals.....	16
7. Sampling Notation.....	16
8. Advance, Sample, Delay.....	17
9. Pseudo Measurement Block Diagram.....	18
10. Reformulated Block Diagram.....	19
11. x , $x^{T/3}$, and the Components of $\hat{x}^{T/3}$	21
12. A Single-Rate Controller, $T = 1.0$ sec.....	22
13. A Multiple-Order Sampling Controller, $T = 1.0$ sec.....	24
14. Continuous System.....	35
15. Open-Loop System.....	39
16. Magnitude Plot for $N = 1, 2, 4$	41
17. Frequency Response and Spectral Components of Output.....	46
18. "Steady-State" Time Response.....	47
19. Illustrative Vector Closed-Loop Configuration.....	48
20. Magnitude Plot for Closed-Loop System.....	52
21. Multi-Rate/Multiple-Order Open-Loop System.....	55
22. Open-Loop System with Switch Decomposition.....	55
23. Closed-Loop System with Switch Decomposition.....	64

	<u>Page</u>
24. Closed-Loop Numerical Example.....	65
25. Composite Magnitude Plot.....	71
26. Magnitude Plot No. 1.....	73
27. Magnitude Plot No. 2.....	73
28. A Simulation Case Study.....	82
29. Case IV, Switch Decomposition Model.....	85
30. Magnitude Plot; Case I, Case II.....	88
31. Magnitude Plot; Case I, Case III.....	89
32. Comparison; Case II and Case III.....	90
33. Magnitude Plot; Case I, Case IV.....	91
34. Comparison, Case II and Case IV.....	92
35. Comparison, All Cases.....	93
36. A Phantom Sampler Formulation of a T/N, T/M Sampling Format.....	94
37. Response of a T/2 Input Sampled, T/3 Output Sampled System.....	96
38. Example Two-Rate Open-Loop System.....	97
39. Switch Decomposition Formulation for Fig. 38.....	97
40. Analog YF-16 Controller.....	104
41. Emulated YF-16 Controller.....	104
42. Bode Plot, Analog Compared with Emulated Controller.....	106
43. Simulation of Actuator via Tustin Transform.....	107
44. Alternate Configuration.....	108
45. A Pseudo Differentiation Configuration.....	110
46. Bode Plot, Pseudo Differentiation Configuration.....	113

	<u>Page</u>
A-1. Fast-Input/Slow-Output Closed-Loop System.....	A-1
A-2. Phantom Sampler Concept.....	A-3
C-1. Switch Decomposition of T/2, T/3 Example.....	C-2

LIST OF TABLES

	<u>Page</u>
1. Some Representative Data Holds.....	8
2. Numerator Coefficients as a Function of Advance Parameter Δ	29
3. Feedback Gains.....	29
4. Data for Composite Magnitude Plot (Figure 25).....	72

SECTION I

INTRODUCTION

Many current digital design procedures attempt only to approach the characteristics of existing analog designs. No explicit methodology exists which can exploit the unique characteristics of multi-rate or multiple-order digital computation and filtering. The objective of this research effort is to develop a multi-rate/multiple-order theory for the design of closed-loop digital control systems with characteristics and attributes that are either difficult or impossible to attain with analog or single-rate controllers. The key idea in this methodology is to use the logic of the computer to take a scalar continuous output signal, sample it at a relatively high rate, and then sort out the various samples into a vector of "pseudo measurements." The potential of such a scheme is significant, since it offers, among other things, the possibility of using fewer sensors and the potential for providing gracefully degrading system performance in the face of sensor failure.

The pseudo measurement concept may be likened to the observer concept of linear system theory. Recall that an "observer" is a dynamic subsystem which processes the available measurements and control inputs to obtain asymptotic estimates of those states which are not measured. The distinction between the observer and pseudo measurement concept is as follows. Additional pseudo states required for proper control action are obtained via design of a multi-rate or multiple-order sampling sequence in the pseudo measurement approach, while the estimate of system states not measured is attained by design of a dynamic subsystem in the observer approach. The pseudo measurement concept is based on using information contained in a scalar measurement, sampled at a high rate, to generate a lower rate measurement vector. This vector is likened to pseudo states since it effectively provides distinctively different information in the form of separate sampling sequences shifted in time. However, it should be noted that the pseudo measurement concept is not a state estimator, but a new design concept.

Several circumstances arise in applications where the pseudo measurement concept, by exploiting the unique characteristics of multi-rate and multiple-order sampling, can have considerable favorable impact.

- It is desirable to minimize the number of sensors, or to
- Provide for gracefully degrading system performance in the face of sensor failure.
- Not all the states are measurable.
- Some measurements are noise free.
- Outer navigation loops are noise free.
- Outer navigation loops are updated at inherently slow rates.

When one or more of these circumstances prevail in a particular application, the contribution of this theory will be in terms of more simple control laws, increased system performance, or more system flexibility in accommodating failures.

The report is organized in three volumes. Volume I contains the theoretical developments as well as illustrative examples and case studies.

Volume II describes two algorithms useful in the analysis of multi-rate systems, while Volume III gives FORTRAN listings for these algorithms. The first algorithm converts a continuous transfer function in the s -domain into alternate descriptions in the z -, w -, and w' -domains. The second algorithm calculates a low data rate discrete transform given a high data rate discrete transfer function. This algorithm is presented in Section IV of Volume I and later derived in Section IV of Volume II.

Volume I is organized as follows. Vector switch decomposition techniques, which provide a straightforward model of the pseudo measurement vector, are reviewed and extended in Section II. Also, in this section the pseudo measurement concept is defined and illustrated with an example.

An important facet of this effort hinges on the ability to interpret the properties of multi-rate/multiple-order closed-loop systems. Frequency response techniques provide effective tools to investigate the spectral characteristics of these systems. Toward this end, the frequency response of the continuous variables of single-rate systems are reviewed in Section III, with the necessary extensions for the analysis of multi-rate systems given in Section IV.

The extensions given in Section IV make it possible to investigate the spectral content of the continuous variables of multi-rate and/or multiple-order configured systems. In addition, an important relationship is deduced which makes it feasible to apply the switch decomposition/frequency response technique to the error analysis of simulations of continuous systems and/or discretely controlled continuous systems. An illustrative example demonstrates significant spectral differences between a closed-loop system (employing an analog or digital controller) and an all-digital simulation of the closed-loop system. The example also treats the problems encountered when simulation software is implemented on two different (independent) computers, each working in a slightly different frame time.

The application of the pseudo measurement concept is discussed further in Section V. In particular, a case study using a longitudinal model of the Y-16 is used to study the practicality of the approach (e.g., investigate the magnitude of the required feedback gains).

A summary and conclusions are presented in Section VI.

SECTION II

VECTOR SWITCH DECOMPOSITION: CONSTRUCTION OF THE PSEUDO MEASUREMENT VECTOR

A. INTRODUCTION

The prime objective of this research effort is the realization of closed-loop digitally controlled systems with desirable attributes not available in continuously controlled (analog) designs. To appreciate the considerable merit of this viewpoint one need only recall that couplers (data holds) which tie the digital computer to the control actuators are themselves filters possessing characteristics which are unrealizable with continuous linear filter sections. For example, the slower data hold forces the control actuator to move with smooth ramp-like deflections which closely approximate the "continuous" deflections. Yet, it inserts deep, wide notches into the frequency response, at multiples of the sampling frequency, which have no counterpart in continuous linear filter theory. The impact of this frequency response characteristic upon system performance can be favorable or unfavorable. It can certainly have an unfavorable effect if unanticipated inputs and/or control inputs are attempted or required at one of the notch frequencies. However, when anticipated, this frequency response characteristic may be used to advantage (for suppressing feedback of structural modes, for example) and its disadvantages avoided.

In short, the ability of the digital computer to perform a variety of unusual operations on input data lends credence to the idea of achieving closed-loop systems with unusual attributes. This is the key point of the present study where the logic of the computer is used to take a scalar continuous output signal, sample it at a relatively high rate, and then sort it out (in a particular fashion) into a vector of "pseudo" measurements. The potential of the idea is significant, since

it offers an alternative path approach for providing gracefully degrading system performance in the face of sensor failure.

To begin, there is a brief review of the multi-rate transform domain (primarily in order to review notation). Then, to put the pseudo measurement concept in proper perspective, we discuss vector switch decomposition and show how it is used to model multi-rate systems. Following this, a multiple-order sampling model is discussed.

Since any viable digital theory must be capable of modeling computational delay, a discussion of non-synchronous sampling is included since it provides a basic theoretical structure for treating time delays.

Completing this background description, we are then in a good position to set forth the pseudo measurement concept and indicate, via an example, its potential for achieving closed-loop configurations with unusual attributes.

B. REVIEW OF THE MULTI-RATE TRANSFORM DOMAIN

A basic property of the transform domain algebra developed in Ref. 1 is that a high sampling rate "operates through" a low one, provided that the ratio of the higher to the lower is an integer value.

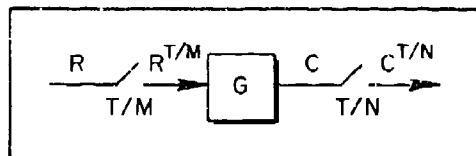


Figure 1. Multi-Rate System

In Fig. 1, the output equation is

$$C = GR^{T/M} \quad (1)$$

Then

$$\begin{aligned} C^{T/N} &= [GR^{T/M}]^{T/N} \\ &= G^{T/N} R^{T/M} \end{aligned} \quad (2)$$

where N/M is an integer. The superscript notation denotes the sampling rate involved. For example, $C^{T/N}$ indicates that the signal C is sampled at N/T samples per second.

The general notation $C^{T/N}$ implies either $C^{T/N}(s)$ or $C^{T/N}(z)$ in this report, where $C^{T/N}(s)$ represents the Laplace transform of the sampled continuous time function $c^{T/N}(t)$ and $C^{T/N}(z)$ its corresponding z transform. The correspondence between a sampled function in the s -domain and its z -transform is given by

$$C^{T/N}(z) = [C^{T/N}(s)]_{z=e^{sT/N}} \quad (3)$$

For continuous, stationary linear systems $C^{T/N}(s)$ is in general a non-algebraic function of s and $C^{T/N}(z)$ is obtained from $C^{T/N}(s)$ using the simple change of variable $z = e^{sT/N}$. However, $C^{T/N}(z)$ could also represent the z -domain model of a completely discrete function (e.g., digital computations in a computer) and thus have no direct counterpart in the continuous domain. In analysis and design no distinction is required between the z -transform function derived from a sampled continuous function [e.g., $C^{T/N}(s)$] and the z -transform function that models a completely discrete function. The z -transform (and its extensions the w - and w' -transforms) thus provides a unified analysis and synthesis technique for systems containing both continuous and discrete elements (i.e., hybrid systems). This ability to model continuous and discrete elements in a common discrete domain is perhaps the most fundamentally useful property of the z -, w -, or w' -domains.

The transform product in Eq. 2 is obtained by establishing a common definition of the z -transform variable. That is,

$$G^{T/N}(z)R^{T/M}(z_m) = G^{T/N}(z)R^{T/M}(z^{N/M}) \quad (4)$$

where

$$z = e^{sT/N}, \quad z_m = e^{sT/M} \quad (5)$$

The procedure is to first calculate the T/N and T/M z -transforms for $G(s)$ and $R(s)$, respectively, and then replace the transform variable z_m in $R^{T/M}(z_m)$ with $z_m = z^{N/M}$.

For a given G and R , a recursion equation can be written for Eq. 2 in a manner that is similar to the single-rate case for which $N = M = 1$. To see this, consider a simple example, for which we define $z = e^{sT/N}$. Let

$$G(s) = \frac{1}{s + 1} \quad (6)$$

Then

$$C^{T/N} = \frac{z}{z - e^{-T/N}} R^{T/M} \quad (7)$$

If the running index of the recursion equation, n , is tied to the z^{-1} operator, the time domain equation can be written directly using the fact that the input is set equal to $R(s)$ whenever n is an integer value of N/M . Therefore,

$$C_n = e^{-T/N} C_{n-1} + \begin{cases} R_n & n/(N/M) = \text{Integer} \\ 0 & n/(N/M) \neq \text{Integer} \end{cases} \quad (8)$$

This agrees with the single-rate case when $N = M = 1$.

$$C_n = e^{-T} C_{n-1} + R_n \quad (9)$$

These results are appreciably different in the presence of data holds. However, the results remain quite tractable and are detailed in Ref. 1 for the zero-order hold as well as the slewer data hold. The slewer data hold is a coupler which produces a smooth ramp output over the inter-sample period and, in addition, provides a continuous output even at the sampling instants. Transfer functions for representative data holds are given in Table 1.

TABLE 1. SOME REPRESENTATIVE DATA HOLDS

DATA HOLD	TRANSFER FUNCTION
Zero-Order Hold	$M_0 = \frac{1 - e^{-sT}}{s}$
First-Order Hold	$M_1 = M_0^2 \left(s + \frac{1}{T} \right)$
Second-Order Hold	$M_2 = M_0^3 \left(s^2 + \frac{3}{2T} s + \frac{1}{T^2} \right)$
Triangular Data Hold	$M_\Delta = \frac{M_0^2}{T} e^{sT}$
Slewer Data Hold	$M_{\text{slew}} = \frac{M_0^2}{T}$

The "T/N" approach is very useful in the analysis of closed-loop multi-rate systems, since the transform domain equations can be written directly, without the need for computing an inverse. Using these equations, the time domain equations can be written in the same manner as in the single-rate case. An example is described in Fig. 2.

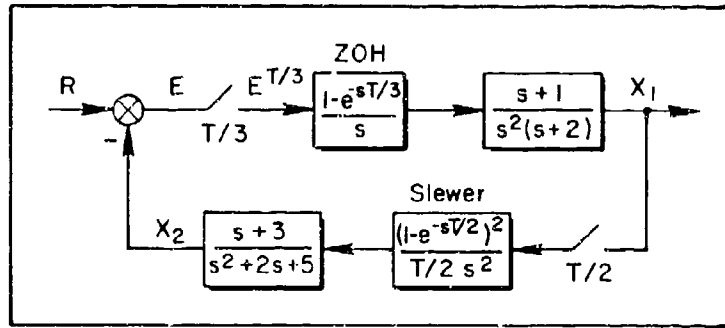


Figure 2. Closed-Loop Multi-Rate System

First, writing the algebraic relationships for X_1 and X_2 gives

$$X_1 = \left[\frac{s+1}{s^2(s+2)} \frac{1-e^{-sT/3}}{s} \right] E^{T/3} \quad (10)$$

$$X_2 = \left[\frac{(1-e^{-sT/2})^2}{(T/2)s^2} \frac{s+3}{s^2+2s+5} \right] X_1^{T/2} \quad (11)$$

Recognizing that

$$E^{T/3} = R^{T/3} - X_2^{T/3} \quad (12)$$

and taking the T/N transform of both sides produces

$$X_1^{T/N} = \left\{ \left[\frac{s+1}{s^2(s+2)} \frac{1-e^{-sT/3}}{s} \right] (R^{T/3} - X_2^{T/3}) \right\}^{T/N} \quad (13)$$

$$X_2^{T/N} = \left\{ \left[\frac{(1-e^{-sT/2})^2}{(T/2)s^2} \frac{s+3}{s^2+2s+5} \right] X_1^{T/2} \right\}^{T/N} \quad (14)$$

Since the outer sampling operator $\{\cdot\}^{T/N}$ operates through the inner one if the ratio of the inner sampling period to the outer sampling period, T/N , is an integer, Eqs. 13 and 14 reduce to

$$X_1^{T/N} = \left[\frac{(1 - e^{-sT/3})(s + 1)}{s^3(s + 2)} \right]^{T/N} (R^{T/3} - X_2^{T/3}) \quad (15)$$

$$X_2^{T/N} = \left[\frac{(1 - e^{-sT/2})^2(s + 3)}{(T/2)s^2(s^2 + 2s + 5)} \right]^{T/N} X_1^{T/2} \quad (16)$$

Observe that two transform domain equations completely define the closed-loop fifth-order system (exclusive of the data holds). Equations 15 and 16 can be used to calculate the inter-sample response with any desired degree of time resolution by increasing N . The only restriction is that N must be divisible by 2 and 3; otherwise, it is arbitrary.

The T/N approach is developed in detail in Ref. 1. It serves as the basis for extending the concept of frequency response, from merely being the magnitude and phase of the sine wave that fits the sample points at the sampling instants, to the case of fitting N sine waves to the sample points and $N - 1$ inter-sample points.

C. VECTOR SWITCH DECOMPOSITION AND MULTI-RATE SAMPLING

In essence, switch decomposition is a procedure wherein systems having multiple sampling operations (occurring at fixed but unequal sampling intervals but with a sampling pattern which is repeated over a fixed, finite time interval) are converted into an equivalent single sample rate format. As originally introduced by Kranc (Ref. 2), the method used a summing point methodology which proved to be extremely cumbersome when the ratios of the sampling periods become high. For this reason (and also because evolving state transition methods were tending to push transform methods into the background), the method fell

into disuse. However, there is much to recommend the switch decomposition concept for use in both time domain and transform domain analyses. In the subsection that follows we will review the basic concept and remove some earlier restrictions by recasting it in vector form. The vector form simplifies matrix block diagram manipulation for multi-loop, multi-rate sampled systems.

An example will make the basic idea quite transparent. Consider the continuous signal shown in Fig. 3a to be sampled at $3/T$ samples per second. This results in the sample sequence shown in Fig. 3b. The sampled values have been numbered for easy reference. Suppose we now sample the continuous signal with a sampling period, T . This results in

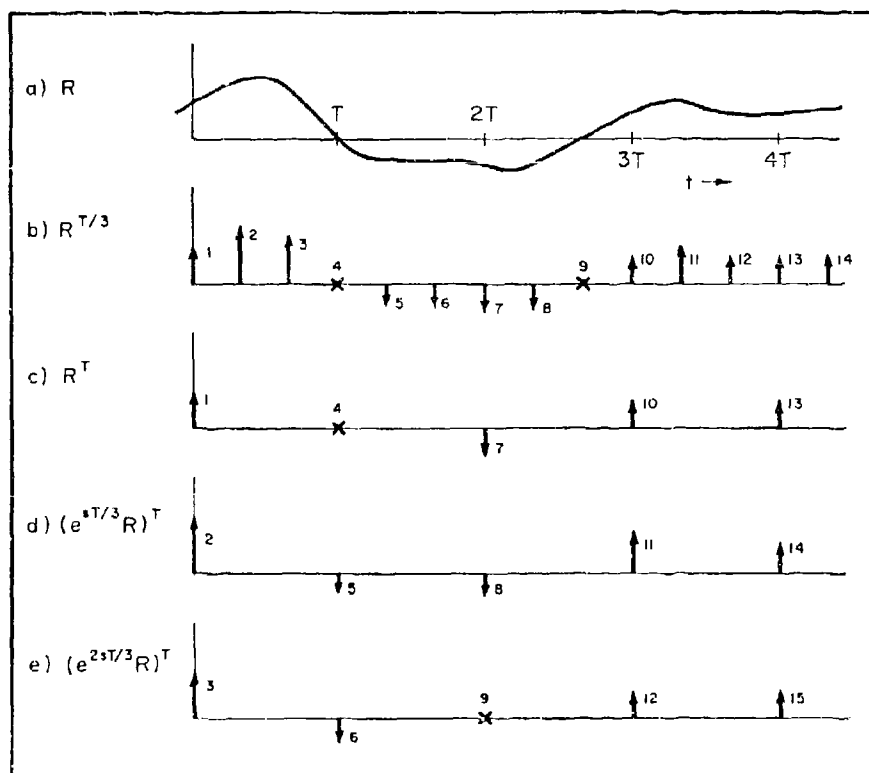


Figure 3. Decomposition of a Sample Sequence

the sample sequence consisting of sample numbers 1, 4, 7, 10, 13, ... shown in Fig. 3c. Define this sample sequence to be R^T .

Next, advance the continuous signal R by $T/3$. Then sample the advanced signal with a sampling period, T . This results in a sample sequence consisting of sample numbers 2, 5, 8, 11, 14, ... shown in Fig. 3d. Define this sample sequence to be $(e^{sT/3}R)^T$. Finally, advance the continuous signal R by $2T/3$, and sample it with a sampling period, T . This results in the sequence consisting of sample numbers 3, 6, 9, 12, 15, ... shown in Fig. 3e. Define this signal sequence to be $(e^{2sT/3}R)^T$.

The significance of the switch decomposition concept resides in its ability to provide an alternative expression for the original sequence $R^{T/3}$ in terms of several quantities which are each sampled simultaneously every T seconds. This alternative expression for $R^{T/3}$ consists of the sum of R^T , $(e^{sT/3}R)^T$, and $(e^{2sT/3}R)^T$:

$$R^{T/3} = R^T + (e^{sT/3} R)^T e^{-sT/3} + (e^{2sT/3} R)^T e^{-2sT/3} \quad (17)$$

Equation 17 has a simple factored equivalent which is the product of two vectors and the scalar R ,

$$R^{T/3} = \begin{bmatrix} 1, & e^{-sT/3}, & e^{-2sT/3} \end{bmatrix} \left\{ \begin{bmatrix} 1 \\ e^{sT/3} \\ e^{2sT/3} \end{bmatrix} R \right\}^T \quad (18)$$

Or, more compactly,

$$R^{T/3} = W(W_*R)^T \quad (19)$$

where

$$W = \begin{bmatrix} 1, & e^{-sT/3}, & e^{-2sT/3} \end{bmatrix} \quad (20)$$

and

$$W_* = \begin{bmatrix} 1 \\ e^{sT/3} \\ e^{2sT/3} \end{bmatrix} \quad (21)$$

The extension of this scalar result to the vector case is discussed in detail in Ref. 1 and will not be covered here. We proceed to a discussion of multiple-order sampling.

D. MULTIPLE-ORDER SAMPLING

Suppose that a group of sampling operations in a system is repeated every T seconds, the intervals between successive samples in the group sequence being unequal. This is depicted in Fig. 4 for an example case of four unequally spaced samples occurring before the sampling sequence repeats. In Fig. 4 the notation X^* is used to denote that X is sampled in a multiple-order manner.

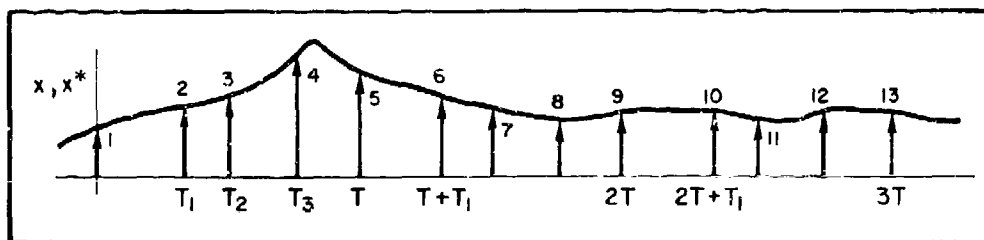


Figure 4. Multiple-Order Sampling

The multiple-order sampling operation can be modeled in terms of a single-rate sampling operation, using the same type of notation given in Eq. 19. Let

$$X^* = W(W_*X)^T \quad (22)$$

where

$$W = [1, e^{-sT_1}, e^{-sT_2}, e^{-sT_3}] \quad (23)$$

and

$$W_* = [1, e^{sT_1}, e^{sT_2}, e^{sT_3}]' \quad (24)$$

The sequence specified by Eq. 22 is shown in Fig. 5. Note that

$$X^* = W(W_*X)^T = W \begin{bmatrix} X^T \\ (e^{sT_1} X)^T \\ (e^{sT_2} X)^T \\ (e^{sT_3} X)^T \end{bmatrix} \quad (25)$$

$$= X^T + e^{-sT_1}(e^{sT_1} X)^T + e^{-sT_2}(e^{sT_2} X)^T + e^{-sT_3}(e^{sT_3} X)^T \quad (26)$$

The extension to the case where X is a vector is straightforward. For example, if X is a two-dimensional vector, let

$$W = \left[\begin{array}{c|c} W_a & 0 \\ \hline 0 & W_b \end{array} \right] \quad (27)$$

where the vectors W_a and W_b are each analogous to the W vector defined by Eq. 23 but each is appropriate to the sampling sequence for the corresponding element of the X vector.

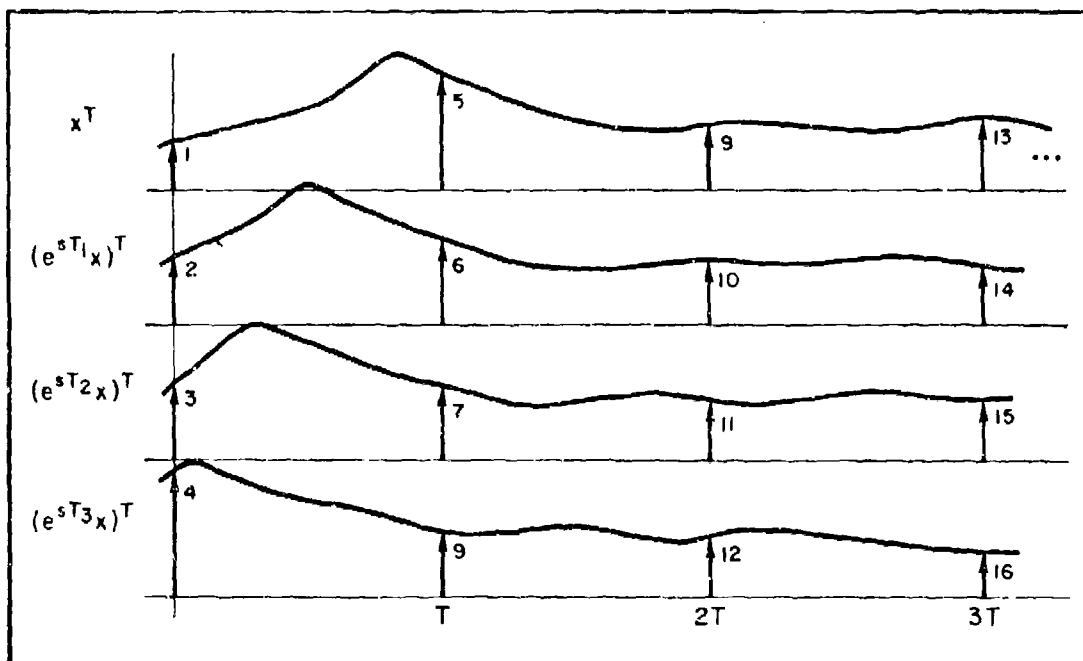


Figure 5. Components of Decomposed Signal

E. NON-SYNCHRONOUS SAMPLING

Non-synchronous sampling is a basic tool useful for modeling distributed computation architecture, data skewness in the A/D and D/A conversion processes as well as the internal computational delay of the digital computer. By definition, non-synchronous sampling occurs when all the systems' sampling operations are repeated at the same rate but occur at different instants of time (refer to Fig. 6).

In Fig. 6 both continuous signals, x_1 and x_2 , are sampled at $1/T$ Hz, but the x_2 sampler is "out of sync" with the x_1 sampler by T_0 seconds. The sampling operation for x_1^T is shown symbolically in Fig. 7a and for x_2^* in Fig. 7b. (* notation on x_2 is used here to indicate an "unconventional" sampling operation.)

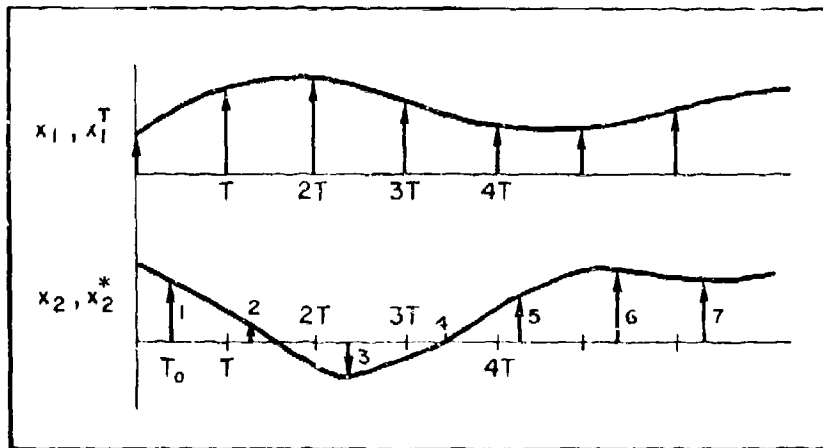


Figure 6. A Set of Non-Synchronously Sampled Signals

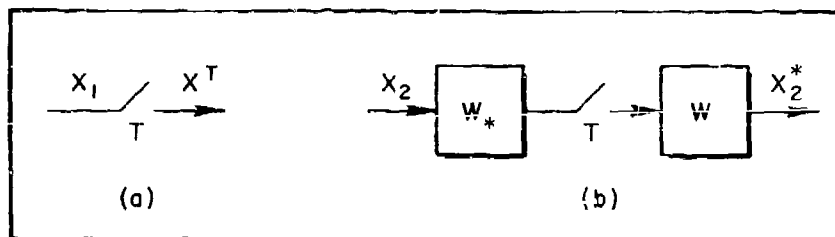


Figure 7. Sampling Notation

Figure 7b models the non-synchronous sampler with a synchronous sampler by preceding the sampler with the operation W_* followed by the operator W . That is,

$$x_2^* = W(W_* x_2)^T \quad (28)$$

where

$$W = e^{-sT_0}, \quad W_* = e^{sT_0} \quad (29)$$

Proceeding according to Eq. 29, one advances x_2 by T_0 seconds, samples at the $1/T$ rate, and then delays $(W_* x_2)^T$ by T_0 seconds to obtain the time sequence (refer to Fig. 8). Note how the non-synchronous sampling operations on x_2 is modeled in terms of a scalar factor; thus the dimension of the equivalent single-rate sampled signal, $(W_* x_2)^T$, is not increased.

The model readily extends to the case where x is a vector.

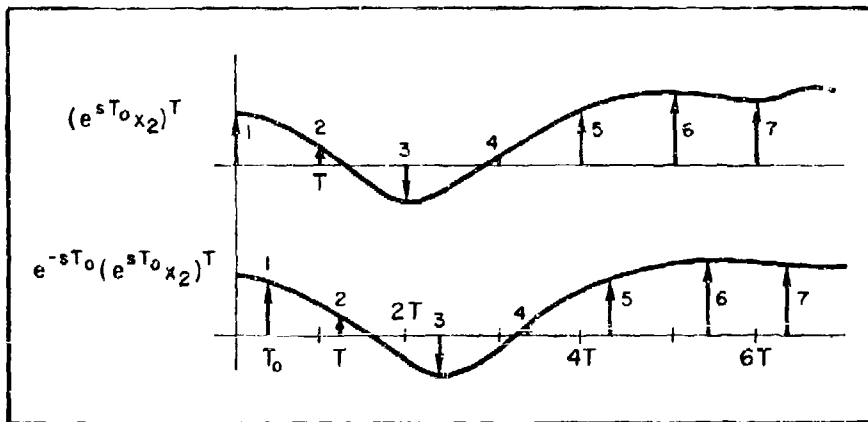


Figure 8. Advance, Sample, Delay

F. THE PSEUDO MEASUREMENT CONCEPT

It has now been shown that vector switch decomposition can be used to model multi-rate and multiple-order sampling operations. Moreover, non-synchronous sampling (i.e., skewed data) can be treated, and therefore, of course, computational time delays can also be included. We are now in a good position to discuss the pseudo measurement concept, using Fig. 9 to indicate the several options available.

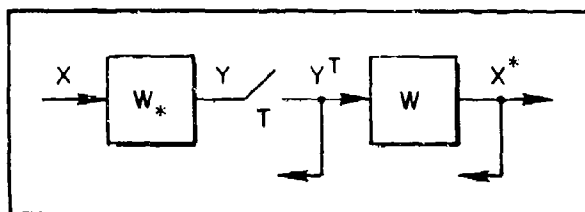


Figure 9. Pseudo Measurement Block Diagram

First of all, the notation W_* , W in Fig. 9 is used to denote either multi-rate or multiple-order sampling operations. The essence of the pseudo measurement idea lies in the following observations:

- X^* is the multi-rate (multiple-order) sampled equivalent of X . It has the same dimension as the vector X .
- Y^T has the row dimension of W which may be considerably greater (but never less than) the dimension of the vector X .

Rather than feed back the entire fixed sequence of samples in a (scalar) element of X^* , one may elect to feed back selected, individual samples in the fixed sequence. These individual samples are elements of the vector signal, Y^T . Of course, one must exercise due regard for physical realizability (a sample cannot be used before it is available). Nevertheless, the digital computer has the ability to sort out individual samples from the sequence and deposit them in their respective appropriate registers. This sorting process in effect creates an enlarged vector of measurements at a slower effective sampling rate. We shall call the elements of this enlarged measurement vector pseudo measurements because they are merely alternative samples of the same basic variables.

As shown in Fig. 9, the Y^T vector is defined in terms of time advance components and therefore caution must be used in interpreting the significance of the various components (again, a sample cannot be used before it is available). To avoid this difficulty, the pseudo measurement operation is redefined in terms of "hat" operators (refer to Fig. 10).

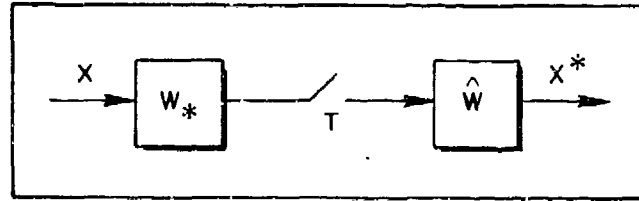


Figure 10. Reformulated Block Diagram

If, for example,

$$W = [1, e^{-sT_0}, e^{-sT_1}, e^{-sT_2}] \quad (30)$$

then

$$\hat{W} = \begin{bmatrix} 1 & 0 & 0 & 0 \\ 0 & e^{-sT_0} & 0 & 0 \\ 0 & 0 & e^{-sT_1} & 0 \\ 0 & 0 & 0 & e^{-sT_2} \end{bmatrix} = W_{\text{diag}} \quad (31)$$

and

$$W_* = \begin{bmatrix} 1 \\ e^{sT_0} \\ e^{sT_1} \\ e^{sT_2} \end{bmatrix} \quad (32)$$

Or, if multi-rate sampling is used, the extended switch decomposition modeling components might appear as:

$$W_* = [1, e^{sT/3}, e^{2sT/3}]' \quad (33)$$

and

$$W = [1, e^{-sT/3}, e^{-2sT/3}] \quad (34)$$

Then

$$\hat{W} = \begin{bmatrix} 1 & 0 & 0 \\ 0 & e^{-sT/3} & 0 \\ 0 & 0 & e^{-2sT/3} \end{bmatrix} \quad (35)$$

Clearly,

$$\begin{aligned} X^* = \hat{X}^{T/3} = \hat{W}(W_*X)^T &= \begin{bmatrix} 1 & 0 & 0 \\ 0 & e^{-sT/3} & 0 \\ 0 & 0 & e^{-2sT/3} \end{bmatrix} \begin{bmatrix} X^T \\ (e^{sT/3}X)^T \\ (e^{2sT/3}X)^T \end{bmatrix} \\ &= \begin{bmatrix} X^T \\ e^{-sT/3}(e^{sT/3}X)^T \\ e^{-2sT/3}(e^{2sT/3}X)^T \end{bmatrix} \end{aligned} \quad (36)$$

Thus, \hat{X} is the desired vector; each component has the samples in the correct temporal sequence (refer to Fig. 11).

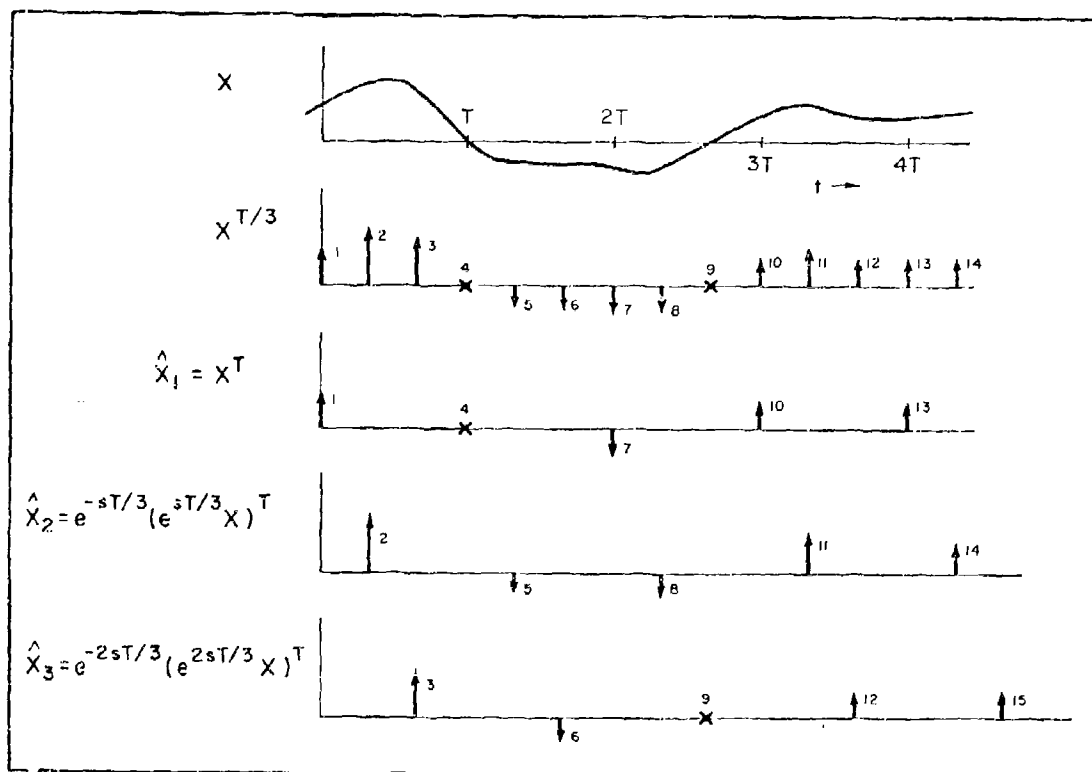


Figure 11. X , $X^{T/3}$, and the Components of $\hat{X}^{T/3}$

G. AN ILLUSTRATIVE EXAMPLE

Consider the single-rate system shown in Fig. 12, where M is a zero-order hold and the plant is

$$G(s) = \frac{3s^3 + 15s^2 + 35s + 13}{(s+1)[(s+2)^2 + (3)^2]} \quad (37)$$

Suppose $G(s)$ (a scalar) is the only output of the system available for feedback. Further, suppose the design objectives are to force a unity steady-state response in G to a unit step input and to obtain an assigned set of poles for the closed-loop system. Let $D(s)$ represent

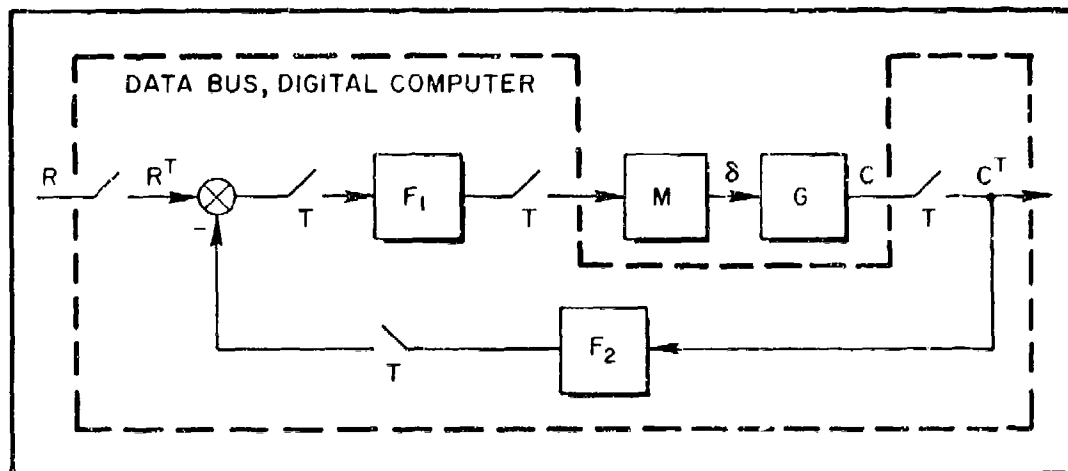


Figure 12. A Single-Rate Controller, $T = 1.0$ sec

the plant poles, i.e., the poles of $G(s)$. The poles for the discretized plant plus data hold are represented by $D(z)$ where

$$(GM)^T = \frac{N(z)}{D(z)} \quad (38)$$

and

$$D(z) = (z - 0.3679)[(z + 0.1340)^2 + (0.019)^2] \quad , \quad T = 1.0 \quad (39)$$

with

$$[s + a]^T \Rightarrow z - e^{-aT}$$

$$\begin{aligned} [(s + a)^2 + b^2] &\Rightarrow [(z - e^{-aT} \cos bT)^2 + (e^{-aT} \sin bT)^2] \\ &= z^2 - (2e^{-aT} \cos bT)z + e^{-2aT} \end{aligned} \quad (40)$$

The assigned poles for the closed-loop system are represented by $\Delta(z)$ where

$$\Delta(z) = (z - 0.1353)[(z - 0.1988)^2 + (0.3096)^2] \quad (41)$$

The roots of $\Delta(z)$ may be thought of as counterparts to

$$\Delta(s) = (s + 2)[(s + 1)^2 + (1)^2] \quad (42)$$

for a continuous system. This particular assignment is quite arbitrary on our part and, moreover, we are not particularly advocating pole assignment as a design method; our objective is to demonstrate that the design goals can be achieved via the properties of multiple-order sampling.

It may be difficult to achieve these goals through design of the filters F_1 and F_2 . For example, from the equation (see Fig. 12)

$$C^T = [1 + (GM)^T F_1^T F_2^T]^{-1} (GM)^T F_1^T R^T \quad (43)$$

It can be appreciated that the gain must be split between F_1 and F_2 filters in order to achieve the unity step response objective. Moreover, it is not readily apparent that one can obtain

$$D(z)[1 + (GM)^T (F_1^T F_2^T)] = \Delta(z) \quad (44)$$

and still maintain a third-order characteristic equation (an implicit requirement of the pole assignment objective).

Having considered a single-rate approach, consider next what multiple-order sampling has to offer. A multiple-order sampled configuration is shown in Fig. 13. In this simple configuration, multiple-order sampling is used only on the plant output variable. Multiple-order sampling could also be employed for sampling the input, R , and at the input to the data hold, U . Restricting the example to sampling the output variable will enable us to demonstrate the possibilities of multiple-order sampling without adding unnecessary complexity. The multiple-order sampling assumption allows us to feed back the pseudo measurement vector C^* instead of the scalar measurement C^T . Furthermore, the intent is to use only a gain matrix, K , to attain the design objectives. The particular choice for W and K is

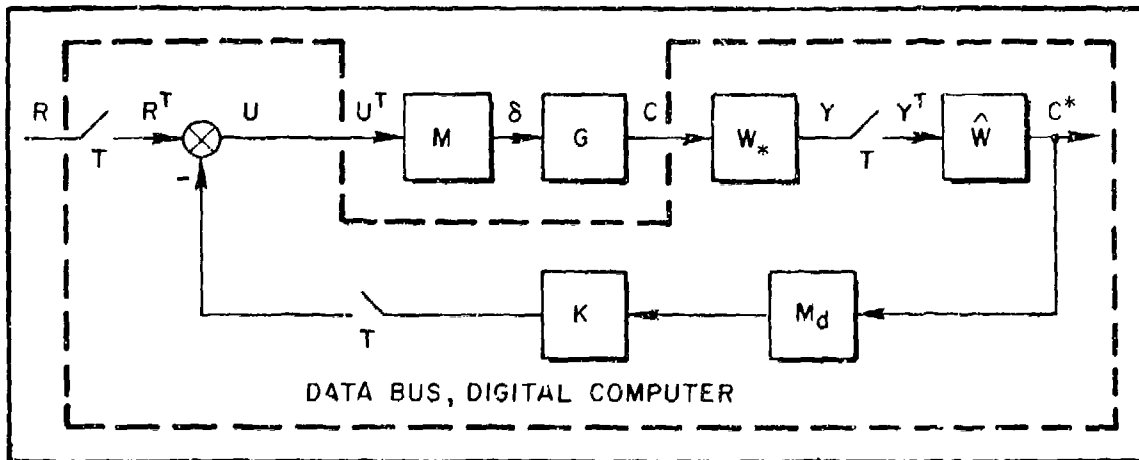


Figure 13. A Multiple-Order Sampling Controller,
 $T = 1.0$ sec

$$W = [1, \quad e^{-(\pi/10)s}, \quad e^{-.4s}, \quad e^{-.6s}, \quad e^{-.7s}] \quad (45)$$

and

$$K = [K_1, \quad K_2, \quad K_3, \quad K_4, \quad K_5] \quad (46)$$

Then

$$\hat{W} = \begin{bmatrix} 1 & 0 & 0 & 0 & 0 \\ 0 & e^{-(\pi/10)s} & 0 & 0 & 0 \\ 0 & 0 & e^{-.4s} & 0 & 0 \\ 0 & 0 & 0 & e^{-.6s} & 0 \\ 0 & 0 & 0 & 0 & e^{-.7s} \end{bmatrix} = W_{\text{diag}} \quad (47)$$

and

$$W_* = \begin{bmatrix} 1 \\ e^{-(\pi/10)s} \\ e^{-.4s} \\ e^{-.6s} \\ e^{-.7s} \end{bmatrix} \quad (48)$$

From Fig. 13 ($T = 1.0$ sec),

$$U^T = [1 + (KM_d \hat{W})^T (W_* GM)^T]^{-1} R^T \quad (49)$$

where

$$M_d = M_{diag} = \begin{bmatrix} M & 0 & 0 & 0 \\ 0 & M & 0 & 0 \\ 0 & 0 & M & 0 \\ 0 & 0 & 0 & M \end{bmatrix}, \quad M = \frac{1 - e^{-sT}}{s} \quad (50)$$

and

$$C^T = (GM)^T U^T \quad (51)$$

But

$$\begin{aligned} (KM_d \hat{W})^T &= \left\{ [K_1 M, K_2 M, K_3 M, K_4 M, K_5 M] \hat{W} \right\}^T \\ &= \left\{ M [K_1, K_2 e^{-(\pi/10)s}, K_3 e^{-.4s}, K_4 e^{-.6s}, K_5 e^{-.7s}] \right\}^T \end{aligned} \quad (52)$$

or

$$(KM_d \hat{W})^T = \left\{ M[K_1, K_2 e^{(9\pi/10)s} e^{-s}, K_3 e^{.6s} e^{-s}, K_4 e^{.4s} e^{-s}, K_5 e^{.3s} e^{-s}] \right\}^T$$

$$\hat{W} = [K_1, K_2 z^{-1}, K_3 z^{-1}, K_4 z^{-1}, K_5 z^{-1}] \quad , \quad z = e^{sT} \quad (53)$$

Reducing Eq. 52 to Eq. 53 requires the use of the advanced z-transform on each term in the Eq. 52 vector. For example, evaluating the second term

$$[M(K_2 e^{(9\pi/10)s} e^{-s})]^T \quad (54)$$

gives

$$(1 - e^{-sT}) e^{-s} \left[\frac{K_2 e^{(2\pi/10)s}}{s} \right]^T \quad (55)$$

Then

$$\frac{z-1}{z} z^{-1} K_2 \frac{z}{z-1} = K_2 z^{-1} \quad (56)$$

The remaining terms in Eq. 53 are evaluated in a similar manner.

Inserting Eqs. 49 and 53 into Eq. 51 gives

$$C^T = (GM)^T \left\{ I + [K_1, K_2 z^{-1}, K_3 z^{-1}, K_4 z^{-1}, K_5 z^{-1}] (W_* GM)^T \right\}^{-1} R^T \quad (57)$$

where

$$W_* = \begin{bmatrix} 1 \\ e^{(\pi/10)s} \\ e^{.4s} \\ e^{.6s} \\ e^{.7s} \end{bmatrix} \quad (58)$$

and

$$G = \frac{N}{D} = \frac{3s^3 + 15s^2 + 35s + 13}{(s+1)[(s+2)^2 + (3)^2]} \quad (59)$$

Carrying out the transform operations indicated in Eq. 57 produces

$$C^T = \left(\frac{z-1}{z} \right) \frac{N(z)_1}{D(z)} \left\{ I + \left(\frac{z-1}{z} \right) [K_1, K_2 z^{-1}, K_3 z^{-1}, K_4 z^{-1}, K_5 z^{-1}] \begin{bmatrix} N(z)_1 \\ N(z)_2 \\ N(z)_3 \\ N(z)_4 \\ N(z)_5 \end{bmatrix} \frac{1}{D(z)} \right\}^{-1} R^T \quad (60)$$

where

$$(W_{*GM})^T = \left(\frac{z-1}{z} \right) \left\{ \begin{bmatrix} N \\ e^{(\pi/10)s} N \\ e^{.42s} N \\ e^{.6s} N \\ e^{.7s} N \end{bmatrix} \frac{1}{sD} \right\}^T = \left(\frac{z-1}{z} \right) \begin{bmatrix} N(z)_1 \\ N(z)_2 \\ N(z)_3 \\ N(z)_4 \\ N(z)_5 \end{bmatrix} \frac{1}{D(z)} \quad (61)$$

Performing the matrix multiplication and taking the inverse in Eq. 60 gives

$$C^T = \left(\frac{z-1}{z} \right) \frac{N(z)_1}{D(z)} \left[\frac{\left(\frac{z}{z-1} \right) D(z)}{\left(\frac{z}{z-1} \right) D(z) + KN(z)} \right] R^T \quad (62)$$

with

$$KN(z) = K_1N(z)_1 + K_2N(z)_2z^{-1} + K_3N(z)_3z^{-1} + K_4N(z)_4z^{-1} + K_5N(z)_5z^{-1} \quad (63)$$

Equation 62 further simplifies to

$$\begin{aligned} C^T &= \left[\frac{N(z)_1}{\left(\frac{z}{z-1} \right) D(z) + KN(z)} \right] R^T \\ &= \left[\frac{(z-1) N(z)_1}{zD(z) + (z-1)KN(z)} \right] R^T \end{aligned} \quad (64)$$

The form of the entries in the column vector $(W_{GM})^T$ (Eq. 61) will be $(a_0z^3 + a_1z^2 + a_2z + a_3)/D(z)$. These are tabulated in Table 2 for a basic sampling cycle period of $T = 1.0$ seconds. The first column corresponds to $N(z)_1$ in Eq. 61, the second column to $N(z)_2$, and so on. The feedback gains that accomplish all design objectives are tabulated in Table 3. The design objectives are repeated below:

- Closed-loop pole assignment as specified by Eq. 41.
- Unity steady-state response in C for a unit step input R .

The first objective is satisfied by equating like coefficients in Eq. 41 and the denominator in Eq. 64. That is,

$$\begin{aligned} zD(z) + (z-1)KN(z) &= \Delta(z) \\ &= (z - 0.1353)[(z - 0.1988)^2 + (0.3096)^2] \end{aligned} \quad (65)$$

TABLE 2
NUMERATOR COEFFICIENTS AS A FUNCTION OF ADVANCE PARAMETER Λ

Λ	0	$\pi/10$.4	.6	.7
a_0	3.000000000	2.475580055	2.251930038	1.773697950	1.584956596
a_1	-2.314717621	-1.623868245	-1.340786259	-0.756522207	-0.537430945
a_2	-0.195116512	-0.029566508	-0.095749095	-0.206712756	-0.235858883
a_3	-0.067316458	-0.009062870	-0.002312250	-0.002620445	-0.001415664

Note: $D(z) = (z - 0.367879441)(z^2 + 0.2677961830z + 0.018315639)$

TABLE 3. FEEDBACK GAINS

K_1	0.091506404
K_2	-1.494955697
K_3	2.832023694
K_4	-4.131755870
K_5	2.703181447

The second objective is realized by applying the final value theorem to Eq. 64 for a unit step input $R^T = (z)/(z - 1)$.

$$CT(\infty) = \lim_{z \rightarrow 1} \frac{(z - 1)}{z} CT(z) \quad (66)$$

Before leaving this example, the physical implications of acquiring the C^* output signal in Fig. 13 will be addressed. The multiple-order sampled signal C^* is given by

$$C^* = \hat{W}(W_* C)^T$$

$$= \begin{bmatrix} 1 & 0 & 0 & 0 & 0 \\ 0 & e^{-(\pi/10)s} & 0 & 0 & 0 \\ 0 & 0 & e^{-.4s} & 0 & 0 \\ 0 & 0 & 0 & e^{-.6s} & 0 \\ 0 & 0 & 0 & 0 & e^{-.7s} \end{bmatrix} \left\{ \begin{bmatrix} 1 \\ e^{(\pi/10)s} \\ e^{.4s} \\ e^{.6s} \\ e^{.7s} \end{bmatrix} C \right\}^T$$

$$= \begin{bmatrix} C^T \\ e^{-(\pi/10)s}(e^{(\pi/10)s}C)^T \\ e^{-.4s}(e^{.4s}C)^T \\ e^{-.6s}(e^{.6s}C)^T \\ e^{-.7s}(e^{.7s}C)^T \end{bmatrix} \quad (67)$$

This sampling scheme analytically models (via single rate sampling) the actual physical operations within an analog-to-digital converter that produce samples of the continuous output variable C in a multiple-order format. These multiple samples must be physically separated according to the selected scheme as indicated by the W_* vector and \hat{W} matrix. In this example, a group of five samples in a multiple-order format must be physically generated every T seconds at intervals of $(0)T$, $(\pi/10)T$,

0.4T, 0.6T, and 0.7T seconds. These individual samples are stored in appropriate storage registers within the computer until all samples within a group are obtained. This group of samples is then added together with each sample first multiplied by an individual gain factor (K_1 , K_2 , K_3 , K_4 , K_5). This process implies that a full frame of delay equal to T seconds is inherently present in every component except the first. That is, as previously pointed out, samples cannot be used to form the scalar feedback signal in Fig. 13 before they are available. This required physical delay shows up in the analytical model as Eq. 53 (repeated here):

$$(KM_d\hat{W})^T = [K_1, K_2z^{-1}, K_3z^{-1}, K_4z^{-1}, K_5z^{-1}] \quad (68)$$

where the z^{-1} delay factors assure that samples from the previous frame time $(n-1)T$ are used to form the scalar feedback signal for the nT frame time.

H. SOME PROPERTIES OF THE PSEUDO MEASUREMENT CONCEPT

While this is not a particularly realistic design problem, a number of properties of the pseudo measurement concept, which accrue from use of multiple-order sampling, have been demonstrated:

- Achieved unity steady-state gain without forward loop compensation.
- Generated a five component multiple-order sample vector from a scalar analog signal.
- Assigned three poles using only the one available analog measurement.
- Avoided compensation networks.
- Accomplished pole placement with multiple samples of a single output variable (in distinction to single samples of several output variables). This has been accomplished without using an observer or Kalman filter to supply estimates of unmeasured states.

We remark in conclusion that the pseudo measurement concept is not the something-for-nothing gambit that it might appear to be. In connection with the illustrative example, a price is paid. This price is more frequent sampling of the plant output variable than for a single-rate system having the same basic sample sequence rate. That is, additional samples of the plant output variable have been used as an alternative to using digital filters (compensation) or as an alternative to measuring additional plant output variables. In more complex multiple-order sampling schemes the general nature of the available tradeoffs will be similar to the alternatives for our simple example. A three-way tradeoff (among number of output variables measured, number of samples of a given set of measurements taken in the sampling sequence interval, and complexity of digital filtering) will exist. Since "number of output variables measured" translates into "number of sensors," the tradeoff against "number of samples" greatly favors taking additional samples in terms of practical system hardware considerations.

The tradeoff of "number of samples of a given set of measurements taken in the sampling sequence interval" and "complexity of digital filtering" also favors taking additional samples. This is the case even though the number of registers required is not affected strongly. However, the number of digital multiplications required may be reduced significantly. This, in turn, can reduce computational burden, which is especially important in a microprocessor computing environment. Hence the potential contribution of the pseudo measurement concept to cost reduction in system hardware is realized.

The pseudo measurement technique also has the potential to provide for gracefully degrading system performance in the face of sensor failure. For example, if a sensor failure can be identified and isolated, then it is possible to divert the computing capacity in the failed sensor path for processing of additional samples of different output variables having operative sensors. For this use, the control law is restructured in a predetermined way following a failure. The way

in which the control law is restructured is dependent upon the particular failure. This may enable significant reduction in number of redundant sensor components when coupled with so-called analytical failure identification techniques. The latter compare the measurements of different output variables for consistency.

Finally, we remark that the sampling sequence, within the basic T frame time of 1, $e^{-\pi/10s}$, $e^{-.4s}$, $e^{-.6s}$, $e^{-.7s}$, was selected only to demonstrate a multiple-order sampling environment. There is nothing especially magic about it; in fact, it might even be a poor choice. We cannot tell this until the tools needed to access the spectral implications of this choice (the topic of the next two sections) are developed.

SECTION III

FREQUENCY RESPONSE OF SINGLE-RATE SYSTEM

A. INTRODUCTION

When a continuous, stable, stationary linear system is excited by a sine wave, its steady-state output is comprised of a single wave at the same frequency as the input. It differs from the input wave only by a phase angle and a magnitude factor. Moreover, it is unnecessary to compute the actual transient response of the system when its behavior over large epochs of time is of interest, since both the magnitude factor and phase angle can be read from a Bode plot.

A similar but more complex situation exists when a sampler and data hold couple the sine wave input to the continuous system. This configuration is referred to as a "discretely excited system." Given that the continuous system is stable, the continuous output waveform will contain a wave at the fundamental frequency and all of its aliases. Thus, if the system is forced with $1 \sin bt$, $0 < b < 2\pi/T$; the output will contain terms at frequencies b , $b + (2\pi/T)$, $b + (4\pi/T)$, The relative amplitudes and phase angles will depend on the data hold employed as well as the system transfer function. Nevertheless, given the data hold and system transfer functions, the magnitude and phase angle for each and every component can be read from a particular "Bode plot." Notice that this concept of frequency response is more comprehensive than the traditional concept of the "sampled spectrum" (see, e.g., see Ref. 3), which is limited to determining the single sinusoid that fits the system output samples at the sampling instants.

In the subsections that follow we review the frequency response concept for continuous systems and then proceed to the frequency response for discretely excited open-loop systems. Finally, the manner of application for single-rate sampled closed-loop systems is given.

B. CONTINUOUS SYSTEM FREQUENCY RESPONSE

It will be helpful to first review the frequency response concept for continuous systems. Let R in Fig. 14 be a unit sine wave input with frequency ω_0 rad/sec. The Laplace transform of the output is

$$C(s) = G(s) R(s) = C(s) \frac{\omega_0}{s^2 + \omega_0^2} \quad (69)$$

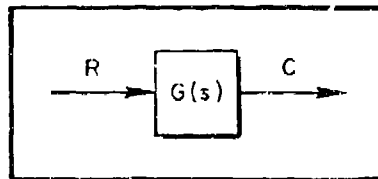


Figure 14. Continuous System

Equation 69 can be expanded in partial fractions as

$$C(s) = \frac{A\omega_0}{s^2 + \omega_0^2} + \frac{Bs}{s^2 + \omega_0^2} + \left[\begin{array}{l} \text{Terms associated} \\ \text{with characteristic} \\ \text{polynomial of } G(s) \end{array} \right] \quad (70)$$

The bracketed term in Eq. 70 determines the characteristic behavior of the system which can be stable (negative eigenvalues) or unstable (positive eigenvalues). Nevertheless, the steady-state sinusoidal behavior is completely defined by the partial fraction coefficients A and B , since once they are known the steady-state time response can be written directly as:

$$\left. \begin{aligned} C(t) \Big|_{t \rightarrow \infty} &= A \sin \omega_0 t + B \cos \omega_0 t \\ &= \sqrt{A^2 + B^2} \sin (\omega_0 t + \phi) \end{aligned} \right\} \quad (71)$$

where $\phi = \tan^{-1} (B/A)$. The details of solving for A and B show clearly the relationship between the Bode plot and the steady-state waveform.

To solve for A and B, multiply Eq. 70 by $[s^2 + \omega_0^2]$ and evaluate the result for $s = j\omega_0$:

$$G(s)\omega_0|_{s=j\omega_0} = (A\omega_0 + Bs)|_{s=j\omega_0} + \left[\begin{array}{c} \text{Terms associated} \\ \text{with characteristic} \\ \text{polynomial of } G(s) \end{array} \right] (s^2 + \omega_0^2)|_{s=j\omega_0} \quad (72)$$

or

$$G(s)|_{s=j\omega_0} = A + jB = \sqrt{A^2 + B^2} e^{j \tan^{-1}(B/A)} = G(j\omega_0) \quad (73)$$

To summarize, we see that a sinusoidal input at frequency ω_0 produces a steady-state sinusoidal output waveform having the same frequency. It differs from the input only by a magnitude factor and a phase shift. Both magnitude factor and phase shift for any given input frequency, ω_0 , can be read directly from a Bode plot for $G(j\omega_0)$. That is, for any given input frequency ω_0 ,

$$A + jB = G(s)|_{s=j\omega_0} \quad (74)$$

The sections that follow expand this "frequency response" viewpoint to include discretely excited systems.

C. MATHEMATICAL PRELIMINARIES

Let R be a sinusoid of unit amplitude and frequency b rad/sec. If R is sampled at $1/T$ samples per second and is then described in terms of a sample sequence having N/T samples per second, the result is:

$$R^T = \frac{z^N \sin bT}{z^{2N} - 2(\cos bT)z^N + 1}, \quad z = e^{sT/N} \quad (75)$$

*The notation follows Ref. 1. The superscript denotes the period of the sampling operator. For example, R^T and $R^{T/3}$ denote sampling periods of T and T/3 seconds, respectively.

The following development is for later use. First, find the N factors of the denominator of Eq. 75. This, in turn, permits partial fraction expansion. This expansion contains terms which correspond to sampled elementary time functions. For example, if $f(t) = \sin bt$, then:

$$f^T(t) = [\sin bt]^T \Rightarrow F(z) = \frac{z \sin bT}{z^2 - 2(\cos bT)z + 1} \quad (76)$$

However, an elementary sampled time function corresponding to

$$F(z) = \frac{z \sin bT}{z^2 + 2(\cos bT)z + 1} \quad (77)$$

is not immediately apparent (the denominator of Eq. 77 is one of the N factors of the denominator of Eq. 75). This situation is remedied by adding π to the trig function arguments so that $F(z)$ in Eq. 77 has a recognizable time domain counterpart. For example, Eq. 77 becomes:

$$F(z) = \frac{-z \sin [b + (\pi/T)]T}{z^2 - 2 \cos [b + (\pi/T)]T z + 1} \Rightarrow [f(t)]^T = \left[-\sin \left(b + \frac{\pi}{T} \right) t \right]^T \quad (78)$$

Consider the denominator of Eq. 75 for the special case of $N = 2$:

$$z^4 - 2 \cos bT z^2 + 1 \equiv \left[z^2 - 2 \left(\cos \frac{bT}{2} \right) z + 1 \right] \left[z^2 + 2 \left(\cos \frac{bT}{2} \right) z + 1 \right] \quad (79)$$

The sign of the coefficient of z in the last factor on the right-hand side of Eq. 79 can be changed by adding π to the argument $bT/2$:

$$z^4 - 2 \cos bT z^2 + 1 \equiv \left[z^2 - 2 \left(\cos \frac{bT}{2} \right) z + 1 \right] \left[z^2 - 2 \left\{ \cos \left[\left(b + \frac{2\pi}{T} \right) \frac{T}{2} \right] \right\} z + 1 \right] \quad (80)$$

Thus, for $N = 2$, the partial fraction expansion contains terms which correspond to sampled sine and cosine functions not only at the input frequency, b , but also at the first alias, $b + (2\pi/T)$, of the input frequency.

The general result is obtained by induction by repeating the exercise for $N = N_1$ and for $N = N_1 + 1$ (Ref. 1).

$$z^{2N} - 2 \cos bT z^N + 1 = \prod_{n=0}^{N-1} \left(z^2 - 2z \cos \left[\left(b + \frac{2\pi n}{T} \right) \frac{T}{N} \right] + 1 \right) \quad (81)$$

$$= \prod_{n=0}^{N-1} \left[\left(z - \cos \left[\left(b + \frac{2\pi n}{T} \right) \frac{T}{N} \right] \right)^2 + \left(\sin \left[\left(b + \frac{2\pi n}{T} \right) \frac{T}{N} \right] \right)^2 \right] \quad (82)$$

Thus, the sampled sine wave, $[\sin bt]^T$, can be described alternatively in terms of a sum of sinusoidal components at frequency b rad/sec and its first $N - 1$ aliases sampled with period T/N .

D. OPEN-LOOP FREQUENCY RESPONSE — CONTINUOUS OUTPUT SAMPLED

Consider the system of Fig. 15 where $G(s)$ represents an arbitrary transfer function and M represents an arbitrary data hold. Suppose R is a unit amplitude sine wave and the output is sampled with period T/N . Using multi-rate sampling results from Section II,

$$\begin{aligned} c^{T/N} &= |GMR|^T \big|_{T/N} = (GM)^{T/N} R^T \\ &= (GM)^{T/N} \frac{z^N \sin bT}{z^{2N} - 2(\cos bT)z^N + 1}, \quad z = e^{sT/N} \end{aligned} \quad (83)$$

Expand the right-hand side of Eq. 83 in partial fractions:

$$C^{T/N} = \sum_{n=0}^{N-1} \frac{A_n z \sin \omega_n(T/N) + B_n z [z - \cos \omega_n(T/N)]}{z^2 - 2z \cos \omega_n(T/N) + 1} + [\text{Terms due to modes of } (GM)^{T/N}] \quad (84)$$

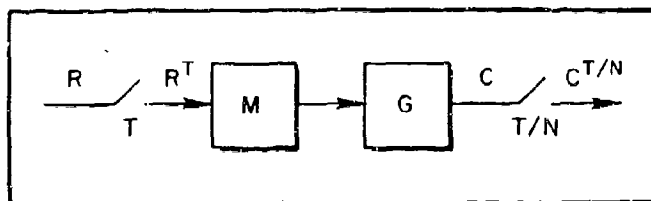


Figure 15. Open-Loop System

Assume that responses in the modes of $(GM)^{T/N}$ approach zero as $t \rightarrow \infty$, i.e., that all modes are stable. This restriction simplifies the notation in the derivation (the development that follows is valid whether the modes of $(GM)^{T/N}$ are stable or unstable). In Eq. 84,

$$\omega_n = b + \frac{2\pi n}{T}, \quad n = 0, 1, 2, \dots, N-1$$

For the present, assume $b \leq 2\pi/T$. The steady-state waveform, at the sampling instants, can be written as:

$$[C(t)]^{T/N} = \left[\sum_{n=0}^{N-1} (A_n \sin \omega_n t + B_n \cos \omega_n t) \right]^{T/N} \quad (85)$$

To solve for A_n and B_n , multiply each side of Eq. 84 by

$$[z^2 - 2z \cos \omega_k(T/N) + 1], \quad 0 \leq k \leq (N-1)$$

and evaluate for $z = e^{j\omega_k(T/N)}$. The only non-zero term on the right-hand side of the result occurs for $n = k$.

$$\begin{aligned}
 & (GM)^{T/N} \frac{z^N \sin bt}{z^N - (2 \cos bT) z^{N-1} + 1} \Big|_{z = 1/\omega_k(T/N)} [z^2 - 2 \cos \omega_k(T/N) z + 1] \\
 & = \sum_{n=0}^{N-1} \frac{[A_n z \sin \omega_n(T/N) + B_n z [z - \cos \omega_n(T/N)]]}{z^2 - 2 \cos \omega_n(T/N) z + 1} \Big|_{z = 1/\omega_k(T/N)} [z^2 - 2z \cos \omega_k(T/N) + 1]
 \end{aligned}
 \tag{86}$$

For any $n \neq k$, the right-hand side of Eq. 86 is identically zero since

$$z^2 - 2[\cos \omega_k(T/N)]z + 1 = [z - \cos \omega_k(T/N)]^2 + (\sin \omega_k(T/N))^2
 \tag{87}$$

vanishes when

$$z = 1/\omega_k(T/N) = \cos \omega_k(T/N) + j \sin \omega_k(T/N)
 \tag{88}$$

Evaluation of Eq. 86, subject to the constraint of Eq. 88, is a tedious chore (Ref. 1). However, the result is relatively simple:

$$A_n + jB_n = \frac{1}{N} (GM)^{T/N} \Big|_{z = 1/\omega_n(T/N)}, \quad z = e^{sT/N}
 \tag{89}$$

Notice in particular the definition of z used in the evaluation.

To summarize, when the system is forced by $\sin bt$, the steady-state output waveform, sampled with period T/N , is given by Eq. 85. The coefficients A_n and B_n in Eq. 85 are computed using Eq. 89.

For example, let

$$M = \frac{1 - e^{-sT}}{s}, \quad G(s) = \frac{a}{s + a}
 \tag{90}$$

so that

$$\frac{1}{N} \langle \text{GM} \rangle T/N = \frac{1 - e^{-aT/N}}{N(z - e^{-aT/N})} \frac{(1 - z^{-N})}{(1 - z^{-1})} \quad (91)$$

It is instructive to plot the amplitude ratio of the frequency response for Eq. 91 with N as a parameter. For the sake of clarity, the plot is versus ω rather than $\log \omega$.

Refer to Fig. 16. Notice that over the range of frequency for the plot, $0 \leq \omega \leq 8\pi/T$, the $N = 1$ case amplitude ratio folds about the frequencies π/T , $3\pi/T$, ..., $7\pi/T$; the $N = 2$ case folds about frequencies $2\pi/T$, $4\pi/T$, $6\pi/T$; and the $N = 4$ case folds about $\omega = 4\pi/T$. However, it can also be observed that the various amplitude ratio plots are periodic with frequency. For $N = 1$ this period is $2\pi/T$; for $N = 2$, $4\pi/T$ and for $N = 4$, $8\pi/T$. Each period contains precisely the number of frequency points (at the input or its positive alias frequencies) required to match the continuous steady-state time response at the sampling instants

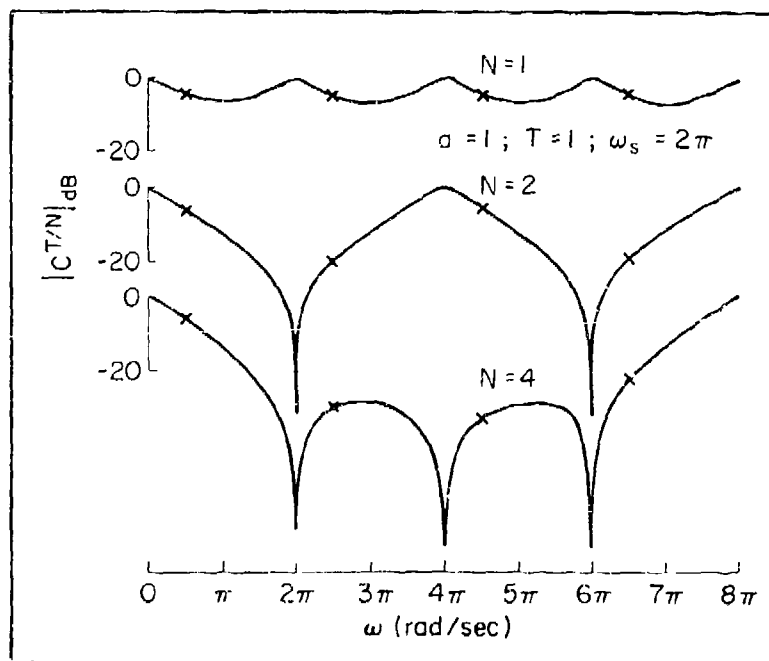


Figure 16. Magnitude Plot for $N = 1, 2, 4$

and at $N - 1$ equally spaced inter-sample points. Consequently, it is the sampling frequency interval rather than the folding frequency interval that is fundamental to generalizing the concept of frequency response.

Consider the use of Fig. 16. Imagine that a unit amplitude sine wave with a frequency $\pi/2$ is input. In the $N = 1$ case, our interest is matching the continuous steady-state time response only at the sampling instants with a single sine wave. The magnitude and phase angle (not shown in Fig. 16) can be read from this plot at $\omega = \pi/2$ (or $\pi/2 + 2\pi/T$, $\pi/2 + 4\pi/T$, $\pi/2 + 6\pi/T$, ...; any of these points gives the correct value). Clearly, if the objective is to match at the sampling instants with a single sinusoid, the frequency could be b plus any $2\pi/T$ multiple. One cannot tell the difference once the waveform is sampled. In fact, the "sub" aliases at $b - (2\pi/T)$, $b - 4\pi/T$ will also work. These "sub" aliases are the difference terms which are prominent in modulation theory.

The $N = 1$ plot in Fig. 16 corresponds to the "sampled spectrum" frequency response of sampled data control theory. Consider the $N = 2$ case wherein the objective is to match one inter-sample point as well as the sample points. Let the input frequency be $\pi/2$ and note that the points at $\omega = \pi/2$, $\pi/2 + 2\pi/T$ give the magnitude (and phase) for the sine waves at those frequencies, as would the points $\pi/2 + 4\pi/T$, $\pi/2 + 6\pi/T$. Suppose next that the input frequency is $b = \pi/2 + 2\pi/T$. Clearly, the second required component could be read from the "first alias" at $b + 2\pi/T$ or the first sub-alias at $b - 2\pi/T$ (or, for that matter, at a host of other frequencies).

In the $N = 4$ case, four sine waves are required to fit three inter-sample points as well as the sample points. If the input frequency were $b = \pi/2 + 6\pi/T$, and if the plot of Fig. 16 with its limited range of 8π were the only one available, clearly it would be to our advantage to use the "difference" frequency points at $\omega = b - 2\pi/T$, $b - 4\pi/T$, and $b - 6\pi/T$ to establish the magnitude and relative phase of the other three sine waves.

Consider now the generalization of these observations. Notice that the N sine wave components required to match the continuous steady-state time response at the sampling instants and at $N - 1$ equally spaced inter-sample points need not have frequencies from within one period of the amplitude ratio plot. However, the frequencies used must each be an alias separated by $(2\pi/T)Nk$ (where k is an arbitrary integer for each frequency) from the N alias-related frequencies falling in any one period of the frequency response. This is evident in the example for $N = 2$. If the input frequency is $\pi/2$, one would ordinarily choose sine wave components with frequencies $\pi/2$ and $[\pi/2 + (2\pi/T)]$ to represent the continuous steady-state response at the sampling instants and one inter-sample point. Alternative choices of frequencies are $\pi/2$ and $[\pi/2 + (6\pi/T)]$, and so on. Choices of $\pi/2$ and $[\pi/2 + (4\pi/T)]$ or $[\pi/2 + (2\pi/T)]$ and $[\pi/2 + (6\pi/T)]$ are not alternatives because these frequency choices do not satisfy the separation criterion stated above.

This brief discussion associates aliases and sub-aliases with the sum and difference frequencies of modulation theory. It is not the case, however, that sum and difference components are necessarily both present simultaneously in the output. It is shown above that only N components are needed.

The case where N is extremely large is also of interest. Let $N \rightarrow \infty$ after evaluating Eq. 91 at $z = 1 - \omega_n(T/N)$:

$$\begin{aligned} & \frac{1 - e^{-aT/N}}{N(z - e^{-aT/N})} \frac{1 - z^{-N}}{1 - z^{-1}} \bigg|_{z=1-\omega_n(T/N)} \\ &= \frac{(1 - e^{-aT/N})(1 - 1 - \omega_n T)}{N[1 - \omega_n(T/N) - e^{-aT/N}][1 - 1 - \omega_n(T/N)]} \bigg|_{\substack{\text{lim} \\ N \rightarrow \infty}} \quad (92) \end{aligned}$$

An indeterminate form is obtained. Therefore, use L'Hôpital's rule twice [substitute $1/\omega_n(T/N) = \cos \omega_n(T/N) + j \sin \omega_n(T/N)$, etc.] and obtain (see Appendix I of Ref. 1):

$$\begin{aligned} \frac{1}{N} \left. \frac{1 - e^{-sT}}{s(s+1)} \right|_{z=1/\omega_n(T/N)} \lim_{N \rightarrow \infty} \\ = \frac{1 - e^{-j\omega_n T}}{j\omega_n T} \frac{1}{1 + j\omega_n} = \frac{1 - e^{-sT}}{sT} \frac{1}{s+1} \bigg|_{s=j\omega_n} \end{aligned} \quad (93)$$

where $z \triangleq e^{sT/N}$. That is, as $N \rightarrow \infty$, simply divide GM by T and evaluate the coefficients at $s = j\omega_n$. This is representative of the general result of the next subsection.

E. OPEN-LOOP FREQUENCY RESPONSE: CONTINUOUS OUTPUT

In the previous subsection it was shown that

$$A_n + jB_n = \frac{1}{N} (GM)^{T/N} \bigg|_{z=1/\omega_n(T/N)}, \quad z \triangleq e^{sT/N} \quad (94)$$

To deduce the behavior for infinite N, rewrite Eq. 94 as

$$\frac{1}{T} \left\{ \frac{T}{N} (GM)^{T/N} \right\} = \frac{1}{T} \left\{ \frac{T}{N} \left[\frac{1}{T/N} \sum_{k=-\infty}^{\infty} (GM) \left(s + j \frac{2\pi k N}{T} \right) \right] \right\} \quad (95)$$

The T/N's cancel, and as N gets very large only the $k = 0$ term contributes since all "aliased" components of the spectrum have moved to infinite frequency. Therefore,

$$\lim_{N \rightarrow \infty} \frac{1}{N} (GM)^{T/N} \Big|_{z=1} \omega_n(T/N) = \frac{GM}{T} \Big|_{s=j\omega_n}, \quad z = e^{sT/N} \quad (96)$$

$$\omega_n = b + \frac{2\pi n}{T}, \quad n = n_0, n_0 + 1, \dots, N - n_0 - 1$$

where

$$n_0 = - \left(\frac{b}{\omega_s / \text{INT}} \right), \quad \omega_s = \frac{2\pi}{T}$$

The example of the previous section with N finite can now be studied for N infinite. This result gives the frequency response for the continuous output.

$$A_n + jB_n = \frac{1 - e^{-sT}}{sT} \frac{1}{s + 1} \Big|_{s=j\omega_n} \quad (97)$$

A Bode plot for this result is shown in Fig. 17. Components for the input frequency $b = 1.0$ rad/sec and its aliases have been indicated with the square symbols.

Interpretation of Fig. 17 is as follows. Suppose a unit sine wave at 1 rad/sec is input to the sampler. Then, if the amplitude ratios and phase angles for sine waves with frequencies 1, $(1 + 2\pi/T)$, $(1 + 4\pi/T)$, ..., are read from Fig. 17, and these components are added together, the resultant waveform will be an exact match of the actual steady-state output waveform in Fig. 18. One might expect this waveform to be very nearly sinusoidal, since the first alias is attenuated on the order of 30 dB, relative to the input component. However, the steady-state time response does not bear this out, as can be seen in Fig. 18. The reason is that the summation of alias terms is significant despite their small individual size.

Again, in connection with Figs. 17 and 13, consider a $(1 + 4\pi/T)$ rad/sec unit sine wave input to the sampler. The steady-state output will contain sub-aliases at 1 rad/sec and $(1 + 2\pi/T)$ rad/sec; a component at the input frequency, $(1 + 4\pi/T)$ rad/sec; and other aliases at $(1 + 6\pi/T)$, $(1 + 8\pi/T)$, ..., rad/sec. The amplitude ratio and phase angle for each component is again read from Fig. 17 (at points indicated

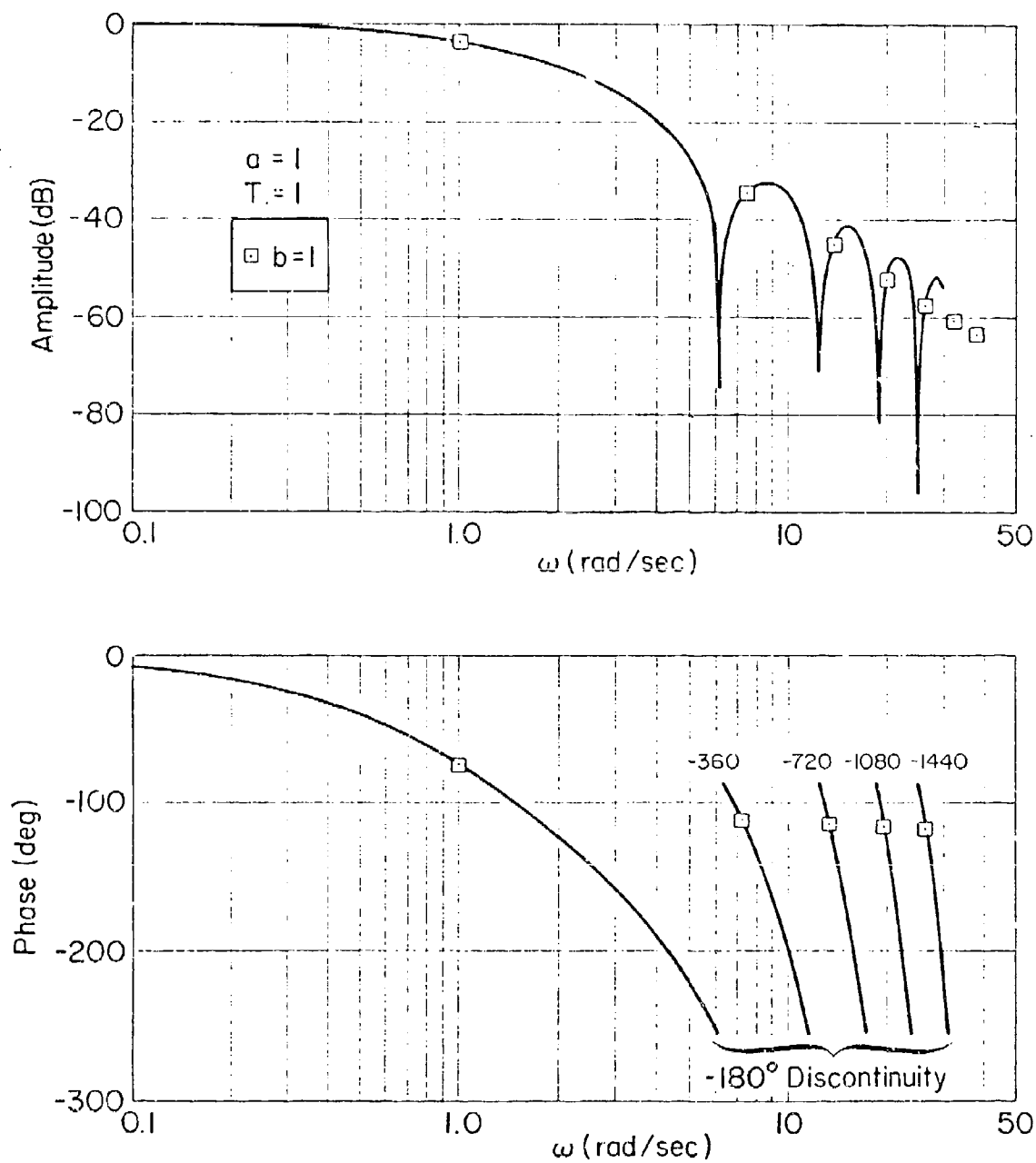


Figure 17. Frequency Response and Spectral Components of Output

by the square symbols). When these components are added the steady-state time response is again that in Fig. 18. Thus, the continuous response spectrum and steady-state time response are the same for a sine wave input of given frequency as for a sine wave input having a positive frequency which is an alias of the given frequency.

Another observation is that the aliases do not represent "harmonic" components but rather represent modulation components which must add together properly in order to match conditions at the sampling instants for the basic period, T . It can be seen in Fig. 18 that the "steady state" does not necessarily imply "periodic." Periodic waveforms occur only when the input frequency and the sampling frequency have an integer relationship with respect to one another.

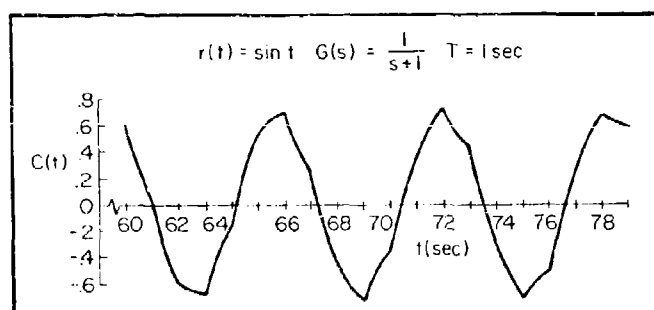


Figure 18. "Steady-State" Time Response

F. SINGLE-RATE CLOSED-LOOP FREQUENCY RESPONSE

Closed-loop results are dependent upon the configuration of the digital loops. However, the basic analysis procedure is independent of configuration. It is important to understand this procedure, and in particular the simplifications that occur in analysis of closed-loop systems.

Consider the (vector) system shown in Fig. 19. The objective is to find the coefficients that characterize the spectral components of the continuous response, C , i.e., the frequency response. The procedure for this example is typical. First, solve for the vector component at the input of the data holds.

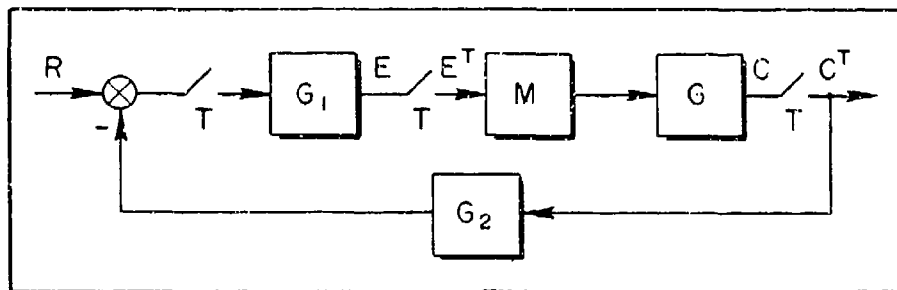


Figure 19. Illustrative Vector Closed-Loop Configuration

$$E^T = G_1^T R^T - G_1^T G_2^T (GM)^T E^T \quad (98)$$

Therefore,

$$E^T = [I + G_1^T G_2^T (GM)^T]^{-1} G_1^T R^T \quad (99)$$

Solve for $C(s)$:

$$C = (GM)[I + G_1^T G_2^T (GM)^T]^{-1} G_1^T R^T \quad (100)$$

The spectrum of $C(s)$ is of interest. It is determined by first finding the spectrum of $C^{T/N}$ and taking the limiting case as $N \rightarrow \infty$.

Let the input be a unit sine wave at frequency b rad/sec and let

$$z = e^{sT/N} \quad (101)$$

so that

$$R^T = \frac{z^N \sin bT}{z^{2N} - 2z^N (\cos bT) + 1} \quad (102)$$

Using Eq. 102 and the results of Section II,

$$C^{T/N} = (GM)^{T/N} [I + G_1^T G_2^T (GM)^T]^{-1} G_1^T R^T \quad (103)$$

For the sake of brevity write Eq. 103 as

$$C^{T/N} = G_A^{T/N} G_B^{T/N} \quad (104)$$

Expand the right-hand side of Eq. 104 in partial fractions:

$$\begin{aligned} C^{T/N} &= G_A^{T/N} G_B^{T/N} \frac{z^N \sin bT}{z^{2N} - 2z^N \cos bT + 1} \\ &= \sum_{n=0}^{N-1} \frac{A_n z \sin \omega_n(T/N) + B_n z [z - \cos \omega_n(T/N)]}{z^2 - 2z \cos \omega_n(T/N) + 1} \\ &\quad + [\text{Terms due to modes of } G_A^{T/N} G_B^{T/N}] \end{aligned} \quad (105)$$

Assume that responses in the modes of $G_A^{T/N} G_B^{T/N}$ approach zero as $t \rightarrow \infty$, i.e., that all closed-loop system modes are stable. In Eq. 105,

$$\omega_n = b + \frac{2\pi n}{T}, \quad n = 0, 1, 2, \dots, N-1 \quad (106)$$

Notice that Eq. 105 is exactly the same as Eq. 83, except $(GM)^{T/N}$ has been replaced by $G_A^{T/N} G_B^{T/N}$. Hence a crucial result is obtained using Eq. 89:

$$A_n + jB_n = \frac{1}{N} G_A^{T/N} G_B^{T/N} \Big|_{z=e^{j\omega_n T}} \quad (107)$$

But,

$$G_B^T(\bar{z}) \triangleq G_B^T(z^N), \quad \bar{z} = e^{sT} \quad (108)$$

because of the local definition of z as $e^{sT/N}$. Therefore, using

$$\begin{aligned}
[14\omega_n(T/N)]^N &= 14\omega_n T \\
&= \cos \omega_n T + j \sin \omega_n T \\
&= \cos [b + (2\pi n/T)]T \\
&\quad + j \sin [b + (2\pi n/T)]T \\
&= \cos bT + j \sin bT
\end{aligned}$$

we obtain

$$G_B^T(z^N) \Big|_{14\omega_n(T/N)} \equiv G_B^T(\bar{z}) \Big|_{\bar{z}=14bT} \quad (109)$$

Thus, z^N in G_B^T can be replaced with \bar{z} provided it is evaluated for $\bar{z} = 14bT$ instead of for $z = 14\omega_n(T/N)$. This amounts to a simple (and very convenient) change of variable. At this point the result is:

$$A_n + jB_n = \frac{1}{N} G_A^{T/N}(z) \Big|_{z=14\omega_n(T/N)} G_B^T(\bar{z}) \Big|_{\bar{z}=14bT}, \quad z = e^{sT/N} \quad (110)$$

Equation 110 is the basic result for the finite N case. To reiterate, to find the coefficients of the N sine waves matching the T/N sampled output, C , compute the usual pulsed transfer functions for

$$G_B^T(\bar{z}) = [I + G_1^T G_2^T (GM)^T]^{-1} G_1^T, \quad \bar{z} = e^{sT} \quad (111)$$

and evaluate it for

$$\bar{z} = 14bT \quad (112)$$

Next, compute the usual T/N pulsed transfer function for G_A as a function of z and evaluate it for $z = 14\omega_n(T/N)$ where $\omega_n = b + (2\pi n/T)$.

Thus, it is superfluous to consider G_B^T as a function of z^N ; it suffices to consider it as a function of z . Moreover, only $G_A^{T/N}$ is a function of N ; this simplifies obtaining the limiting case tremendously. For the case of $N \rightarrow \infty$, the continuous case, we obtain

$$A_n + jB_n = \left(\left[\frac{M(s)G_A(s)}{T} \right]_{s=j\omega_n} \right) \left(\left[G_B^T(z) \right]_{z=14bT} \right), \quad z \triangleq e^{sT} \quad (113)$$

Equation 113 is the desired result for the given closed-loop configuration.* However, it is the procedure which is key. One can follow the details through for other configurations quite easily.

An illustrative closed-loop frequency response example is shown in Fig. 20.

G. SECTION SUMMARY

The "sampled spectrum" frequency concept of sampled data control theory is concerned with determining the single sinusoid that fits the output of a single-rate system at the sampling instants. In this report the frequency response concept has been extended to encompass the continuous spectrum for the continuous variables of a discretely controlled system. Moreover, the theory is sufficiently comprehensive to cover cases wherein a group of N sinusoids is used to match the continuous variables not only at the sample points but at $N - 1$ equally spaced inter-sample points as well. N may be finite or infinite. Infinite N corresponds to the true continuous spectrum. The practical value of knowing the true continuous spectrum for continuous physical variables

*Accurate numerical determination of $G_B^T(z)|_{z=14bT}$ may prove difficult at high sampling rates. This is the result of small differences between large numbers which occur in the computations as poles and zeros approach the unit circle. In this event, one is well advised to carry out equivalent computations in a domain where numerical conditioning is much improved (e.g., in terms of w' or w).

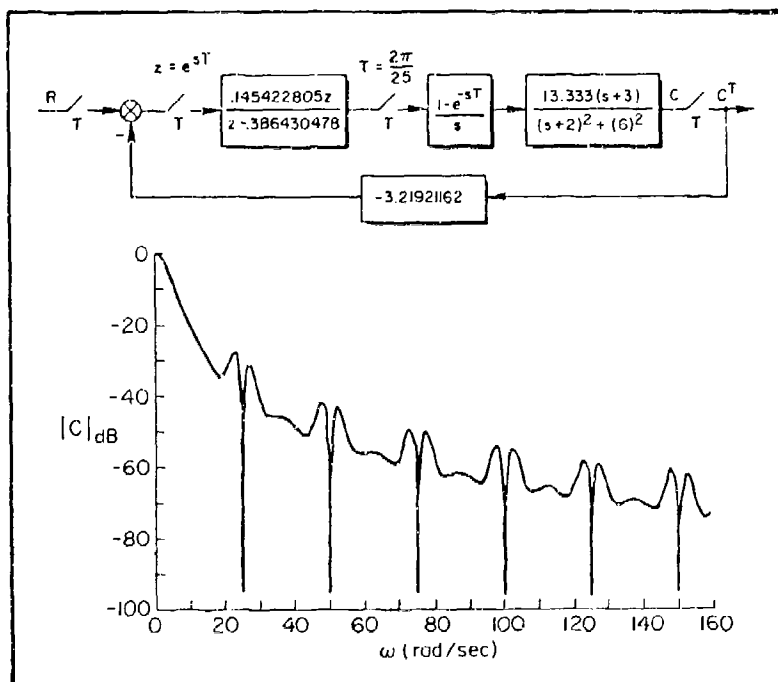


Figure 20. Magnitude Plot for Closed-loop System

is self-evident. For example, this information can be used for evaluating inter-sample ripple and for guiding continuous filter selection. Cases wherein N is finite also have important practical application as, for example, in the bench validation of the digital controller hardware/software combination. Digital controller characteristics are often specified in terms of end-to-end "frequency response." On the bench, if continuous outputs (say from data holds) are sampled at a finite rate (N is finite), the difference between the measured frequency response and the true continuous frequency response ($N \rightarrow \infty$) may be significant. The results of this report can be used to predict, minimize, or correct for the difference between measured and true frequency responses.

Results for closed-loop cases depend upon the specific configuration of the digital loops. However, the basic analysis procedure is independent of the loop configuration. The procedure is to obtain the pulsed transfer function matrix relating the outputs to the data holds and the

inputs through which the (sampled) sine wave inputs enter. The continuous system (including data holds) is placed in cascade with the output of the pulsed system. Frequency response is then evaluated in exactly the same manner as for any discretely excited open-loop continuous system.

Corresponding results for two rate sampled closed-loop systems are contained in Ref. 1. Extensions for true multi-rate sampled closed-loop systems will be developed in Section IV. In addition, the theory, in Section IV, is extended to provide a tool for quantifying fidelity of digital simulations of continuous systems.

SECTION IV

FREQUENCY RESPONSE OF MULTI-RATE SYSTEMS

A. INTRODUCTION

The frequency response of digitally controlled single-rate systems was discussed in the previous section. The manner in which one treats two-rate systems is given in Ref. 1. We will omit a review of the two-rate case and move directly to a discussion of multi-rate/multiple-order configurations. It will be shown that the basic tools developed in this section are ideally suited to a variety of situations such as defining a Bode plot for digitally controlled closed-loop systems, a Bode plot for the simulation of a closed-loop system, and the Bode plot associated with a simulation wherein more than one independent processor (e.g., multiple computers or microprocessors) is used to implement the computer code.

B. A BASIC RESULT

Let the general multi-rate/multiple-order open-loop system of Fig. 21 have a sine wave input.

In Fig. 21,

$$C_1^\beta = (G_1 R^\alpha)^\beta \quad (114)$$

$$C^{T/N} = [G(G_1 R^\alpha)^\beta]^{T/N} \quad (115)$$

where α , β represent sampling schemes with a basic period of T seconds. For example, α might represent a multiple-order sampling format; β might represent a multi-rate and/or pseudo measurement format (Section II).

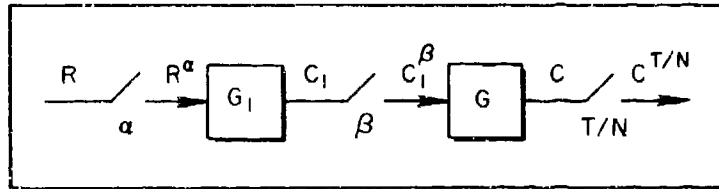


Figure 21. Multi-Rate/Multiple-Order Open-Loop System

Using switch decomposition, Fig. 21 takes on the representation of Fig. 22. Clearly,

$$C_1^\beta = W_2(W_{2*}G_1W_1)^T(W_{1*}R)^T \quad (116)$$

and

$$C^{T/N} = (CW_2)^{T/N} (W_{2*}G_1W_1)^T (W_{1*}R)^T \quad (117)$$

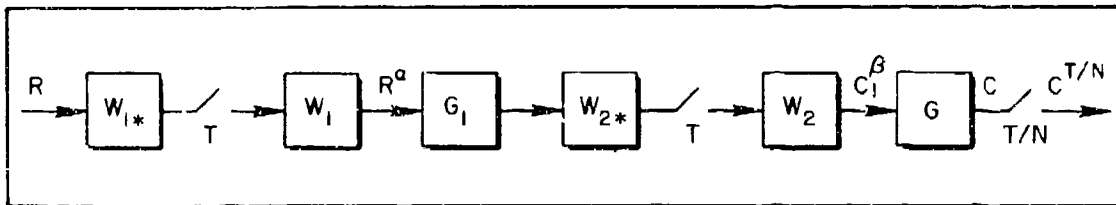


Figure 22. Open-Loop System with Switch Decomposition

If α represents multiple-order sampling and β a pseudo measurement format using multi-rate sampling, the switch decomposition modeling components might appear as:

$$W_1 = [1, e^{-T_0s}, e^{-T_1s}, e^{-T_2s}] \quad (118)$$

$$W_{1*} = \begin{bmatrix} 1 \\ e^{T_0s} \\ e^{T_1s} \\ e^{T_2s} \end{bmatrix} \quad (119)$$

and

$$W_2 \Rightarrow \hat{W}_2 = \begin{bmatrix} 1 & 0 & 0 \\ 0 & e^{-sT/3} & 0 \\ 0 & 0 & e^{-2sT/3} \end{bmatrix} \quad (120)$$

$$W_{2*} = \begin{bmatrix} 1 \\ e^{sT/3} \\ e^{2sT/3} \end{bmatrix} \quad (121)$$

Comparing Eq. 117 with Eqs. 83 (or Eq. 104), we see that only one new facet has entered the problem, namely $(W_{1*}R)^T$ replaces R^T . Consider, therefore, a generic component of $(W_{1*}R)^T$ — for instance the scalar $(e^{\Delta Ts}R)^T$, where $0 \leq \Delta \leq 1.0$.

For $R = \sin bt$ and Δ zero ($e^{\Delta Ts} - 1$), the output equation (Eq. 117) becomes

$$C^{T/N} = (GW_2)^{T/N} (W_{2*}G_1W_1)^T \frac{z^N \sin bT}{z^{2N} - (2 \cos bT)z^N + 1}, \quad z = e^{sT/N} \quad (122)$$

where R^T is described in terms of a N/T samples per second model. For the sake of brevity write Eq. 122 as

$$C^{T/N} = G_A^{T/N} G_B^T \frac{z^N \sin bT}{z^{2N} - (2 \cos bT)z^N + 1} \quad (123)$$

Expand the right-hand side of Eq. 123 in partial fractions:

$$\begin{aligned}
 C^{T/N} &= G_A^{T/N} G_B^T \frac{z^N \sin bT}{z^{2N} - (2 \cos bT)z^N + 1} \\
 &= \sum_{n=0}^{N-1} \frac{A_n z \sin \omega_n(T/N) + B_n z [z - \cos \omega_n(T/N)]}{z^2 - [2 \cos \omega_n(T/N)]z + 1} \\
 &\quad + [\text{Terms due to modes of } G_A^{T/N} G_B^T] \quad (124)
 \end{aligned}$$

For non-zero Δ , we use the advanced z-transform on $(e^{\Delta T s_R})^T$ and Eq. 124 becomes

$$\begin{aligned}
 C^{T/N} &= G_A^{T/N} G_B^T \frac{z^N [(\sin b\Delta T)z^N + \sin [b(1 - \Delta)T]]}{z^{2N} - (2 \cos bT)z^N + 1} \\
 &= \sum_{n=0}^{N-1} \frac{A_n z \sin \omega_n(T/N) + B_n z [z - \cos \omega_n(T/N)]}{z^2 - [2 \cos \omega_n(T/N)]z + 1} \\
 &\quad + [\text{Terms due to modes of } G_A^{T/N} G_B^T] \quad (125)
 \end{aligned}$$

Assume that responses in the modes of $G_A^{T/N} G_B^T$ approach zero as $t \rightarrow \infty$, i.e., that all modes are stable. In Eqs. 124 and 125

$$\omega_n = b + \frac{2\pi n}{T}, \quad n = 0, 1, 2, \dots, N-1 \quad (126)$$

[More generally, $n = n_0, n_0+1, \dots, N-n_0-1$, where $n_0 = -(b/\omega_s)_{INT}$]. The steady-state waveform, at the sampling instants, can be written as

$$\left[C(t) \right]^{T/N} = \left[\sum_{n=0}^{N-1} (A_n \sin \omega_n t + B_n \cos \omega_n t) \right]^{T/N} \quad (127)$$

To solve for A_n and B_n , multiply each side of Eqs. 124 and 125 by

$$\{z^2 - [2 \cos \omega_k(T/N)]z + 1\}, \quad 0 \leq k \leq (N-1) \quad (128)$$

and evaluate for $z = e^{j\omega_k(T/N)}$. Since the only terms which can survive on the right-hand side occur when $n = k$, the Σ will, of course, disappear. Then, if we so choose, the k notation can be changed back to n . To illustrate,

$$\begin{aligned} & G_A^{T/N} G_B^T \frac{z^N \sin bT}{z^{2N} - (2 \cos bT)z^N + 1} \left\{ z^2 - [2 \cos \omega_k(T/N)]z + 1 \right\} \Big|_{z=e^{j\omega_k(T/N)}} \\ &= \sum_{n=0}^{N-1} \frac{A_n z \sin \omega_n(T/N) + B_n z [z - \cos \omega_n(T/N)]}{z^2 - [2 \cos \omega_n(T/N)]z + 1} \left\{ z^2 - [2 \cos \omega_k(T/N)]z + 1 \right\} \Big|_{z=e^{j\omega_k(T/N)}} \quad (129) \end{aligned}$$

$$\begin{aligned} & G_A^{T/N} G_B^T \frac{z^N \{ (\sin b\Delta T)z^N + \sin b(1-\Delta)T \}}{z^{2N} - (2 \cos bT)z^N + 1} \left\{ z^2 - [2 \cos \omega_k(T/N)]z + 1 \right\} \Big|_{z=e^{j\omega_k(T/N)}} \\ &= \sum_{n=0}^{N-1} \frac{A_n z \sin \omega_n(T/N) + B_n z [z - \cos \omega_n(T/N)]}{z^2 - [2 \cos \omega_n(T/N)]z + 1} \left\{ z^2 - [2 \cos \omega_k(T/N)]z + 1 \right\} \Big|_{z=e^{j\omega_k(T/N)}} \quad (130) \end{aligned}$$

For any $n \neq k$, the right-hand side of Eqs. 129 and 130 are identically zero since

$$z^2 - [2 \cos \omega_k(T/N)]z + 1 = [z - \cos \omega_k(T/N)]^2 + [\sin \omega_k(T/N)]^2 \quad (131)$$

vanishes when

$$z = e^{j\omega_k(T/N)} = \cos \omega_k(T/N) + j \sin \omega_k(T/N) \quad (132)$$

Specifically, we obtain

$$[\cos \omega_k(T/N) + j \sin \omega_k(T/N) - \cos \omega_k(T/N)]^2 + [\sin \omega_k(T/N)]^2 \equiv 0 \quad (133)$$

For $n = k$, the cancellation of the common factor guarantees the survival of an $n = k$ term. Factoring out a common z gives

$$\begin{aligned} z \{ A_k \sin \omega_k(T/N) + B_k [\cos \omega_k(T/N) - \cos \omega_k(T/N) + j \sin \omega_k(T/N)] \} \\ = (A_k + j B_k) z \sin \omega_k(T/N) \Big|_{z=1 \pm j \omega_k(T/N)} \end{aligned} \quad (134)$$

Therefore, Eqs. 129 and 130 become

$$z \sin \omega_k(T/N) (A_k + j B_k) = \frac{G_A^{T/N} G_B^T (z^N \sin bT) \{ z^2 - [2 \cos \omega_k(T/N)] z + 1 \}}{z^{2N} - (2 \cos bT) z^N + 1} \Big|_{z=1 \pm j \omega_k(T/N)} \quad (135)$$

$$z \sin \omega_k(T/N) (A_k + j B_k) = \frac{G_A^{T/N} G_B^T z^N [\sin b\Delta T] z^N + \sin b(1-\Delta)T \{ z^2 - [2 \cos \omega_k(T/N)] z + 1 \}}{z^{2N} - (2 \cos bT) z^N + 1} \Big|_{z=1 \pm j \omega_k(T/N)} \quad (136)$$

At this point, divide through by $z \sin \omega_k(T/N)$ and replace k with n :

$$A_n + j B_n = G_A^{T/N} G_B^T \Big|_{z=1 \pm j \omega_n(T/N)} \cdot \frac{z^{N-1} \sin bT}{\sin \omega_n(T/N)} \frac{z^2 - [2 \cos \omega_n(T/N)] z + 1}{z^{2N} - (2 \cos bT) z^N + 1} \Big|_{z=1 \pm j \omega_n(T/N)} \quad (137)$$

$$A_n + j B_n = G_A^{T/N} G_B^T \Big|_{z=1 \pm j \omega_n(T/N)} \frac{z^{N-1} [\sin b\Delta T] z^N + \sin b(1-\Delta)T}{\sin \omega_n(T/N)} \frac{z^2 - [2 \cos \omega_n(T/N)] z + 1}{z^{2N} - (2 \cos bT) z^N + 1} \Big|_{z=1 \pm j \omega_n(T/N)} \quad (138)$$

The last term on the right-hand side of Eqs. 137 and 138 is indeterminate (0/0) when $z = 1 \angle \omega_n(T/N)$. Therefore, applying L'Hôpital's rule first to Eq. 137 ($\Delta = 0$ case),

$$A_n + jB_n = G_A^{T/N} G_B^T \frac{z^{N-1} \sin bT}{\sin \omega_n(T/N)} \frac{2z - 2 \cos \omega_n(T/N)}{2N[z^{2N-1} - (\cos bT)z^{N-1}]} \Big|_{z=1 \angle \omega_n(T/N)} \quad (139)$$

$$= G_A^{T/N} G_B^T \frac{z^{N-1} \sin bT}{\sin \omega_n(T/N)} \frac{2[z - \cos \omega_n(T/N)]}{2Nz^{N-1}(z^N - \cos bT)} \Big|_{z=1 \angle \omega_n(T/N)} \quad (140)$$

$$A_n + jB_n = G_A^{T/N} G_B^T \Big|_{z=1 \angle \omega_n(T/N)} \times \frac{\sin bT [\cos \omega_n(T/N) + j \sin \omega_n(T/N) - \cos \omega_n(T/N)]}{[\sin \omega_n(T/N)]^N \{ [1 \angle \omega_n(T/N)]^N - \cos bT \}} \quad (141)$$

$$A_n + jB_n = G_A^{T/N} G_B^T \Big|_{z=1 \angle \omega_n(T/N)} \times \frac{(\sin bT)[j \sin \omega_n(T/N)]}{[\sin \omega_n(T/N)]^N \{ [1 \angle \omega_n(T/N)]^N - \cos bT \}} \quad (142)$$

but,

$$\begin{aligned} [1 \angle \omega_n(T/N)]^N - \cos bT &= 1 \angle \omega_n T - \cos bT \\ &= \cos \omega_n T + j \sin \omega_n T - \cos bT \\ &= \cos [b + (2\pi n/T)]T + j \sin [b + (2\pi n/T)]T - \cos bT \\ &= \cos bT + j \sin bT - \cos bT \\ &= j \sin bT \end{aligned}$$

Therefore,

$$A_n + jB_n = \frac{1}{N} G_A^{T/N} G_B^T \Big|_{z=14\omega_n(T/N)} \quad (143)$$

Next,

$$G_B^T(\bar{z}) = G_B^T(z^N), \quad \bar{z} = e^{sT} \quad (144)$$

because of the local definition $z = e^{sT/N}$. Therefore,

$$\begin{aligned} G_B^T(z^N) \Big|_{z=14\omega_n(T/N)} &= G_B^T[14\omega_n(T/N)]^N \\ &= G_B^T(14\omega_n T) = G_B^T(14bT) \end{aligned} \quad (145)$$

That is, take the "T" z-transform of G_B^T , and evaluate at $z = 14bT$.

The finite N result for Eq. 137 ($\Delta = 0$) is then

$$A_n + jB_n = \frac{G_A^{T/N}}{N} \Big|_{z=14\omega_n(T/N)} \hat{z} e^{sT/N} G_B^T \Big|_{z=14bT} \hat{z} e^{sT} \quad (146)$$

As $N \rightarrow \infty$, the coefficients of the continuous spectrum are given by

$$A_n + jB_n = \frac{1}{T} G_A \Big|_{s=j\omega_n} G_B^T \Big|_{z=14bT} \hat{z} e^{sT} \quad (147)$$

The superscript notation in Eqs. 146 and 147 is for the purpose of calling out the definition of z being used in the evaluation.

We next treat the indeterminate part of Eq. 138 (the $\Delta \neq 0$ case). Applying L'Hôpital's rule to the last term on the right-hand side of Eq. 138 results in

$$A_n + jB_n = \frac{(GW_2)^{T/N}}{N} \left| \begin{matrix} z^{\hat{a}} e^{sT/N} \\ z = 1 \angle \omega_n (T/N) \end{matrix} \right| (W_{2*} G_1 W_1)^T \left| \begin{matrix} z^{\hat{a}} e^{sT} \\ z = 1 \angle \omega_n T \\ z = 1 \angle bT \end{matrix} \right| W_{1*} \Big|_{s=jb} \quad (151)$$

$$\omega_n = b + \frac{2\pi n}{T}, \quad n = 0, 1, \dots, N-1 \quad (152)$$

As in Eq. 146, letting $N \rightarrow \infty$ gives the "continuous" result

$$A_n + jB_n = \frac{GW_2}{T} \Big|_{s=j\omega_n} (W_{2*} G_1 W_1)^T \left| \begin{matrix} z^{\hat{a}} e^{sT} \\ z = 1 \angle bt \\ \text{or } z = 1 \angle \omega_n T \end{matrix} \right| W_{1*} \Big|_{s=jb} \quad (153)$$

In Eqs. 151 and 153 it is important to observe that an option exists with regard to $(W_{2*} G_1 W_1)^T$; it may be evaluated at either $1 \angle bT$ or $1 \angle \omega_n T$. However, there is no option with regard to W_{1*} since it must be evaluated at $s = jb$. Clearly, the most efficient procedure is to evaluate $(W_{2*} G_1 W_1)^T$ at $z = 1 \angle bT$ and W_{1*} at $s = jb$, save the result in a polar format, and then evaluate $(GW_2/N)^{T/N}$ (or GW_2/T) over the appropriate range of n .

It can be appreciated that the results of Section III are contained in Eqs. 151 and 153, since Section III considers only the special case of $W_{1*} = 1.0$ (a scalar). Also, note that W_1 and W_2 are symbolic representations that can represent either multi-rate or multiple-order sampling formats (e.g., it is permissible for $W_2 = \hat{W}$, etc.). However, in arriving at the spectrum of the continuous variable, uniformly spaced time samples, in a T/N time frame, were used.

C. A CLOSED-LOOP APPLICATION

The ability to cast any multi-rate or multiple-order sampling sequence into a switch decomposition format makes the analysis of closed-loop systems a straightforward task. Consider the system of Fig. 23. Proceed as in the single-rate case. Since $C = G_1 W_1 E^T$, one must first solve for E^T :

$$E^T = (W_{1*} R)^T - (W_{1*} G_2 W_2)^T (W_{2*} G_1 W_1)^T E^T \quad (154)$$

or

$$E^T = [I + (W_{1*} G_2 W_2)^T (W_{2*} G_1 W_1)^T]^{-1} (W_{1*} R)^T \quad (155)$$

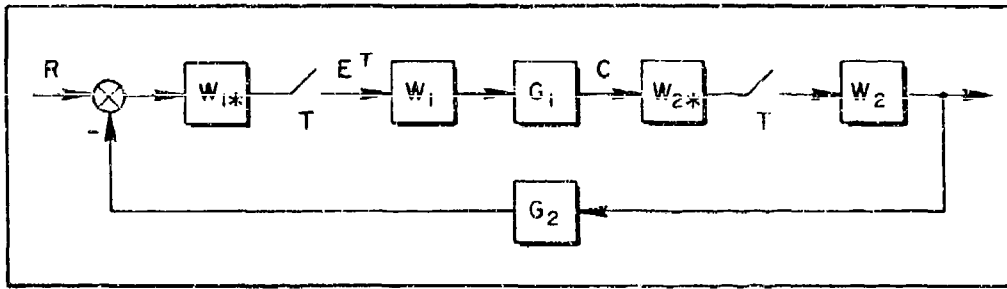


Figure 23. Closed-Loop System with Switch Decomposition

Therefore

$$C^{T/N} = (G_1 W_1)^{T/N} [I + (W_{1*} G_2 W_2)^T (W_{2*} G_1 W_1)^T]^{-1} (W_{1*} R)^T \quad (156)$$

The coefficients for the steady-state waveform are then

$$A_n + jB_n = \left. \frac{G_1 W_1}{T} \right|_{s=j\omega_n} \left[I + (W_{1*} G_2 W_2)^T (W_{2*} G_1 W_1)^T \right]^{-1} \left. \frac{z \hat{e}^{sT}}{z-1} \right|_{z=1 \pm jbT} W_{1*} \Big|_{s=jb} \quad \text{or } z=1 \pm j\omega_n T \quad (157)$$

The following numerical example will help clarify the specific details of Eq. 157. (An alternate solution based on the "two-rate" theory of Ref. 1 is contained in Appendix A.) Consider the system of Fig. 24.

With reference to Eq. 157, $W_1 = W = [1, e^{-sT/2}]$ and $W_2 = 1.0$. The T/N output equation for Fig. 24 is

$$C^{T/N} = (G_1 M_2 W)^{T/N} E^T \quad (158)$$

where

$$E^T = [I + (W_* G_2 M)^T (G_1 M_2 W)^T]^{-1} (W_* R)^T \quad (159)$$

Then

$$C^{T/N} = (G_1 M_2 W)^{T/N} [I + (W_* G_2 M)^T (G_1 M_2 W)^T]^{-1} (W_* R)^T \quad (160)$$

The steady-state coefficients for Eq. 160 are given by

$$A_n + jk_n = \left. \frac{G_1 M_2 W}{T} \right|_{s=j\omega_n} [I + (W_* G_2 M)^T (G_1 M_2 W)^T]^{-1} \left. \frac{z^{\Delta} e^{sT}}{z-1} \right|_{z=1} \left. W_* \right|_{s=j\omega_n} \quad (161)$$

or $z = 1 + j\omega_n T$

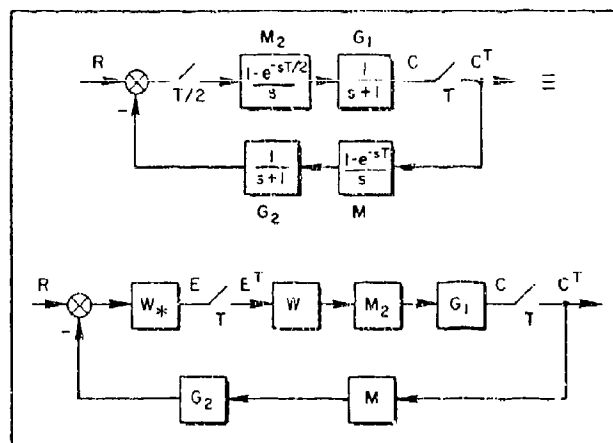


Figure 24. Closed-Loop Numerical Example

where

$$\omega_n = b + \frac{2\pi n}{T}, \quad n = 0, 1, 2, \dots, N-1 \quad (162)$$

The inverse expression in Eq. 161 is formed using the following steps ($z = e^{sT}$):

$$(W_* G_2 M)^T = \left\{ \left[\frac{1}{e^{sT/2}} \right] \frac{1 - e^{-sT}}{s(s+1)} \right\}^T = \frac{\left[\frac{1 - e^{-T}}{(1 - e^{-T/2})z + (e^{-T/2} - e^{-T})} \right]}{z - e^{-T}} \quad (163)$$

where

$$\left[\frac{1 - e^{-sT}}{s(s+1)} \right]^T = \frac{z-1}{z} \left[\frac{1}{s} - \frac{1}{s+1} \right]^T \quad (164)$$

and

$$\left[\frac{e^{sT/2}(1 - e^{-sT})}{s(s+1)} \right]^T = \frac{z-1}{z} \left[\frac{e^{sT/2}}{s} - \frac{e^{sT/2}}{s+1} \right]^T \quad (165)$$

with

$$\left[\frac{e^{\Delta Ts}}{s} \right]^T = \frac{z}{z-1}, \quad \left[\frac{e^{\Delta Ts}}{s+a} \right]^T = \frac{ze^{-\Delta T}}{z - e^{-aT}} \quad (166)$$

Applying the advanced z-transform relationships in Eq. 166 to Eqs. 164 and 165 gives Eq. 163. Next,

$$(G_1 M_2 W)^T = \left\{ \frac{1 - e^{-sT/2}}{s(s+1)} [1 \quad e^{-sT/2}] \right\}^T = \left[\frac{e^{-T/2} - e^{-T}}{z - e^{-T}} \quad \frac{1 - e^{-T/2}}{z - e^{-T}} \right] \quad (167)$$

where

$$\left[\frac{1 - e^{-sT/2}}{s(s+1)} \right]^T = \left[\frac{(1 - e^{-sT/2})}{s} + \frac{(-1 + e^{-sT/2})}{s+1} \right]^T \quad (168)$$

and

$$\left[\frac{e^{-sT/2}(1 - e^{-sT/2})}{s(s+1)} \right]^T = \left[\frac{e^{-sT/2}(1 - e^{-sT/2})}{s} + \frac{e^{-sT/2}(-1 + e^{-sT/2})}{s+1} \right]^T \quad (169)$$

Placing Eqs. 168 and 169 in an advanced z-transform format produces

$$\left[\frac{(1 - e^{-sT/2})}{s} + \frac{(-1 + e^{-sT/2})}{s+1} \right]^T = z^{-1} \left[\frac{-e^{sT/2}}{s} + \frac{e^{sT/2}}{s+1} \right]^T + \left[\frac{1}{s} - \frac{1}{s+1} \right]^T \quad (170)$$

$$\left[\frac{e^{-sT/2}(1 - e^{-sT/2})}{s} + \frac{e^{-sT/2}(-1 + e^{-sT/2})}{s+1} \right]^T = z^{-1} \left[\frac{e^{sT/2}}{s} - \frac{1}{s} - \frac{e^{sT/2}}{s+1} + \frac{1}{s+1} \right]^T \quad (171)$$

Equation 166 can now be applied directly to Eqs. 170 and 171, resulting in Eq. 167. Now, assume $T = -\ln(.81)$, which gives a set of convenient numbers when Eqs. 163 and 167 are evaluated. The result is

$$\begin{aligned}
(W_* G_2 M)^T (G_1 M_2 W)^T &= \frac{\begin{bmatrix} .019 \\ \hline .1z + .09 \\ z - .81 \end{bmatrix}}{\frac{z - .81}{z - .81}} \begin{bmatrix} .09 & .1 \end{bmatrix} \\
&= \frac{\begin{bmatrix} .0171 & .019 \\ \hline .009z + .0081 & .01z + .009 \end{bmatrix}}{(z - .81)^2} \quad (172)
\end{aligned}$$

and

$$I + (W_* G_2 M)^T (G_1 M_2 W)^T = \frac{\begin{bmatrix} z^2 - 1.62z + .6732 & .019 \\ \hline .009z + .0081 & z^2 - 1.61z + .6651 \end{bmatrix}}{z^2 - 1.62z + .6561} \quad (173)$$

where

$$I(z - .81)^2 = \begin{bmatrix} (z - .81)^2 & 0 \\ \hline 0 & (z - .81)^2 \end{bmatrix} \quad (174)$$

Taking the inverse of Eq. 173 produces

$$[I + (W_* G_2 M)^T (G_1 M_2 W)^T]^{-1} = \frac{\begin{bmatrix} z^2 - 1.61z + .6651 & -.019 \\ \hline -(.009z + .0081) & z^2 - 1.62z + .6732 \end{bmatrix}}{z^2 - 1.61z + .6822}$$

$$= \frac{\begin{bmatrix} N_1(z) & N_2(z) \\ \hline N_3(z) & N_4(z) \end{bmatrix}}{D(z)} \quad (175)$$

Substituting Eq. 175 into Eq. 161 gives

$$A_n + jB_n = \frac{1 - e^{-sT/2}}{Ts(s+1)} \left[1 \mid e^{-sT/2} \right] \bigg|_{s=j\omega_n} \frac{\begin{bmatrix} N_1(z) & N_2(z) \\ N_3(z) & N_4(z) \end{bmatrix}}{D(z)} \bigg|_{z=e^{j\omega_n T}} \begin{bmatrix} 1 \\ e^{jbT/2} \end{bmatrix} \quad (176)$$

Performing the matrix operations reduces Eq. 176 to Eq. 177.

$$A_n + jB_n = \frac{1 - e^{-sT/2}}{Ts(s+1)} \frac{N_1(z) + N_2(z)e^{jbT/2} + N_3(z)e^{-sT/2} + N_4(z)e^{-sT/2}e^{jbT/2}}{D(z)} \bigg|_{\substack{s=j\omega_n \\ \text{and } z=e^{j\omega_n T}}} \quad (177)$$

where

$$\omega_n = b + \frac{2\pi n}{T} \quad n = 0, 1, 2, \dots, N-1 \quad (178)$$

In Eq. 177, $N_1(z)$, $N_2(z)$, $N_3(z)$, $N_4(z)$, $N_5(z)$, and $D(z)$ are evaluated at $e^{j\omega_n T} = e^{jbT}$ and the remaining terms at $s = j\omega_n$.

In this two-rate, closed-loop example where the input sampling interval is one-half ($T/2$) the output sampling interval (T), two separate sets of Bode plots are required to present the magnitude factor and phase shift information for the entire frequency spectrum. That is, the fundamental and alias components are still directly read from individual magnitude and phase plots, but now two separate magnitude plots and two separate phase plots exist. One set of Bode plots (i.e., magnitude plot and its accompanying phase plot) is valid for a specific range of input excitation frequencies ($r = 1 \sin bt$) and the second set for an alternate range. In this example, these two frequency ranges are given by

$$K\omega_s \leq b \leq (K+1)\omega_s \quad (179)$$

where $\omega_s = 2\pi/T$ and one set of Bode plots is applicable for even K's (0, 2, 4, 6, etc.) and the other for odd K's (1, 3, 5, 7, etc.). Therefore, the first set of Bode plots is valid for

$$\begin{aligned} 0 &< b < \omega_s \\ 2\omega_s &< b < 3\omega_s \\ 4\omega_s &< b < 5\omega_s \\ &\cdot \\ &\cdot \\ &\cdot \end{aligned} \quad (180)$$

and the second set is used for input excitation frequencies which fall in the following ranges

$$\begin{aligned} \omega_s &< b < 2\omega_s \\ 3\omega_s &< b < 4\omega_s \\ 5\omega_s &< b < 6\omega_s \\ &\cdot \\ &\cdot \\ &\cdot \end{aligned} \quad (181)$$

It is seen that the ranges covered by the two sets of Bode plots alternate along the frequency axis.

A composite magnitude plot for Eq. 177 is shown in Fig. 25. The solid curve represents one magnitude plot and the dotted curve the second. As pointed out, these curves are valid for the input excitation frequencies defined by Eqs. 180 and 181. Sample printouts are shown in Table 4 for Eq. 177 evaluated at $b = 1, 40, \text{ and } 80 \text{ rad/sec}$. The format of the printout is magnitude (dB), phase angle (deg), $\omega_n = b + 2\pi/T$ (rad), and an index number to indicate the aliased component. Figure 25 was generated by evaluating Eq. 177 for a large number of input frequencies, leading to the appearance of a multi-valued Bode plot. However, a careful check of the spectral components listed in Table 4 will show

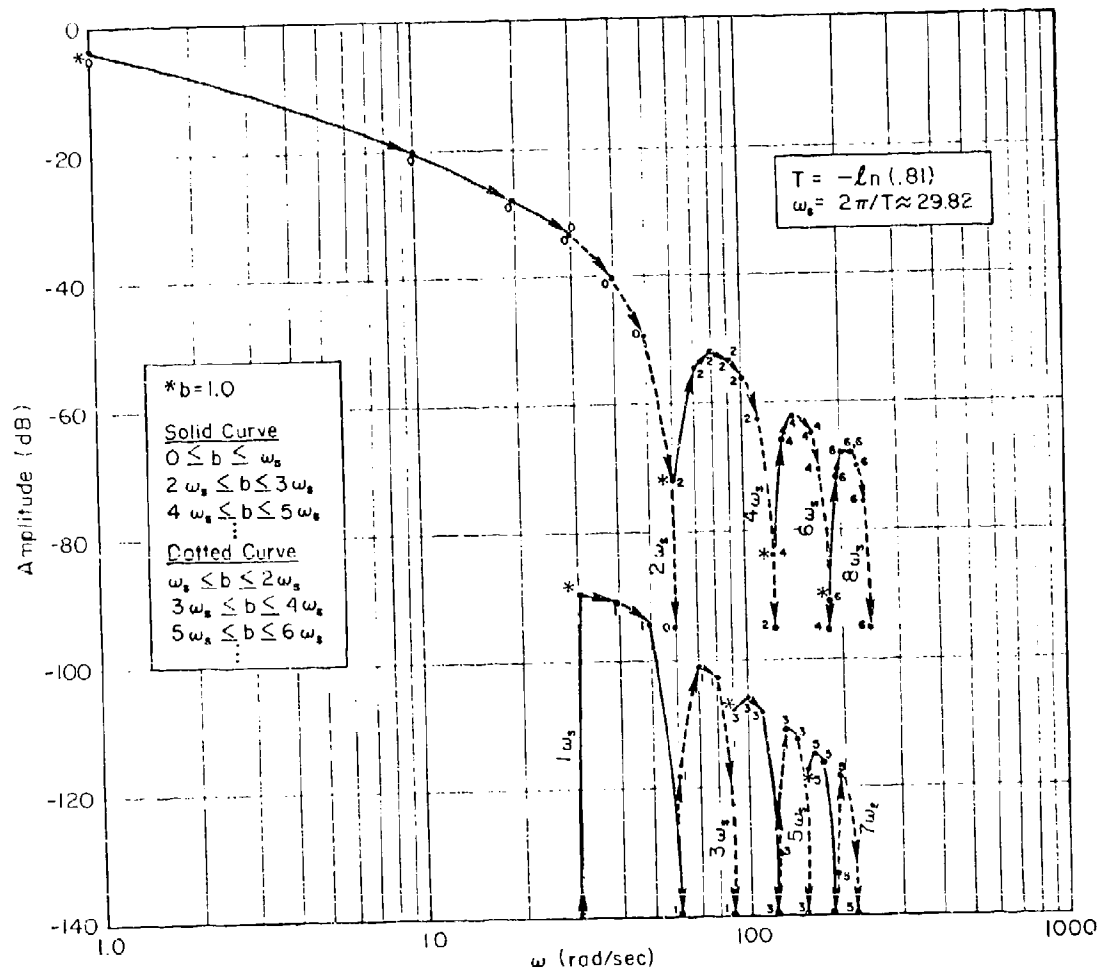


Figure 25. Composite Magnitude Plot

TABLE 4. DATA FOR COMPOSITE MAGNITUDE PLOT (FIGURE 25)

	<u>b = 1</u>	<u>b = 40</u>	<u>b = 80</u>
Magnitude (dB)	-3.300	-39.849	-51.897
Phase (deg)	-19.924	-209.290	-150.751
Frequency (rad/sec)	1.000	40.000	30.000
Spectral Component Index	0.000	0.000	0.000
	-88.518	-99.387	-107.245
	-117.241	60.648	-428.657
	30.818	69.818	109.818
	1.000	1.000	1.000
	-71.690	-55.701	-61.372
	-63.879	-210.147	-151.057
	-60.635	99.635	139.635
	2.000	2.000	2.000
	-107.219	-116.112	-114.780
	-118.466	60.270	-428.840
	90.453	129.453	169.453
	3.000	3.000	3.000
	-83.587	63.850	-67.550
	-64.348	-210.362	-151.180
	120.270	159.270	199.270
	4.000	4.000	4.000
	-116.016	-116.694	-120.018
	-119.718	60.130	-428.928
	150.088	189.088	229.088
	5.000	5.000	5.000
	-90.582	-69.374	-72.098
	-64.506	-210.460	-151.246
	179.905	218.905	258.905
	6.000	6.000	6.000

that the various aliased components will alternate between the top and bottom curves, or they will remain totally on the solid curve or totally on the dotted curve. To illustrate this, the fundamental and aliased components are highlighted with a star symbol in Fig. 25 for an input frequency of $b = 1.0$. The two magnitude plots in Fig. 25 are shown separately in Figs. 26 and 27 to further emphasize that two completely independent magnitude plots exist, each valid for different ranges of input frequencies.

This multiplicity in Bode plots is directly associated with the $(WR)^T$ term in Eq. 160 and exists for any general closed-loop system

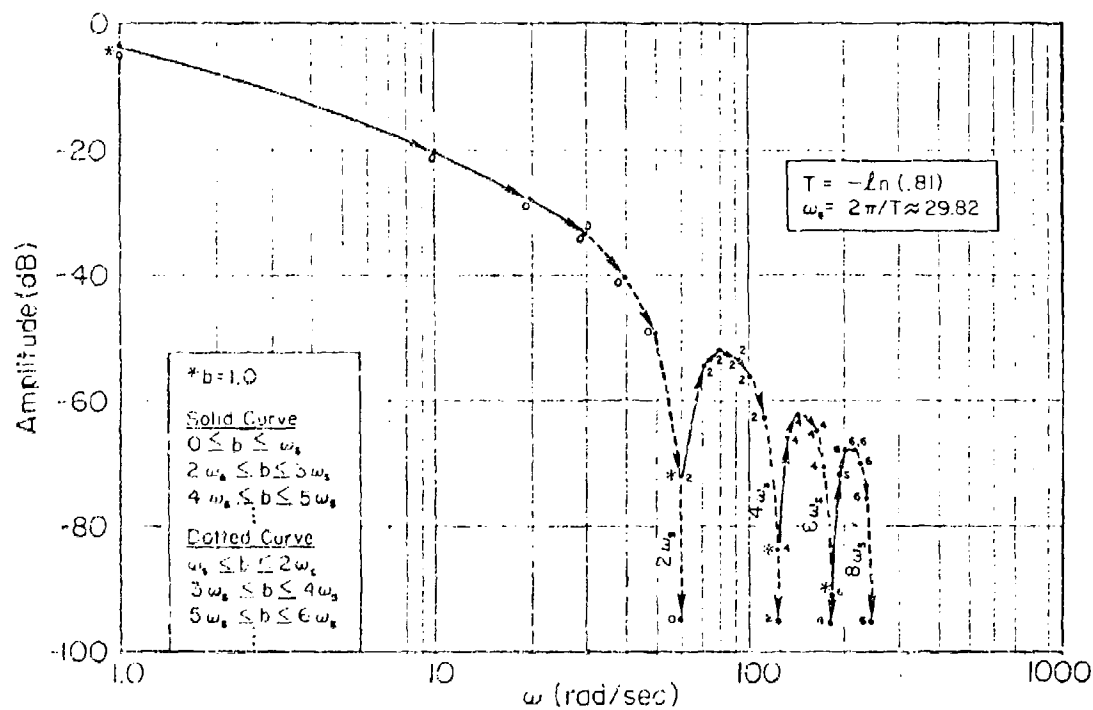


Figure 26. Magnitude Plot No. 1

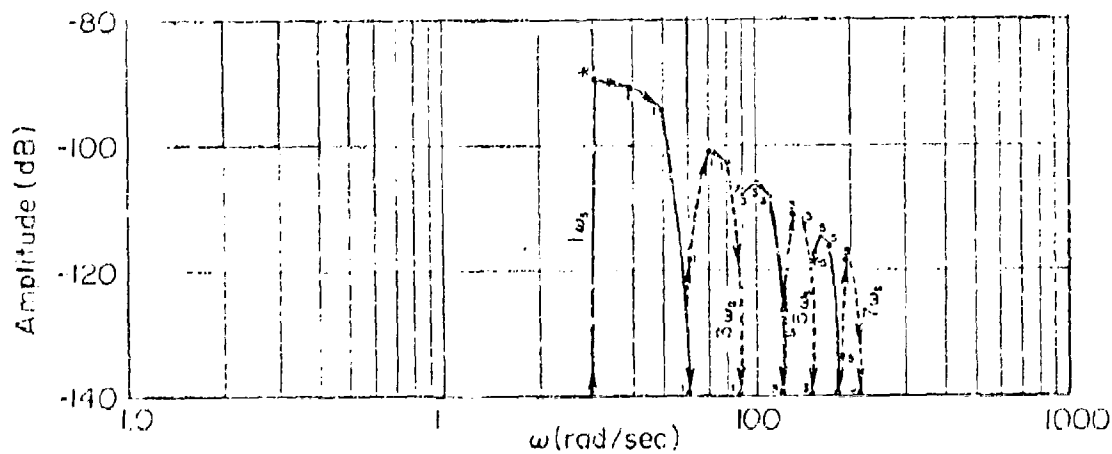


Figure 27. Magnitude Plot No. 2

with high-input/slow-output sampling. For other general multi-rate/multiple order systems, a single magnitude and phase plot covers the entire frequency spectrum. It should be emphasized that the $(W_R)^T$ term alone does not guarantee multiple Bode plots. In many open-loop and closed-loop systems the $(W_R)^T$ term appears and only a single set of Bode plots is required (e.g., Case IV example in Subsection D). Thus, the multiplicity in Bode plots is directly tied to closed-loop systems with high-input/slow-output sampling. For these systems, the properties of the multiple Bode plots are then determined by the $(W_R)^T$ term.

In Eq. 161 (or Eq. 177), those terms that are evaluated at $z = 14\omega_n T$ and $s = j\omega_n$ are inherently generic with respect to the input frequency. For example, given a sampling frequency of $\omega_s = 2\pi/T = 10.0$ rad/sec and an input frequency of $b = 1.0$ rad/sec, these terms contribute to the following fundamental and aliased components:

Fundamental:	1.0 rad/sec
1st Alias:	11.0 rad/sec
2nd Alias:	21.0 rad/sec
3rd Alias:	31.0 rad/sec
	.
	.
	.
nth Alias:	$b + 2\pi n/T$ rad/sec

Now, for $b = 11.0$ rad/sec, contributions to the following frequency components are obtained:

Fundamental:	11.0 rad/sec
1st Alias:	21.0 rad/sec
2nd Alias:	31.0 rad/sec
3rd Alias:	41.0 rad/sec
	.
	.
	.
nth Alias:	$b + 2\pi n/T$ rad/sec

It is seen that the contributions to the 1st, 2nd, 3rd, etc., aliased component for $b = 1.0$ rad/sec identically match the contributions to the fundamental and 1st, 2nd, 3rd, etc., aliased component for $b = 11.0$. We could then replace $\omega_n = b + 2\pi n/T$ with simply $\omega_n = b$ to obtain the fundamental and aliased components for the Bode plot if it were not for the $(W_R)_*^T$ term in Eq. 160. Indeed, a single set of generic Bode plots can be constructed for any general multi-rate/multiple-order closed-loop system except those employing fast-input/slow-output sampling.

The $(W_R)_*^T$ term, unlike the remaining terms in Eq. 160, must be evaluated at $s = jb$ (and not $s = j\omega_n$). Therefore, this frequency response term is solely a function of the input frequency b and not a function of the input plus aliased component. The multiple Bode plots are a consequence of this singular dependence on the input frequency b and the resulting cyclic or periodic nature of the $e^{jbT/2}$ element in

$$W_* \Big|_{s=jb} = \begin{bmatrix} 1 \\ e^{sT/2} \end{bmatrix}_{s=jb} \quad (182)$$

For this example, this periodicity is at the input sampling frequency $[2\pi/(T/2) = 2\omega_s]$ since

$$e^{jbT/2} \Big|_{b=2\pi/(T/2)} = \cos 2\pi + j \sin 2\pi \quad (183)$$

and the contribution from the $(W_R)_*^T$ term then repeats itself for input frequencies equal to

$$b = 2\pi n/(T/2) \quad n = 1, 2, 3, \dots \quad (184)$$

This cyclic behavior shows up directly in the composite magnitude plot in Fig. 25 where the fundamental frequency range covered by the combination of both Bode plots equals the input sampling frequency, $2\omega_s = 59.6351$ rad/sec. However, each Bode plot contains aliased components

which are a function of the output and not the input sampling frequency (i.e., $b + 2\pi/T$, $b + 4\pi/T$, $b + 6\pi/T$, etc.).

D. GENERAL RESULTS

Some general conclusions can be formed by extending the two-rate vector switch decomposition example from the previous subsection. The final expression (Eq. 161) for the spectral coefficients is repeated below for easy reference.

$$A_n + jB_n = \frac{G_1 M_2 W}{T} \bigg|_{s=j\omega_n} \left[I + (W_* G_2 M)^T (G_1 M_2 W)^T \right]^{-1} \bigg|_{\substack{z=e^{sT} \\ z=1 \pm j\omega_n T \\ \text{or } z=1 \pm j b T}} W_* \bigg|_{s=jb} \quad (185)$$

Vector switch decomposition modeling for a different input sampling interval only requires alterations to the W and W_* vectors. This change does not disturb those terms evaluated at $s = j\omega_n$ and $z = 1 \pm j\omega_n T$. It is known that the W_* term evaluated at $s = jb$ dictates the structure of the frequency response spectrum and the Bode diagrams. As was shown, for an input sampling frequency that is twice the output sampling frequency, two separate sets of Bode plots are required as a result of the $e^{jbT/2}$ element in the $W_*|_{s=jb}$ term. If this is extended to an input sampling interval of $T/3$, the W_* vector will contain the following elements:

$$W_* = \begin{bmatrix} 1 \\ e^{sT/3} \\ e^{sT2/3} \end{bmatrix} \quad (186)$$

Both $e^{jbT/3}$ and $e^{jbT2/3}$ elements now appear in the spectral coefficient expression. The $e^{jbT/3}$ factor is periodic in $b = 2\pi n/(T/3)$ and $e^{jbT2/3}$ in $b = 2\pi n/(2T/3)$. This periodicity results in not two but three separate sets of Bode plots to cover the entire frequency response spectrum. Again, as in the $T/2$ case, all alias components will be directly related to multiples of the output sampling frequency, $\omega_s = 2\pi/T$ (i.e.,

$b + 2\pi/T$, $b + 4\pi/T$, $b + 6\pi/T$, etc.). The individual range of input frequencies that are applicable to these three sets of Bode plots is given by:

$$(k)\omega_s \leq b \leq (k+1)\omega_s$$

$$(k+1)\omega_s \leq b \leq (k+3/2)\omega_s \quad (187)$$

$$(k+3/2)\omega_s \leq b \leq (k+3)\omega_s$$

$$\omega_s = 2\pi/T, \quad k = 0, 2, 4, 6, 8, \text{etc.}$$

The fundamental frequency range covered by all three Bode plots again occurs at the input sampling frequency, ω_s .

Further extensions of this example provide the following general conclusions for fast-input/slow-output sampled closed-loop systems:

- The number of separate sets of Bode plots required to display the entire frequency spectrum is equal to the number of elements in the $W|_{s=j\omega}$ switch decomposition modeling vector.
- The frequency range that is applicable to each Bode plot is determined by the periodicity of the $W|_{s=j\omega}$ elements.
- The alias components in all Bode plots are a direct function of the output sampling frequency, $\omega_s = 2\pi/T$ (i.e., $b + \omega_s$, $b + 2\omega_s$, $b + 3\omega_s$, etc.).
- The fundamental frequency range covered by the combination of Bode plots is equal to the input sampling frequency.

In addition to these general conclusions, the fast-input/slow-output sampling scheme gives rise to new frequency response identities. These new identities, along with those presented in Ref. 1, allow the frequency response expression $(A_n + jB_n)$ to be written directly from inspection of each term in the C^T/N output equation. Any general multi-rate/multiple-order sampling architecture can be handled with this complete set of identities. This includes vector switch decomposition modeling

of multi-rate/multiple-order systems, computational delays, and nonsynchronous sampling.

For the two-rate example in the previous subsection (Fig. 24), the $C^{T/N}$ output equation using multi-rate theory (Eq. A-6), and the $C^{T/N}$ equation using vector switch decomposition modeling (Eq. 160) follows:

$$C^{T/N} = (G_1 M_2)^{T/N} R^{T/2} - (G_1 M_2)^{T/N} (G_2 M)^{T/2} \times \left\{ 1 + [(G_1 M_2)(G_2 M)^{T/2}]^T \right\}^{-1} (G_1 M_2 R^{T/2})^T \quad (188)$$

$$C^{T/N} = (G_1 M_2 W)^{T/N} [I + (W_* G_2 M)^T (G_1 M_2 W)^T]^{-1} (W_* R)^T \quad (189)$$

In the $C^{T/N}$ equation arrived at using multi-rate theory (Eq. 188), the first term on the right-hand side introduces spectral components at $\omega_n = b + 2\pi n/(T/2)$, $n = 1, 2, \dots$, and the second term introduces spectral components at $\omega_k = b + 2\pi k/T$, $k = 0, 1, 2, \dots$. The unique factor in this expression is $(G_1 M_2 R^{T/2})^T$ which corresponds to the $(W_* R)^T$ factor in the $C^{T/N}$ equation based on vector switch decomposition modeling (Eq. 189). These two factors directly determine the multiple Bode plot structure. The new frequency response identities for these two factors are

$$(G_1 M_2 R^{T/2})^T \rightarrow (G' R^{T/M})^T \rightarrow G'(z) \Big|_{z=e^{j\omega} s T/M} \quad (190)$$

$$(W_* R)^T \rightarrow W_* \Big|_{s=j\omega} \quad (191)$$

All the remaining terms and factors in the $C^{T/N}$ equation can be handled by the following identities from Ref. 1.

Finite N

$$(GM)^{T/N} \rightarrow \frac{1}{N} (GM)^{T/N}(z) \left| \begin{matrix} z \hat{=} e^{sT/N} \\ z = 14\omega_n(T/N) \end{matrix} \right. \quad (192)$$

$$G_A^T \rightarrow G_A^T(z) \left| \begin{matrix} z \hat{=} e^{sT} \\ z = 14bT \end{matrix} \right. \quad (193)$$

$$G_K^{T/M_k} \rightarrow G_K^{T/M_k}(z) \left| \begin{matrix} z \hat{=} e^{sT/M_k} \\ z = 14\omega_n(T/M_k) \end{matrix} \right. \quad (194)$$

$$\begin{aligned} A_n + jB_n = & \left[\frac{1}{N} (GM)^{T/N}(z) \left| \begin{matrix} z \hat{=} e^{sT/N} \\ z = 14\omega_n(T/N) \end{matrix} \right. \right] \left[G_A^T(z) \left| \begin{matrix} z \hat{=} e^{sT} \\ z = 14bT \end{matrix} \right. \right] \\ & \times \left[\prod_k^k G_K^{T/M_k}(z) \left| \begin{matrix} z \hat{=} e^{sT/M_k} \\ z = 14\omega_n(T/M_k) \end{matrix} \right. \right] \end{aligned} \quad (195)$$

N → ∞

$$(GM)^{T/N} \rightarrow \frac{1}{T} (GM)(s) \Big|_{s=j\omega_n} \quad (196)$$

$$G_A^T \rightarrow G_A^T(z) \left| \begin{matrix} z \hat{=} e^{sT} \\ z = 14bT \end{matrix} \right. \quad (197)$$

$$G_K^{T/M_k} \rightarrow G_K^{T/M_k}(z) \left| \begin{matrix} z \hat{=} e^{sT/M_k} \\ z = 14\omega_n(T/M_k) \end{matrix} \right. \quad (198)$$

$$\begin{aligned} A_n + jB_n = & \left[\frac{1}{T} (GM)(s) \Big|_{s=j\omega_n} \right] \left[G_A^T(z) \left| \begin{matrix} z \hat{=} e^{sT} \\ z = 14bT \end{matrix} \right. \right] \\ & \times \left[\prod_k^k G_K^{T/M_k}(z) \left| \begin{matrix} z \hat{=} e^{sT/M_k} \\ z = 14\omega_n(T/M_k) \end{matrix} \right. \right] \end{aligned} \quad (199)$$

$$\omega_n = b + \frac{2\pi n}{T}$$

$$n = n_0, n_0 + 1, \dots, 0, 1, 2, \dots, N - n_0 - 1$$

$$n_0 = -(b/\omega_s)_{\text{INT}}$$

The notation used in these identities indicates the definition of "T" to be used in calculating each z-transform expression and the subsequent evaluation performed to calculate coefficients for the fundamental and alias terms in the output waveform ($A_n + jB_n$). That is:

- Take the T/N z-transform of (GM) and evaluate at $z = 14\omega_n(T/N)$.
- Take the T z-transform of G_A and evaluate at $z = 14bT$.
- Take the T/ M_k z-transform of each G_k term and evaluate at $z = 14\omega_n(T/M_k)$.

For the (GM) term, calculate the normal z-transform expression and replace each "T" in this expression with "T/N." Follow the same procedure for G_A and G_k with "T" replaced with "T/ M_k " in the resulting z-transform expression for the G_k terms. With (GM), G_A , and G_k in z-transform form, each term is then individually evaluated at the appropriate value of "z" as indicated by the notation.

Example

$$c^{T/100} = (GM)^{T/100} G_A^T G_1^{T/10} G_2^{T/20} G_3^{T/50} R^T \quad (200)$$

$$\begin{aligned} A_n + jB_n &= \frac{1}{N} (GM)^{T/100}(z) \left| \begin{array}{l} z^{\Delta} e^{sT/100} \\ z = 14\omega_n(T/100) \end{array} \right. G_A^T(z) \left| \begin{array}{l} z^{\Delta} e^{sT} \\ z = 14bT \end{array} \right. G^{T/10}(z) \left| \begin{array}{l} z^{\Delta} e^{sT/10} \\ z = 14\omega_n(T/10) \end{array} \right. \\ &\times G_2^{T/20}(z) \left| \begin{array}{l} z^{\Delta} e^{sT/20} \\ z = 14\omega_n(T/20) \end{array} \right. G_3^{T/50}(z) \left| \begin{array}{l} z^{\Delta} e^{sT/50} \\ z = 14\omega_n(T/50) \end{array} \right. \end{aligned} \quad (201)$$

$$\omega_n = b + (2\pi n/T)$$

$$n = n_0, n_0-1, \dots, 0, 1, 2, \dots, N-n_0-1$$

$$n_0 = -(b/\omega_s)_{INT}$$

It is apparent that once the $C^{T/N}$ expression has been determined for the system, simple substitution produces the exact frequency response expression for either the finite N case or the limiting case of $N \rightarrow \infty$. Using this expression, the coefficients $(A_n + jB_n)$ for the fundamental and its aliases present in the output waveform can then be determined. A summary of the steps required follows:

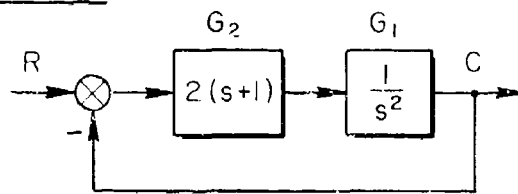
- Obtain the $C^{T/N}$ output equation using block diagram/signal flow algebra.
- Apply the identities outlined in this subsection to each term in $C^{T/N}$ to obtain the frequency response expression $A_n + jB_n$.
- Calculate the individual z -transforms using the appropriate definition of z .
- Evaluate each term in the $A_n + jB_n$ expression at appropriate values of z and s .

E. APPLICATION TO SIMULATION ERROR ANALYSIS

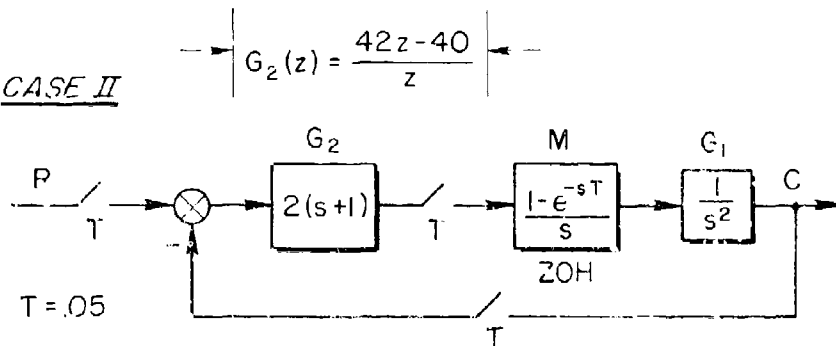
There is a natural extension of the previous results which makes the switch decomposition/frequency response technique ideal for the error analysis of simulations (either simulations of continuous systems or the simulation of continuous plants under the influence of direct digital control). One may obtain a clearer understanding of this statement by considering the four diagrams of Fig. 28.

The situation described by Case I in Fig. 28 assumes a controlled element $(1/s^2)$ under the influence of a continuous feedback controller with an (idealized) compensation network $2(s + 1)$ in the forward path. Case II depicts the same controlled element under the influence of a discrete feedback controller which smooths the output of the digital

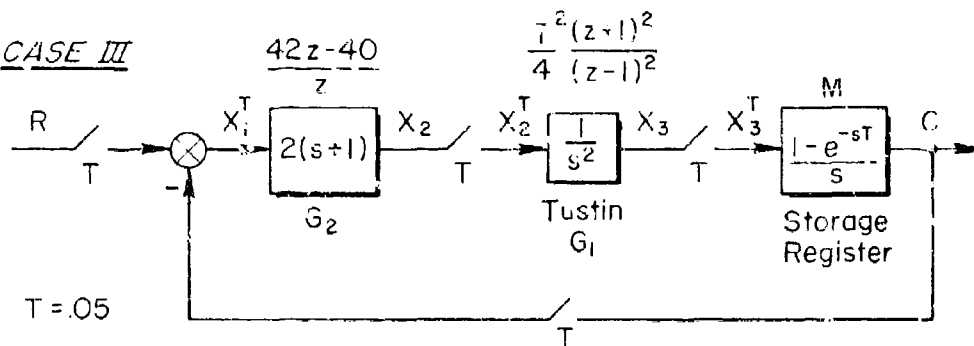
CASE I



CASE II



CASE III



CASE IV

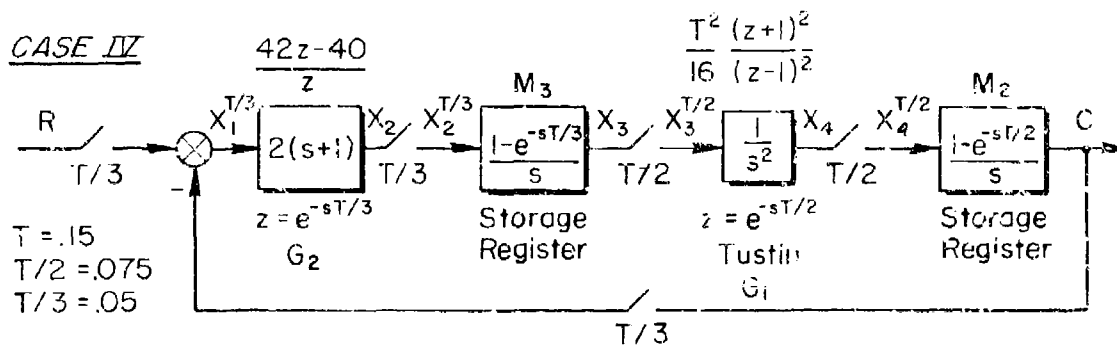


Figure 28. A Simulation Case Study

computer with a ZOH (passing on a "staircased" signal to the control point). The discretized version of $2(s + 1)$ was computed, using the first back difference algorithm resulting in the model $(42z - 40)/z$ (at a sampling rate of 20 Hz).

Case III depicts a simulation of Case II (or I) wherein the plant, $1/s^2$, is modeled using a "substitution-for-s" rule (Tustin transform). The output variable C is modeled as the output of a storage register (ZOH).

Finally, Case IV depicts a common situation wherein one part of a simulation is coded for one computer while another part is coded on a second computer. Typically, the computers are working in slightly different frametimes and therefore will, on occasion, pass "old data" back and forth. In this example it is assumed that the compensation is modeled in a 0.05 sec time frame, while the plant is modeled in a 0.075 sec time frame. Data transfer between the two computers is via appropriate buffer registers, modeled as a ZOH in a $T/3$ time frame (M_3) and a ZOH in a $T/2$ time frame (M_2).

This completes the problem description; we may now write the appropriate equations for each case and discuss the analytical difficulties.

Case I is straightforward since

$$C(s) = [I + G_1 G_2]^{-1} G_1 G_2 R \quad (202)$$

Case II appears straightforward but does present a contradiction in the output equation

$$C^T = [I + (G_1 M)^T G_2^T]^{-1} (G_1 M)^T G_2^T R^T \quad (203)$$

That is,

$$(G_1 M)^T = \left[\frac{1 - e^{-sT}}{s} \frac{1}{s^2} \right]^T = \frac{T^2}{2} \frac{(z + 1)}{(z - 1)^2} \quad (204)$$

is readily computed using a transform table. However, it was not the intent of the designer, who used a substitution technique to model $2(s + 1)$ as $(42z - 40)/z$, to compute

$$G_2^T = [2(s + 1)]^T \quad (205)$$

using the z -transform. Indeed, what does $[s]^T$ mean? Clearly, the intent was to assign $G_2^T = (42z - 40)/z$, which is legitimate if one interprets z^{-1} as a delay operator.

This difficulty surfaces again in Case III since

$$C^T = [I + G_1^T G_2^T]^{-1} G_1^T G_2^T R^T \quad (206)$$

after taking due note that $M^T \equiv I$.

Now it is necessary to interpret both G_1^T and G_2^T as given functions of z rather than z -transform operations. For example, assign (via the Tustin transform)

$$G_1^T = \frac{T^2}{4} \frac{(z + 1)^2}{(z - 1)^2} \quad (207)$$

rather than (via the z -transform)

$$G_1^T = \left[\frac{1}{s^2} \right]^T = \frac{Tz}{(z - 1)^2} \quad (208)$$

Difficulties in the "assignment" procedure also surface when we write the output equation for Case IV (see Fig. 29).

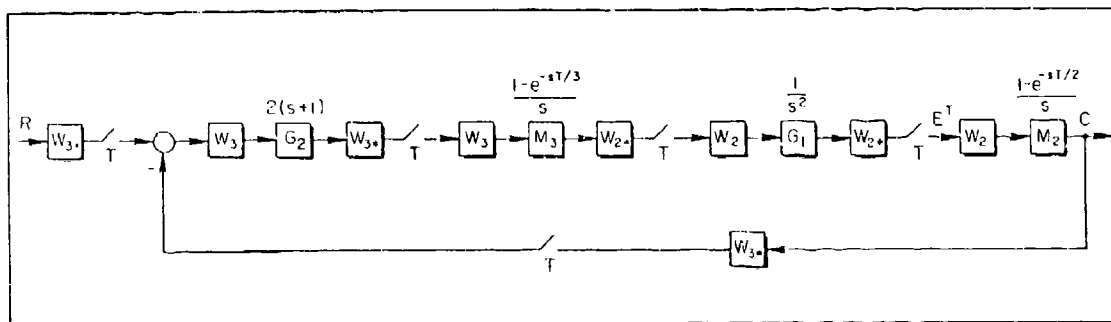


Figure 29. Case IV, Switch Decomposition Model

$$C = (M_2 W_2) [I + (W_{2*} G_1 W_2)^T (W_{2*} M_3 W_3)^T (W_{3*} G_2 W_3)^T (W_{3*} M_2 W_2)^T]^{-1} \\ \times (W_{2*} G_1 W_2)^T (W_{2*} M_3 W_3)^T (W_{3*} G_2 W_3)^T (W_{3*} R)^T \quad (209)$$

where

$$W_2 = [1, e^{-sT/2}] \quad , \quad W_3 = [1, e^{-sT/3}, e^{-sT2/3}] \quad (210)$$

The meaning of some terms in Eq. 209 are clear; others are not. For example, a straightforward computation yields (see Appendix B)

$$(W_{3*} M_2 W_2)^T = \begin{bmatrix} 1 & 0 \\ 1 & 0 \\ 0 & 1 \end{bmatrix} \quad ; \quad (W_{2*} M_3 W_3)^T = \begin{bmatrix} 1 & 0 & 0 \\ 0 & 1 & 0 \end{bmatrix} \quad (211)$$

However, the meaning of $(W_{3*} G_2 W_3)^T$ or $(W_{2*} G_1 W_2)^T$ is not clear. When the designer specified $G_2 = (42z - 40)/z$, he intended (for a T time frame) the recursion relationship

$$X_2(n) = 42(R_n - C_n) - 40(R_{n-1} - C_{n-1}) \quad (212)$$

In a like manner, the Tustin substitution for $1/s^2$ was meant to yield

$$X_4(n) = 2X_4(n-1) - X_4(n-2) + \frac{T^2}{16} [X_3(n) + 2X_3(n-1) + X_3(n-2)] \quad (213)$$

Clearly, the information available in Case IV is

$$G_2^{T/3} = \frac{42z - 40}{z}, \quad T/3 = 0.05, \quad z = e^{sT/3} \quad (214)$$

and

$$G_1^{T/2} = \frac{T^2}{16} \frac{(z+1)^2}{(z-1)^2}, \quad T/2 = 0.075, \quad z = e^{sT/2} \quad (215)$$

Using only the given computer code, how does one compute $(W_3 \star G_2 W_3)^T$ and $(W_2 \star G_1 W_2)^T$? This problem is treated in the next subsection. In order to complete the analysis of the present problem, the reader is asked to temporarily accept the assignments

$$(W_3 \star G_2 W_3)^T = \begin{bmatrix} 42 & 0 & -40/z \\ -40 & 42 & 0 \\ 0 & -40 & 42 \end{bmatrix}, \quad z = e^{sT} \quad (216)$$

and

$$(W_2 \star G_1 W_2)^T = \frac{\begin{bmatrix} \frac{T^2}{16} (z^2 + 6z + 1) & (T^2/4)(z+1)/z \\ \frac{T^2}{4} z(z+1) & \frac{T^2}{16} (z^2 + 6z + 1) \end{bmatrix}}{(z-1)^2} \quad (217)$$

With these assignments, all terms in Eq. 209 are defined and the Bode plots descriptive of Cases I-IV can be computed. The results (magnitude plots only) are shown in Figs. 30 through 35.

Inspection of Fig. 30 discloses no surprises. The digitally controlled system is a reasonably faithful reproduction of the analog system until the folding frequency (approximately equal to 62.8 rad/sec) is passed. Notice that in the discretely controlled system, minimum response points in the Bode plot (notches) occur at multiples of sampling frequency (approximately equal to 125.66 rad/sec).

The comparison of the single-rate simulation against the baseline design exhibits fidelity over a shorter low-frequency range (Fig. 31). Of particular importance is that the aliased bands exhibit a much higher amplitude response than did the aliased bands of the digitally controlled system (Case II). Moreover, the "notches" now occur at multiples of the folding frequency rather than the sampling frequency. In addition, there are very sharp notches which occur close to odd multiples of the folding frequency; these are a consequence of the zeros of the Tustin transform introduced by $(z + 1)^2$. A direct comparison between Cases II and III is given in Fig. 32.

Figure 33 compares the two independent processor case (Case IV) against the continuous baseline design. Large, sharp resonant peaks have been introduced in the aliased bands and, in addition, there is a significant overshoot in the first fold. A comparison between the two rate simulation (Case IV) and the digitally controlled continuous system (Case II) is given in Fig. 34. Figure 35 (a very "busy" figure) compares all the cases.

There are significant differences in the spectral content of the four cases which would be hidden if one only looked at the sampled spectrum (that is, looked only at the frequency content from zero to the first folding frequency). Even in the first fold, there is a significant difference in the Bode plot of the continuous case and the two-rate simulation; the reason for the added overshoot in the two-rate simulation will be discussed in the next subsection. After this, we return to the theoretical issue of computing such terms as $(h_3^* G_2 W_3)^T$ when only a $G_2^{T/3}$ assignment in z has been given (or, equivalently, the recursion equation is given).

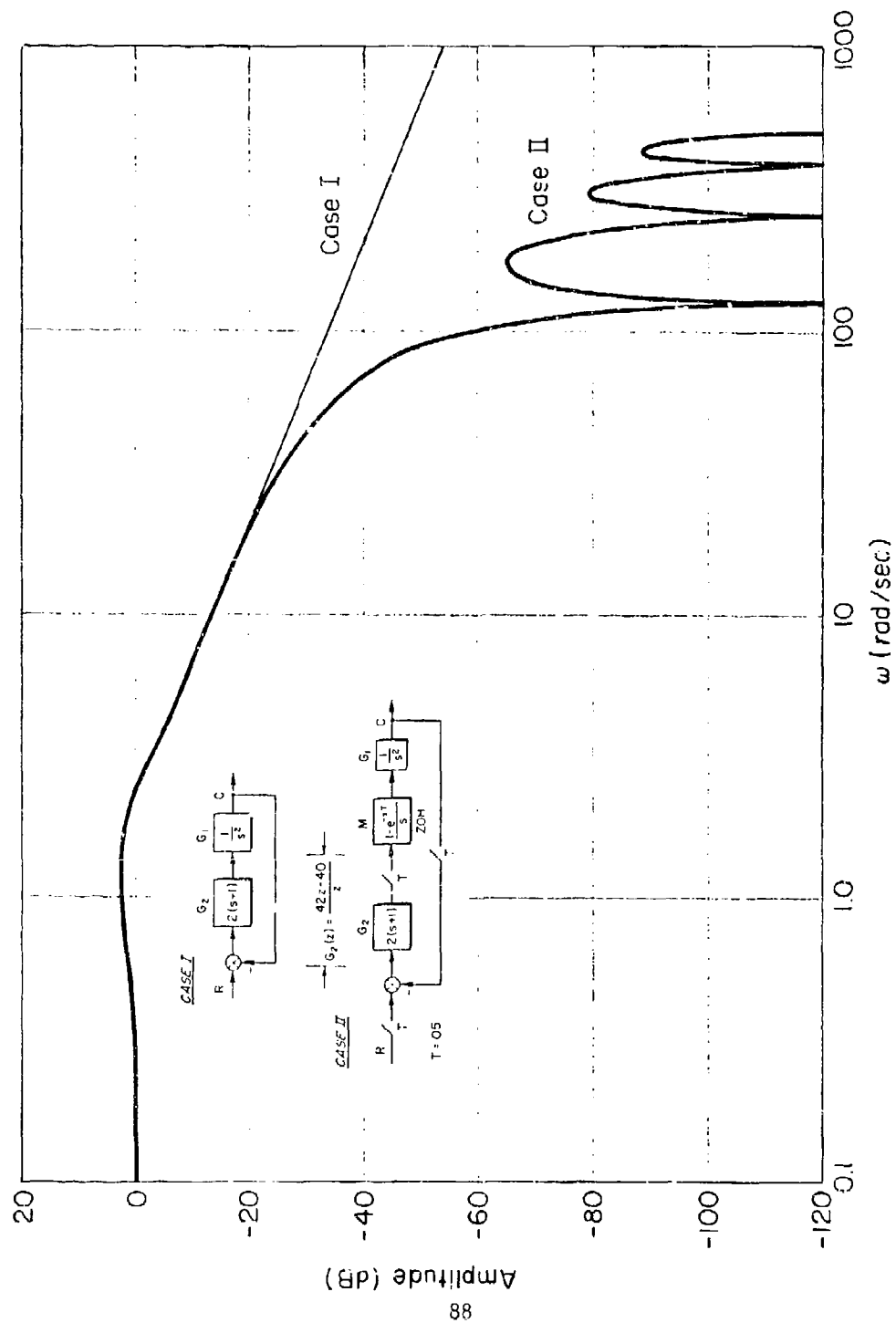


Figure 30. Magnitude Plot; Case I, Case II

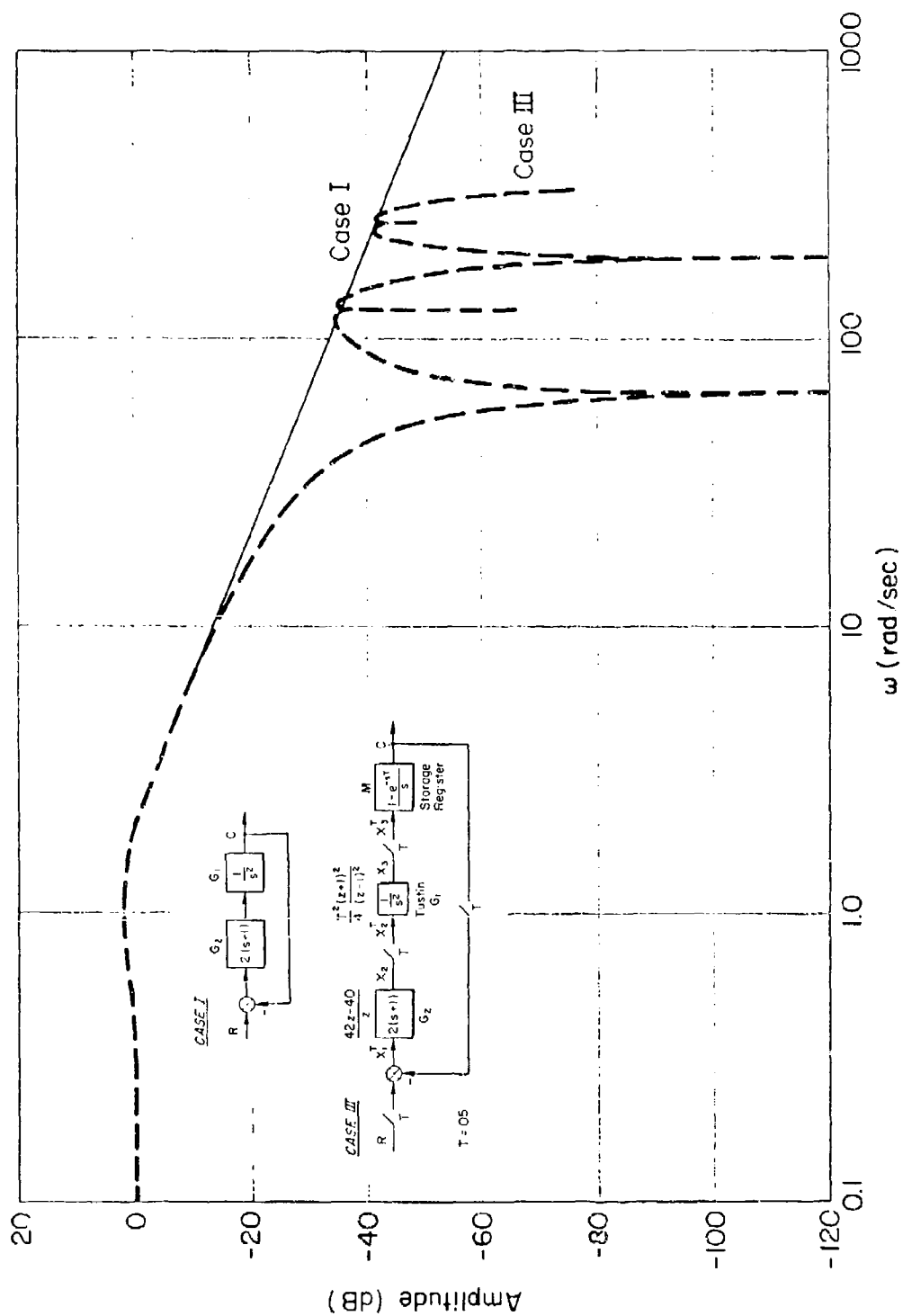


Figure 31. Magnitude Plot; Case I, Case III

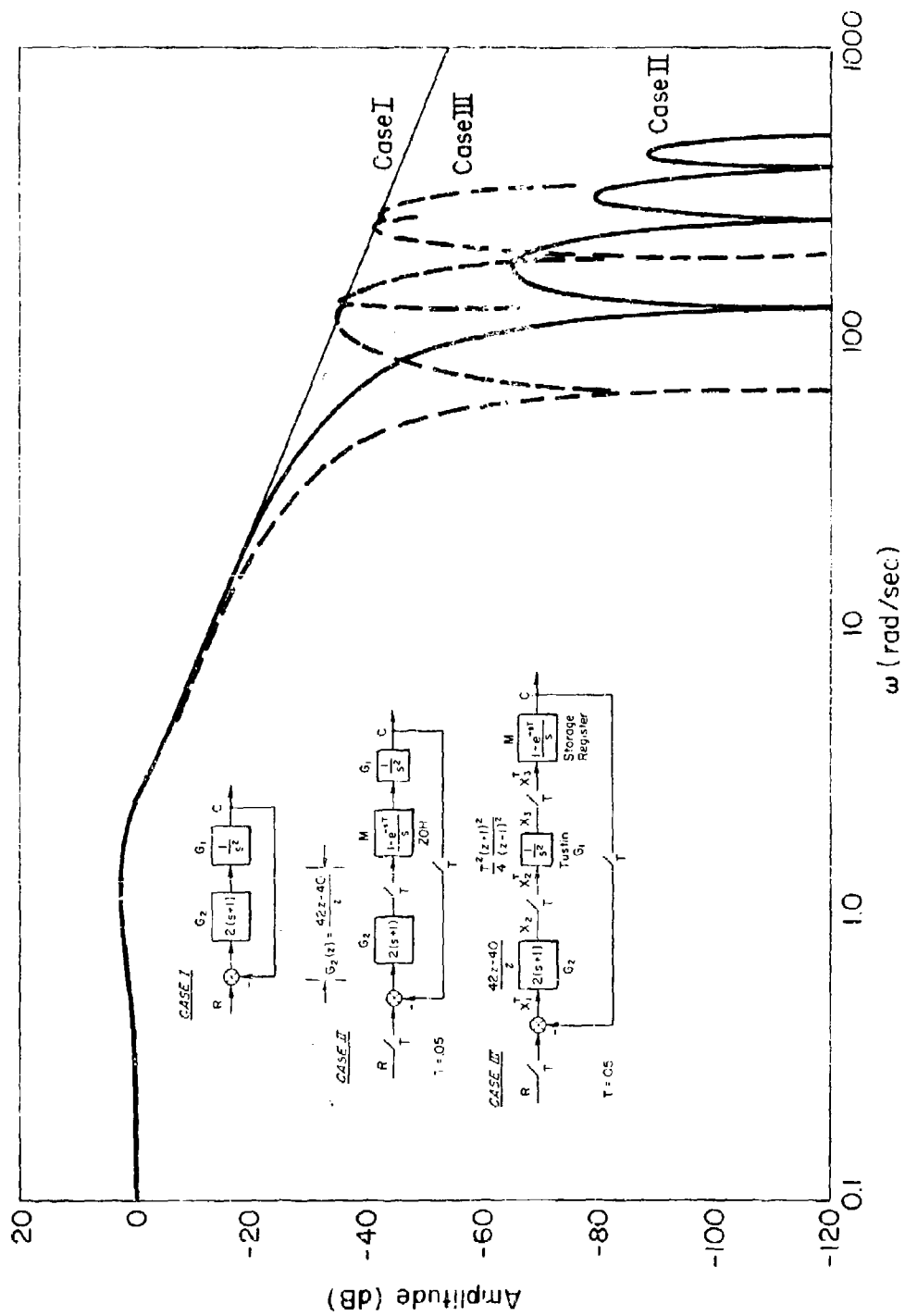
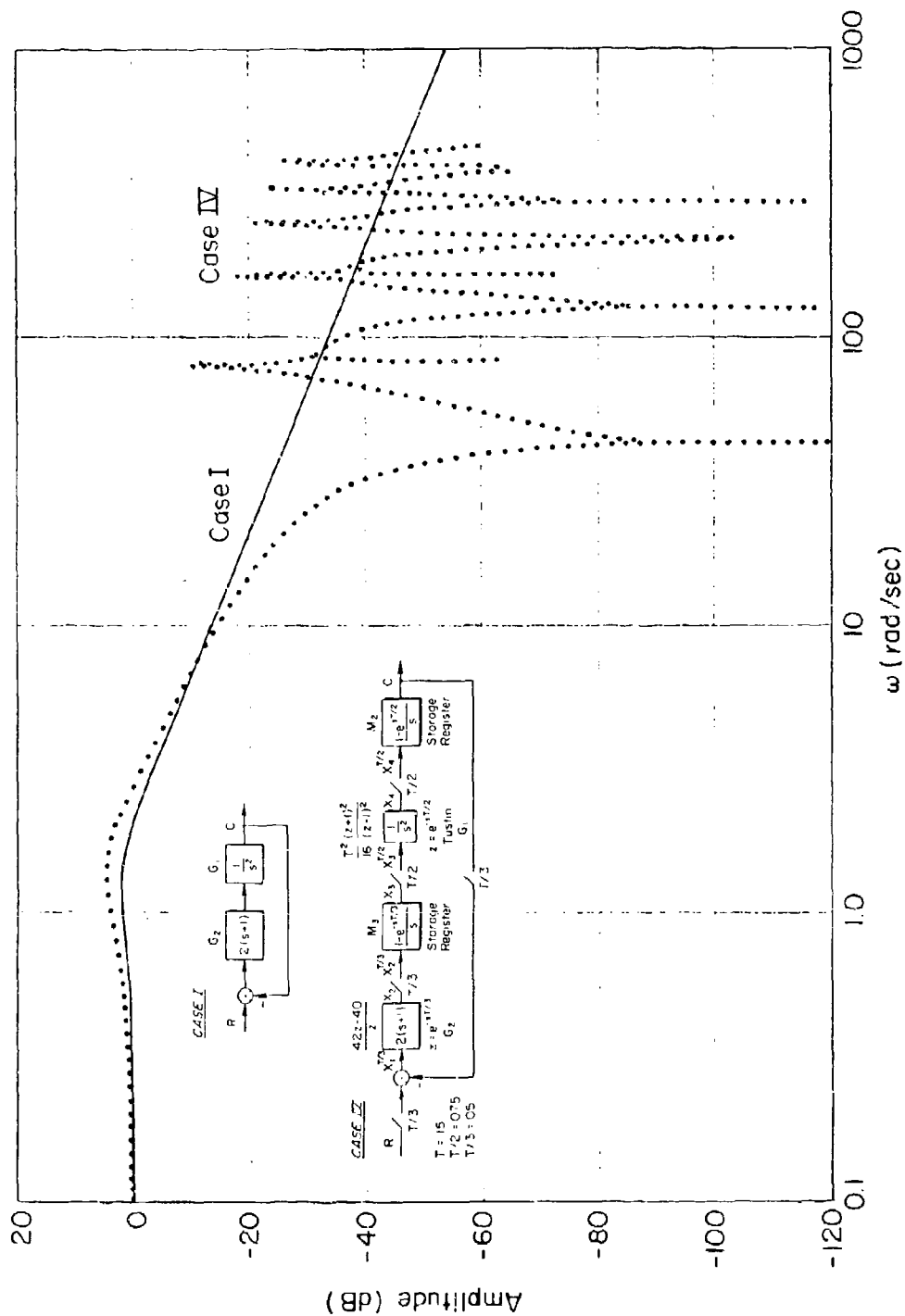


Figure 32. Comparison; Case II and Case III



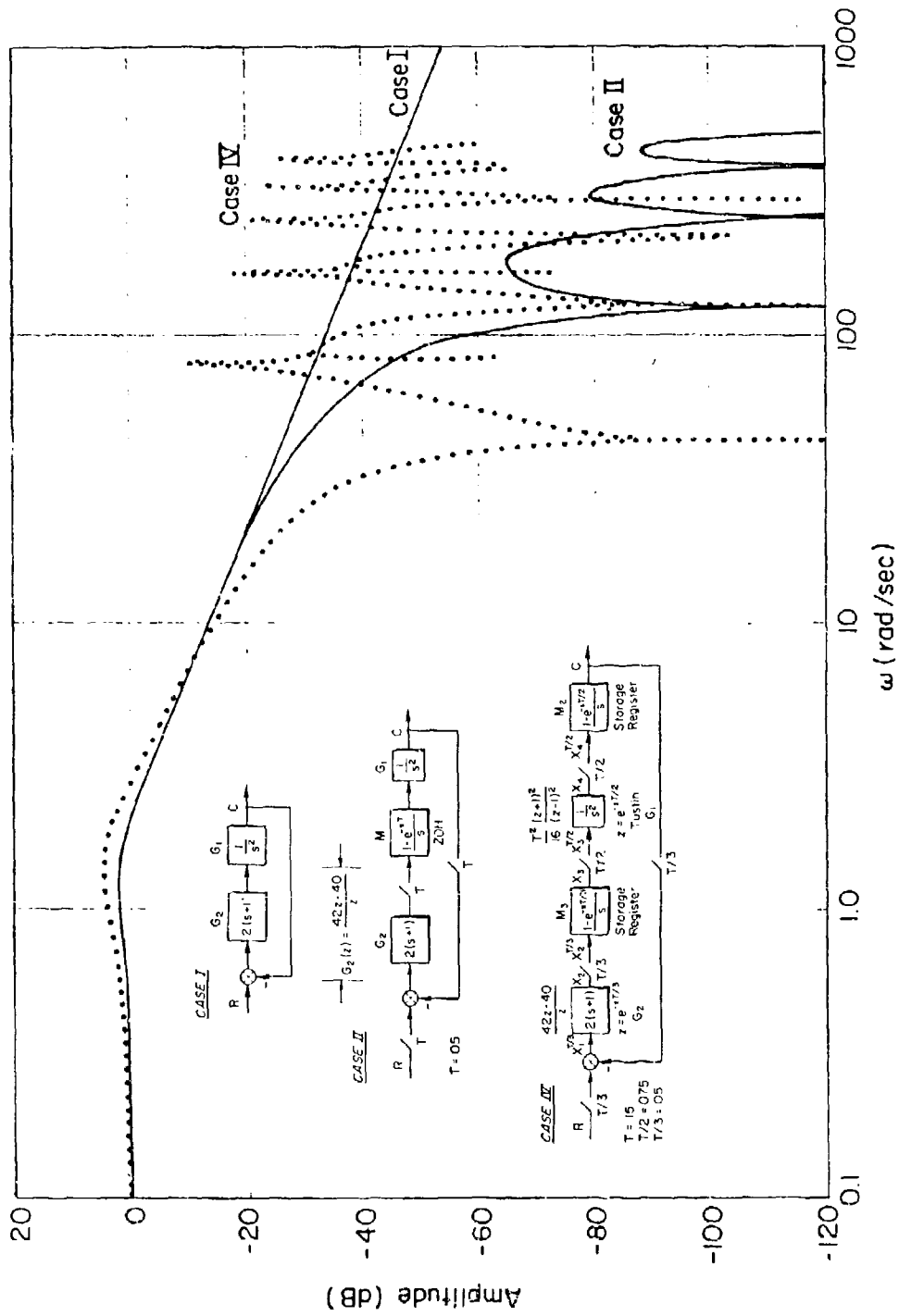


Figure 34. Comparison, Case II and Case IV

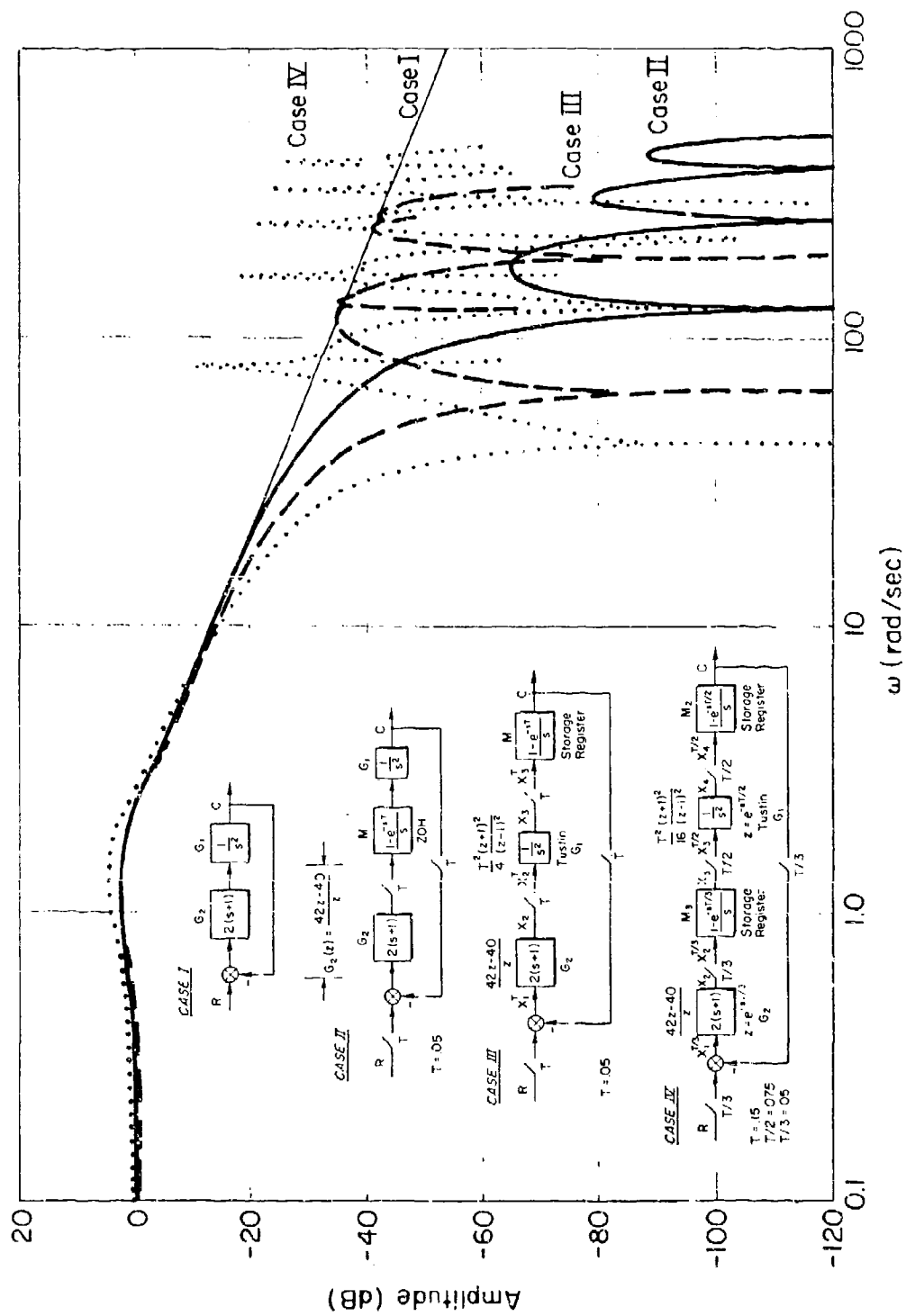


Figure 35. Comparison, All Cases

F. AN IMPORTANT ALGORITHM

Of fundamental concern is the evaluation of terms such as $(W_{\star} G W)^T$ when G is specified only in terms of software statements (i.e., given as a function of z). As a first step, consider how one might evaluate the system of Fig. 36. As indicated, it is permissible to insert

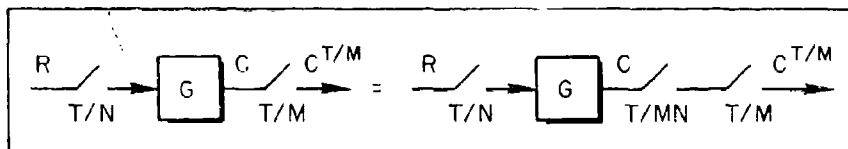


Figure 36. A Phantom Sampler Formulation of a T/N, T/M Sampling Format

a phantom sampler between G and the T/M sampler since T/MN and T/M are integerly related. Thus,

$$C^{T/M} = [G R^{T/N}]^{T/M} \equiv [G^{T/MN} R^{T/N}]^{T/M} \quad (218)$$

M and N are integers.

To compute the entries of Eq. 218 one may:

- 1) Compute R by table lookup.
- 2) Replace T by T/N .
- 3) Replace z (in R) with z^M .
- 4) Compute G by table lookup.
- 5) Replace T with T/MN .
- 6) z remains the same (in G).
- 7) Compute $C^{T/M}$ using Eq. 219.

$$C^{T/M} = \frac{1}{2\pi j} \int_{\Gamma} G(p) R(p^M) \frac{z}{z - p^N} \frac{dp}{p} \quad (219)$$

Equation 219 is mechanized in a digital computer program (TXCONV) which is discussed in Volume II.

For example, let

$$z = e^{sT/6}, \quad M = 3, \quad N = 2 \quad (220)$$

$$G = \frac{1}{s+2}, \quad G^{T/6} = \frac{z}{z - e^{-T/3}} \quad (221)$$

$$R = \frac{1}{s+1}, \quad R^{T/2} = \frac{z^3}{z^3 - e^{-T/2}} \quad (222)$$

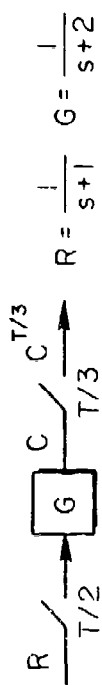
so that

$$\begin{aligned} C^{T/3} &= \frac{1}{2\pi j} \int \frac{p^4 z}{(p - e^{-T/3})(p^3 - e^{-T/2})(z - p^2)} \frac{dp}{p} \\ &= \frac{1}{2\pi j} \int \frac{p^3 z}{(p - e^{-T/3})(p - e^{-T/6})(p^2 + e^{-T/6}p + e^{-2T/6})(z - p^2)} dp \\ &= \text{res} \Big|_{p=e^{-T/3}} + \text{res} \Big|_{p=e^{-T/6}} + \text{res} \Big|_{p=-(e^{-T/6})/2 + je^{-T/6}(\sqrt{3}/2)} \\ &\quad + \text{res} \Big|_{p=-(e^{-T/6})/2 - je^{-T/6}(\sqrt{3}/2)} \end{aligned} \quad (223)$$

Thus, there are four residues to evaluate. Relegating the numerical details to Appendix C, we proceed directly to the final result,

$$C^{T/3} = \frac{z^2(z^2 + e^{-5T/6})}{(z - e^{-2T/3})(z - e^{-T/3})(z^2 + e^{-T/3}z + e^{-2T/3})}, \quad z = e^{sT/3} \quad (224)$$

and observe that the $T/2$, $T/3$ sampling format has produced additional lightly damped modes in the output response. The reality of the additional modes can be better appreciated by first plotting the continuous variable $C(t)$ and then picking off the $T/3$ sample points. This is done in Fig. 37. Joining the sample points with a smooth curve emphasizes the lightly damped nature of the response. This effect was also present in the two-rate simulation analysis of the previous subsection (recall the additional "overshoot" in the first fold of Fig. 33).



$$C^{T/3} = \frac{z^2(z^2 + e^{-5/6T})}{(z - e^{-2T/3})(z - e^{-T/3})(z^2 + e^{-T/3}z + e^{-2T/3})}$$

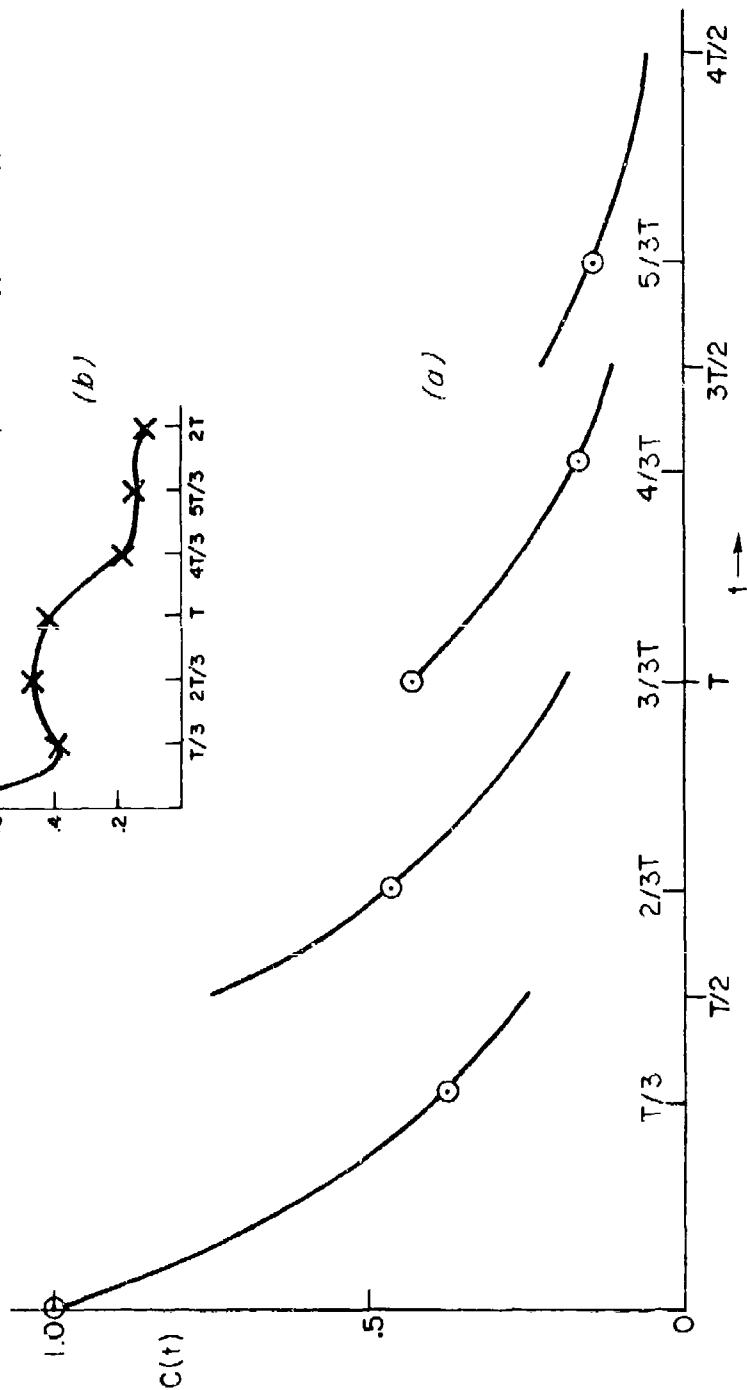
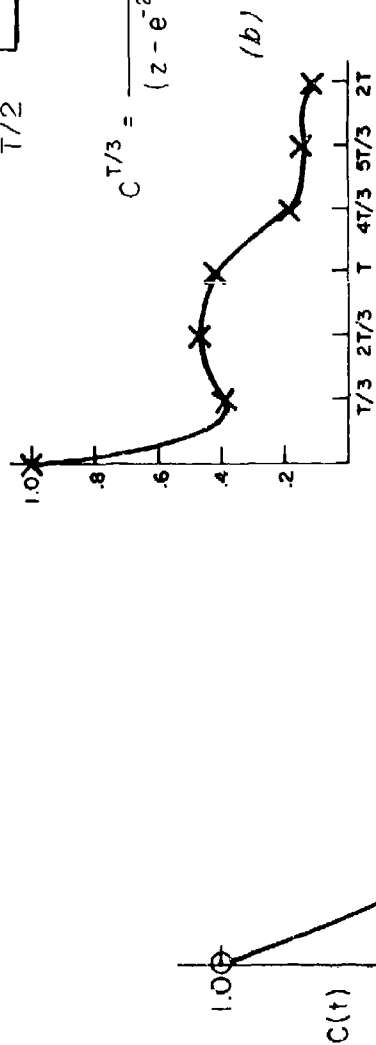


Figure 37. Response of a T/2 Input Sampled, T/3 Output Sampled System

G. COMPUTATION OF $(W_*CW)^T$, $G^{T/N}$ GIVEN

With the aid of Eq. 218, we are in a position to evaluate configurations such as those of Fig. 38 (the vector switch decomposition equivalent is shown in Fig. 39).

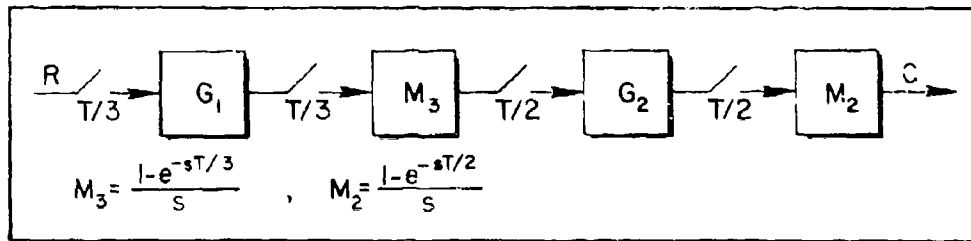


Figure 38. Example Two-Rate Open-Loop System

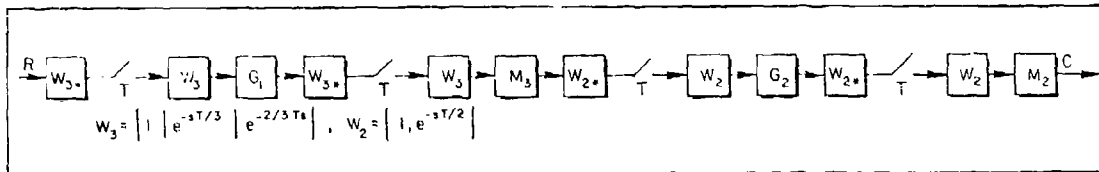


Figure 39. Switch Decomposition Formulation for Fig. 38

From Fig. 39,

$$C = M_2 W_2 (W_{2*} G_2 W_2)^T (W_{2*} M_3 W_3)^T (W_{3*} C_1 W_3)^T (W_{3*} R)^T \quad (225)$$

As noted previously, the evaluation of terms such as $(W_{2*} M_3 W_3)^T$ is routine (Appendix B); our concern is with terms like $(W_{3*} G_1 W_3)^T$ when $G^{T/3}$ is given as a software specification (e.g., computer algorithm). Focusing on $(W_{3*} G_1 W_3)^T$, we find

$$\begin{aligned}
(W_{3*}G_1W_3)^T &= \left\{ \begin{bmatrix} 1 \\ e^{sT/3} \\ e^{2sT/3} \end{bmatrix} G_1 \begin{bmatrix} 1 & e^{-sT/3} & e^{-2sT/3} \end{bmatrix} \right\}^T \\
&= \left\{ G_1 \begin{bmatrix} 1 & e^{-sT/3} & e^{-2sT/3} \\ e^{sT/3} & 1 & e^{-sT/3} \\ e^{2sT/3} & e^{sT/3} & 1 \end{bmatrix} \right\}^T \quad (226)
\end{aligned}$$

$$(W_{3*}G_1W_3)^T = \left\{ G_1 \begin{bmatrix} 1 & e^{-sT} \{ e^{2sT/3} \} & e^{-sT} \{ e^{sT/3} \} \\ \{ e^{sT/3} \} & 1 & e^{-sT} \{ e^{2sT/3} \} \\ \{ e^{2sT/3} \} & \{ e^{sT/3} \} & 1 \end{bmatrix} \right\}^T \quad (227)$$

Observe the super-diagonal terms. They are simply appropriate sub-diagonal terms multiplied by e^{-sT} . Indeed, it is only necessary to compute the first column entries in order to completely determine $(W_{3*}G_1W_3)^T$.

Next, observe the problem statement stipulates $G_1^{T/3}$, perhaps defined through a substitution rule. If $e^{sT/3}$ is defined as z we have, using Eq. 218,

$$(W_{3*}G_1W_3)^T = \begin{Bmatrix} G_1^{T/3} & z^{-3}(z^2G_1^{T/3}) & z^{-3}(zG_1^{T/3}) \\ zG_1^{T/3} & G_1^{T/3} & z^{-3}(z^2G_1^{T/3}) \\ z^2G_1^{T/3} & zG_1^{T/3} & G_1^{T/3} \end{Bmatrix}^T, \quad z = e^{sT/3} \quad (228)$$

Although each term in Eq. 228 can be evaluated, using Eq. 219, only the first column entries need be computed (i.e., the three entries of column one are sufficient to define all nine entries).

To summarize,

$$(W_{3*}G_1W_3)^T = (W_{3*}G_1^{T/3}W_3)^T \quad (229)$$

For example, recall the $G_1^{T/3}$ transfer function from the simulation example (Case IV) had the form

$$G_1^{T/3} = \frac{a_0z + a_1}{z}, \quad z = e^{sT/3} \quad (230)$$

One must therefore compute

$$\left(\frac{a_0z + a_1}{z}\right)^T, \quad \left(\frac{z(a_0z + a_1)}{z}\right)^T, \quad \left(\frac{z^2(a_0z + a_1)}{z}\right)^T \quad (231)$$

in order to define the 3×3 matrix $(W_{3*}G_1W_3)^T$. To illustrate,

$$\begin{aligned} \left(\frac{a_0z + a_1}{z}\right)^T &= \frac{1}{2\pi j} \int_{\Gamma} \frac{a_0p + a_1}{p} \cdot \frac{z}{z - p^3} \frac{dp}{p} \\ &= \frac{d}{dp} \left(\frac{(a_0p + a_1)z}{z - p^3} \right) \Big|_{p=0} = a_0 \end{aligned} \quad (232)$$

$$\begin{aligned}
(a_0 z + a_1)^T &= \frac{1}{2\pi j} \int_{\Gamma} \frac{(a_0 p + a_1)z}{p(z - p^3)} dp \\
&= \left. \frac{(a_0 p + a_1)z}{z - p^3} \right|_{p=0} = a_1
\end{aligned} \tag{233}$$

$$[(z)(a_0 z + a_1)]^T = \frac{1}{2\pi j} \int \frac{(a_0 p + a_1)z}{z - p^3} dp \equiv 0 \tag{234}$$

(no poles enclosed). Therefore,

$$(W_{3*} G_2 W_3)^T = \begin{bmatrix} a_0 & 0 & a_1/z \\ a_1 & a_0 & 0 \\ 0 & a_1 & a_0 \end{bmatrix}, \quad z = e^{sT} \tag{235}$$

Setting $a_0 = 42$, $a_1 = -40$ verifies Eq. 216 of the previous subsection.

The other assignment made was

$$(W_{2*} G_1 W_2)^T = \frac{\begin{bmatrix} (T^2/16)(z^2 + 6z + 1) & [(T^2/4)(z + 1)]/z \\ (T^2/4)[z(z + 1)] & (T^2/16)(z^2 + 6z + 1) \end{bmatrix}}{(z - 1)^2} \tag{236}$$

given

$$G_1^{T/2} = \frac{T^2}{16} \frac{(z+1)^2}{(z-1)^2}, \quad z = e^{sT/2} \quad (237)$$

To verify this, write

$$(W_{2*} G_1^{T/2} W)^T = \left[\begin{bmatrix} 1 \\ z \end{bmatrix} \begin{bmatrix} 1 & z^{-1} \end{bmatrix} G_2^{T/2} \right]^T = \left\{ \frac{T^2}{16} \frac{(z+1)^2}{(z-1)^2} \begin{bmatrix} 1 & z^{-1} \\ z & 1 \end{bmatrix} \right\}^T \quad (238)$$

The first term of column one is

$$\begin{aligned} \left\{ \frac{T^2(z+1)^2}{16(z-1)^2} \right\}^T &= \frac{1}{2\pi j} \int_{\Gamma} \frac{T^2}{16} \frac{(p+1)^2}{(p-1)^2} \frac{z}{z-p^2} \frac{dp}{p} = \text{res} \Big|_{p=0} + \text{res} \Big|_{p=1} \\ &= \frac{T^2}{16} + \frac{T^2}{16} \frac{d}{dp} \frac{(p+1)^2 z}{p(z-p^2)} \Big|_{p=1} = \frac{T^2}{16} \left[1 + \frac{8z}{(z-1)^2} \right] \\ &= \frac{T^2}{16} \frac{(z^2 + 6z + 1)}{(z-1)^2}, \quad z = e^{sT} \quad (239) \end{aligned}$$

The second term of the first column is easier to compute:

$$\begin{aligned} \frac{1}{2\pi j} \int_{\Gamma} \frac{T^2}{16} \frac{p(p+1)^2}{(p-1)^2} \frac{z}{(z-p^2)} \frac{dp}{p} &= \text{res} \Big|_{p=1} \\ &= \frac{T^2}{16} \frac{d}{dp} \frac{z(p+1)^2}{(z-p^2)} \Big|_{p=1} \\ &= \frac{T^2}{4} \frac{z(z+1)}{(z-1)^2} \quad (240) \end{aligned}$$

The only remaining terms are the 2,2 term (which is the same as the 1,1 term) and the 1,2 term. The 1,2 term is the product of z^{-2} with the 2,1 term. Thus, we verify Eq. 236 of this subsection and Eq. 217 of the previous subsection.

H. SECTION SUMMARY

Important extensions to the frequency response concept for single-rate systems have been given. These extensions make it possible to investigate the spectral content of the continuous variables of multi-rate and/or multiple-order configured systems. In addition, an important relationship was deduced which makes it feasible to apply the switch decomposition/frequency response technique to the error analysis of simulations of continuous systems and/or discretely controlled continuous systems. An illustrative example was used to demonstrate the significant spectral differences that occur when a closed-loop system (either an analog or digital controller) is compared with an all-digital simulation of the closed-loop system. The example also treated, as a particular case, the problems encountered when a simulation software is put up on two different (independent) computers, each working in a slightly different frame time.

At this juncture, the important spectral analysis tools have been developed, and we return (in the next section) to the study of the multiple-order vector concept.

SECTION V

A PSEUDO MEASUREMENT EXERCISE

The pseudo measurement approach achieves certain well-defined goals, as demonstrated in Section II. This section addresses the important issue of whether or not the gains required will be reasonable when plant dynamics typical of modern aircraft are used.

To provide a digital controller baseline for the numerical ranges involved, we first "emulate" an analog controller for the YF-16. Next, the pseudo measurement approach provides alternate loops for the basic airframe. The numerical range of the compensation can then be meaningfully evaluated, though the intent is not to force the pseudo measurement design to "copy" the emulated baseline controller. A basic frame time of $T = 0.04$ sec (25 Hz) is used throughout.

A. ANALOG CONTROLLER — YF-16

An analog flight controller for the longitudinal YF-16 is given in Fig. 40 ($M = 0.6$, $h = 30,000$ ft). This figure (and the transfer functions for the aircraft model) were developed using data from Ref. 5.

A listing of transfer functions for this flight condition can be found in Appendix D.

A digital controller configuration, using a ZOH together with compensation defined by the Tustin transform, is shown in Fig. 41.

For frequency response purposes, note for example

$$\alpha = \left(\frac{N_{\delta}^{\alpha}}{D} G_1 M \right) G_2^T \delta_{e_c}^T \quad (241)$$

where

$$\begin{aligned} \delta_{e_c}^T &= \left[I + G_3^T \left(\frac{N_{\delta_e}^{\alpha}}{D} G_1 M \right)^T + G_2^T G_4^T \left(\frac{N_{\delta_e}^q}{D} G_1 M \right)^T + G_2^T G_5^T \left(\frac{N_{\delta_e}^{an}}{D} G_1 M \right)^T \right]^{-1} G_2^T R^T \\ &= G_A^T R^T \end{aligned} \quad (242)$$

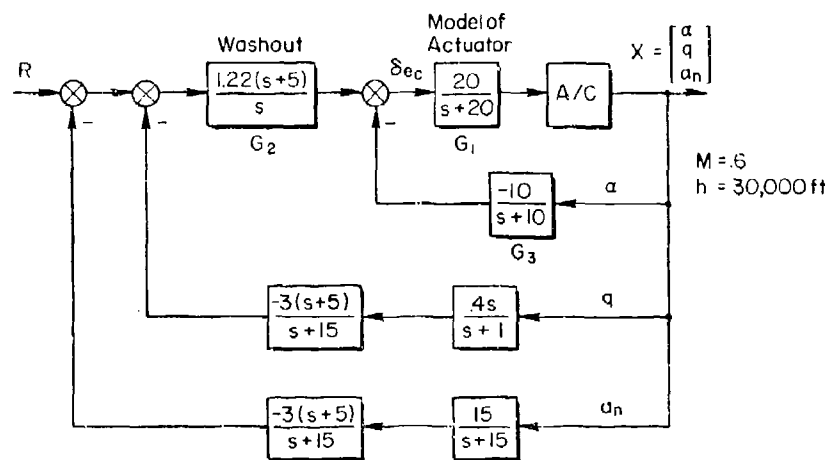


Figure 40. Analog YF-16 Controller

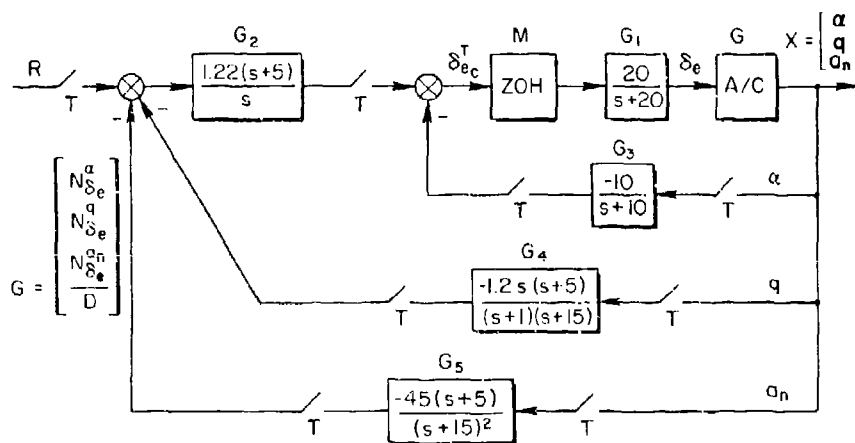


Figure 41. Emulated YF-16 Controller

That is, the coefficients for the frequency response components are defined (for α):

$$A_n + jB_n = \left. \frac{N_{\delta_e}^{\alpha}}{D} G_1 M \right|_{s=j\omega_n} \left(G_2^T G_A^T \right)(z) \Big|_{z=1} \omega_n T \quad (243)$$

There is a need to know the Tustin transform of such elements as G_2^T , G_3^T , G_4^T , etc. A significant computational burden can be neatly side-stepped at this point by noting that the bilinear w' -transformation applied to a z -domain transfer function (which itself was derived using the Tustin transform) yields the same form as the s -domain function. For example, the compensation network

$$\frac{-1.2s(s+5)}{(s+1)(s+15)} \Rightarrow \frac{-1.2w'(w'+5)}{(w'+1)(w'+15)} \quad (244)$$

$$\frac{-10}{s+10} \Rightarrow \frac{-10}{w'+10}, \text{ etc.} \quad (245)$$

By working in w' , the computational burden imposed by poles and zeros very close to the unit circle is avoided. Of course, Eq. 243 must be modified to indicate the dependence on w' rather than z :

$$A_n + jB_n = \left. \frac{N_{\delta_e}^{\alpha}}{D} G_1 M \right|_{s=j\omega} \left(G_2^T G_A^T \right)(w') \Big|_{w'=j(2/T) \tan \omega_n(T/2)} \quad (246)$$

In addition, the transfer functions $[(N_{\delta_e}^{\alpha}/D)G_1 M]^T$, etc., which define the effects of the ZOH on the open-loop plant must be tabulated. These are also listed in Appendix D.

B. FREQUENCY RESPONSE

Using Eqs. 243 and 246, the frequency response of the continuous controller can be contrasted against the discrete controller results (see Fig. 42) for the α component of the state vector. The magnitude plot for the discrete controller is a good replica out to about 70 rad/sec; however, the phase angle plots begin to deviate much earlier (about 7 rad/sec). These results are typical of systems designed via the emulation approach.

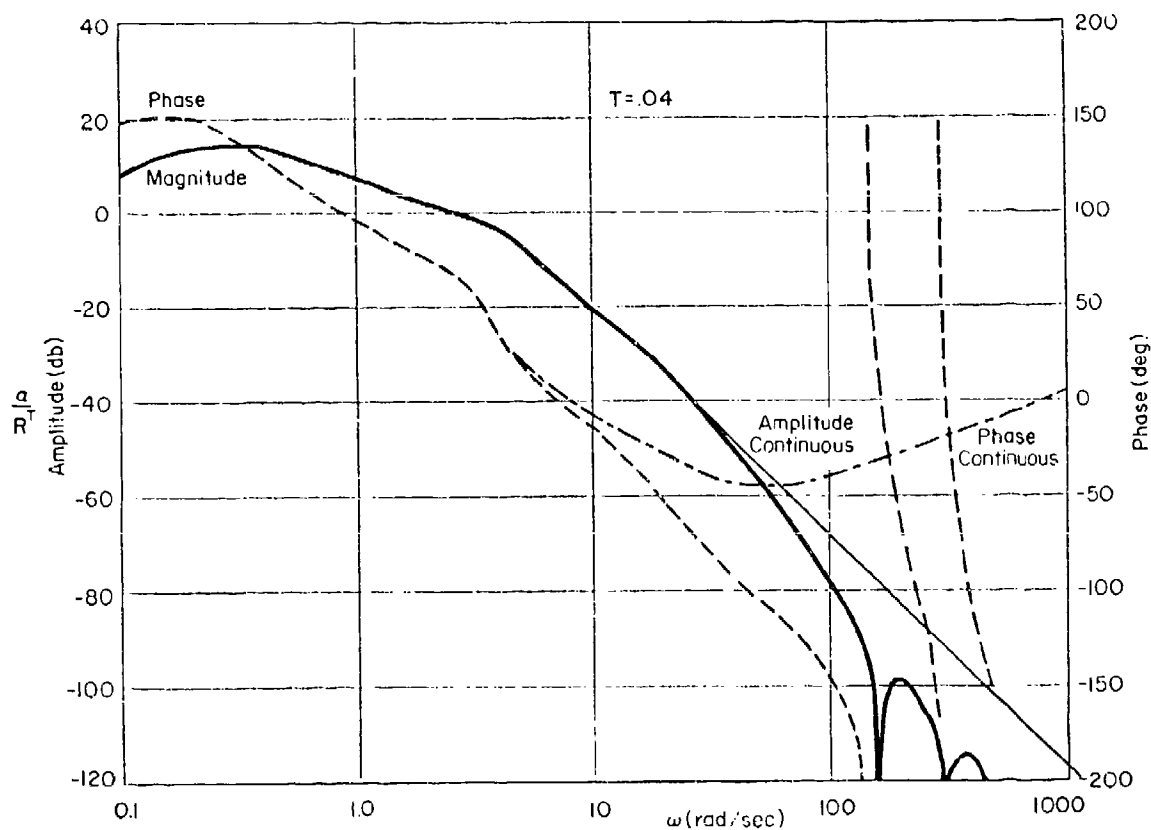


Figure 42. Bode Plot, Analog Compared with Emulated Controller

C. A COMMENT ON A SIMULATION ARTIFACT

Suppose the system of Fig. 41 is simulated in a particular manner. Specifically, the compensation is Tustin transformed, the aircraft is simulated on an analog computer, but a discrete model of the actuator is used (Tustin transformed). The Bode plot for the α response (Fig. 43) discloses additional "notches" (compare with Fig. 42) at odd multiples of the folding frequency (62.83 rad/sec). These additional notches are introduced as a consequence of the algorithm used to form the actuator model. That is, the Tustin transform of

$$\frac{20}{s + 20} \Rightarrow \frac{\frac{20}{(2/T) + 20} (z + 1)}{z + \frac{20 - (2/T)}{20 + (2/T)}} \quad (247)$$

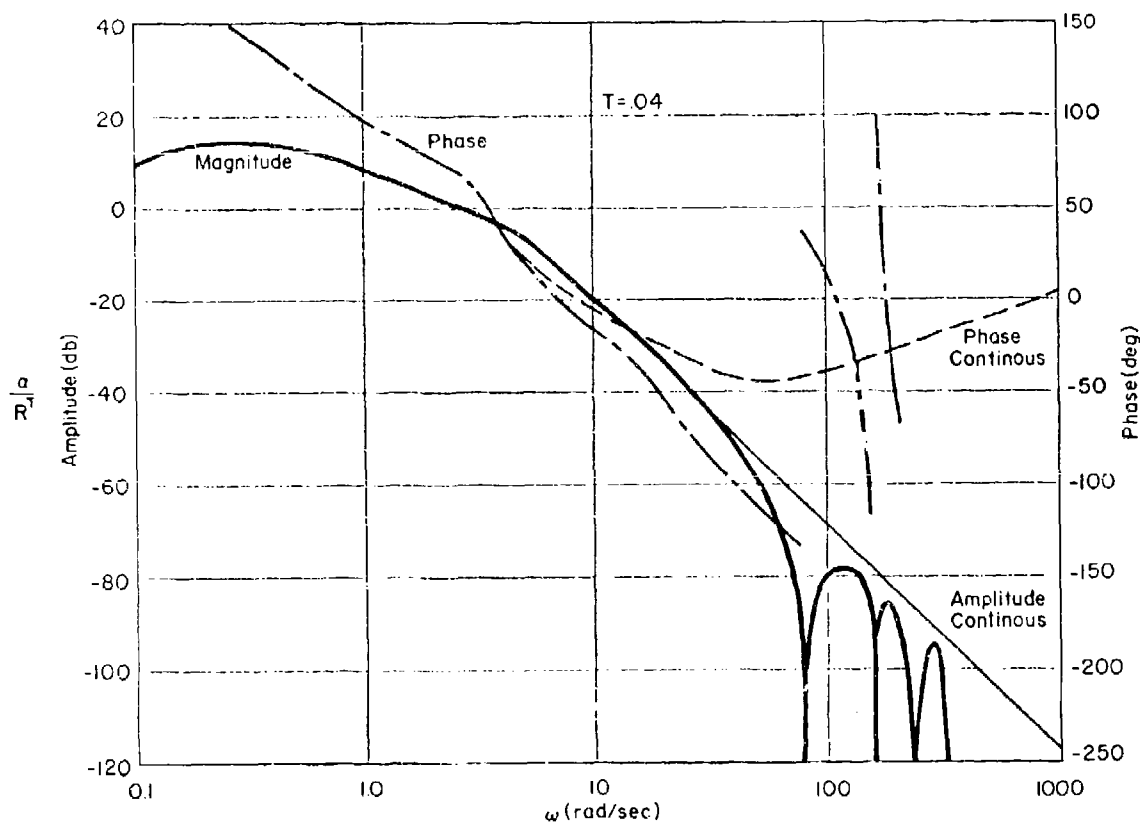


Figure 43. Simulation of Actuator via Tustin Transform

introduces, because of the $(z + 1)$ numerator, nulls at odd multiples of π/T . This points up a general result: low-frequency checks on computational algorithms (perhaps with the aid of the "discrete" frequency response) overlook nulls introduced in the higher folds.

D. THE PSEUDO MEASUREMENT DESIGN

Assume the availability of only an angle of attack (α) measurement. A set of loops around the airframe (ignoring the washout network of the baseline configuration) is shown in Fig. 44. The K_f feedforward gain is used, in the absence of the washout, to set the steady-state gain. First, survey the w' -plane transfer functions associated with the time-

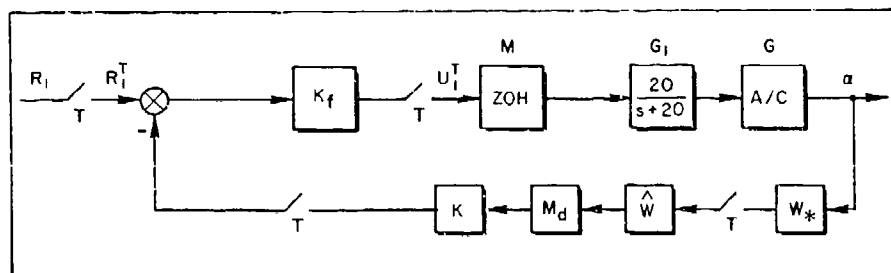


Figure 44. Alternate Configuration

advanced elements of $(W_*GG_1M)^T$ (these are listed in Appendix D). This listing places in clear view the w' -plane property of generating transfer functions where the order of the numerator and denominator are equal. For example, the transfer function for a time advance of $0.5T$ is given in Eq. 248.

$$G_{.5} = \frac{(.3672 \times 10^{-3})[(w' + .0083)^2 + (.07455)^2](w' + 47.34)(w' - 61.72)(w' + 130.5)}{(w' - 1.137)[(w' + .009)^2 + (.077)^2](w' + 2.07)(w' + 19)} \quad (248)$$

The expected result of having the phugoid cancel in the α -related transfer functions, for a zero time advance, is seen to persist for non-zero time advances as well. The greatest effect, as Δ varies, appears in the high-frequency modes.

Comparing, for example, the transfer function for $\Delta = 0.2$ and $\Delta = 0.8$ exposes what appears to be an interesting general trend (Eq. 249). That is, the numerator polynomials have essentially the same coefficients up to the w'^3 term, which suggests subtracting the two signals $[e \cdot 2sT(N_{\delta_e}^{\alpha}/D)G_1M]^T$ and $[e \cdot 8sT(N_{\delta_e}^d/D)G_1M]^T$ to form an effective transfer function with a free w' (see Fig. 45).

$$\begin{aligned} G_{.2} &= \frac{(.8525 \times 10^{-7})[(w' + .008)^2 + (.07455)^2](w' - 51.82)(w' + 50.31)(w' + 6.3 \times 10^7)}{D} \\ &= \frac{.8525 \times 10^{-7} w'^5 + .5372 \times 10^{-1} w'^4 - .08056 s^3 - 140.1 w'^2 - 2.242 w' - .7873}{D} \end{aligned} \quad (249a)$$

$$\begin{aligned} G_{.8} &= \frac{(.4629 \times 10^{-3})[(w' + .008)^2 + (.07455)^2](w' + 47.79)(w' + 68.83)(w' - 91.98)}{D} \\ &= \frac{.4629 \times 10^{-3} w'^5 + .01141 w'^4 - 3.442 w'^3 - 140.1 w'^2 - 2.261 w' - .7873}{D} \end{aligned} \quad (249b)$$

From Fig. 45,

$$U_1^T = \{I + K_f^T K_1^T (GG_1 M)^T + K_f^T K_2^T z^{-1} [e \cdot 2sT GG_1 M]^T - [e \cdot 8sT GG_1 M]^T\}^{-1} K_f^T R_1^T \quad (250)$$

The presence of z^{-1} premultiplying the pseudo differentiator term requires the modification of the $G_{.2}$ and $G_{.8}$ transfer functions by $z^{-1} = (-w' + 50)/(w' + 50)$ since the synthesis is being performed in w' rather than the z -domain.

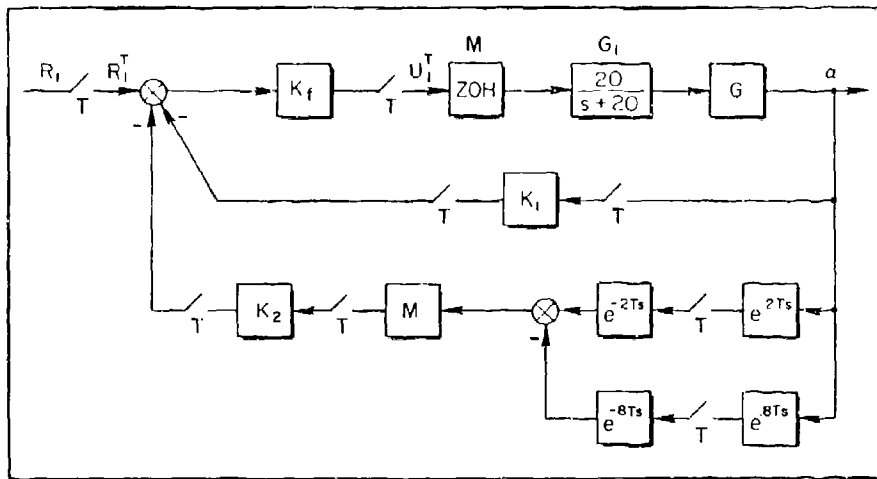


Figure 45. A Pseudo Differentiation Configuration

Since the open-loop polynomial is third order (phugoid essentially cancels), we may attempt a first cut at a design by using the simplified expression for $\Delta(w')$, the closed-loop characteristic equation:

$$\begin{aligned} \Delta(w') &\doteq w'^3 + 19.933w'^2 + 15.379w' - 44.598 \\ &\quad + K_1^T K_f^T (1.039)w' - K_1^T K_f^T (140.048) \\ &\quad + K_2^T K_f^T (32.956)w' \end{aligned} \quad (251)$$

Using $(w' + 3)^2 + (2)^2$ as a goal for the closed-loop short period then produces, after a short root locus exercise, the gains

$$\begin{aligned} K_1^T K_f^T &= -1.62 \\ K_2^T K_f^T &= 2.5 \end{aligned} \quad (252)$$

Using these gains as a guide, the exact equation for $\Delta(w')$,

$$\Delta(w') = D\{I + K_f^T K_1^T (GG_1 M)^T + K_f^T K_2^T \frac{(-w'+50)}{w'+50} [(e^{.2sT} GG_1 M)^T - (e^{.8sT} GG_1 M)^T]\} \quad (253)$$

is used to fine tune the gains. This results in

$$K_1^T K_f^T = -1.5 \quad (254)$$

$$K_2^T K_f^T = 2.2$$

with (ignoring the phugoid)

$$\begin{aligned} \Delta(w') &= 1.01062083w'^3 + 17.89902448w'^2 + 86.32467180w' + 165.4746084 \\ &\approx 1.01[(w' + 3.086)^2 + (2.159)^2](w' + 11.537) \end{aligned} \quad (255)$$

The design appears to be reasonably insensitive to gain variations (see Eqs. 256-258):

$$\begin{aligned} \Delta(w') &= [(w' + 1.36)^2 + (1.2)^2](w' + 16.2) \quad , \quad \begin{aligned} K_1^T K_f^T &= -0.7 \\ K_2^T K_f^T &= 1.0 \end{aligned} \end{aligned} \quad (256)$$

$$\begin{aligned} \Delta(w') &= [(w' + 1.003)^2 + (1.45)^2](w' + 17.2) \quad , \quad \begin{aligned} K_1^T K_f^T &= -0.7 \\ K_2^T K_f^T &= 0.7 \end{aligned} \end{aligned} \quad (257)$$

$$\begin{aligned} \Delta(w') &= [(w' + 6.16)^2 + (8.74)^2](w' + 3.214) \quad , \quad \begin{aligned} K_1^T K_f^T &= -3.0 \\ K_2^T K_f^T &= 4.4 \end{aligned} \end{aligned} \quad (258)$$

The gains used are comparable in magnitude to those in the baseline design (refer to Fig. 41). The (w') characteristic equation for the configuration of Fig. 41 is Δ_c :

$$\begin{aligned} \Delta_c = & [(w' + 2.154)^2 + (3.503)^2][(w' + .5)^2 + (.303)^2](w' + .00172) \\ & \times (w' + 10.7)[(w' + 14.12)^2 + (14.48)^2](w' + 13.55) \end{aligned} \quad (259)$$

The design which uses q and A_n feedback has introduced additional damping in the phugoid term, which α feedback alone cannot do. Again, no attempt to "copy" the baseline design was made; the sole objective was to establish feasibility and determine if reasonable gains were required. It appears that the concept is sound and warrants further investigation. Further, the ability to generate a "pseudo differentiator" by differencing time delay components of a signal is interesting in itself.

The Bode plot of Fig. 46 was generated on the assumption of a sinusoidal input for R_1 (see Fig. 45).

E. SECTION SUMMARY

The pseudo measurement controller, which gives closed-loop dynamics similar to an emulated baseline design, was shown to be feasible using gains of reasonable magnitude. Moreover, by differencing two time delayed signals, it was possible to generate a new transfer function containing a free w' in the numerator, making it a relatively simple task to independently control two coefficients in the closed-loop characteristic equation.

As an aside, a simulation artifact introduced in the higher folds, as a consequence of using the Tustin transform, was pointed out.

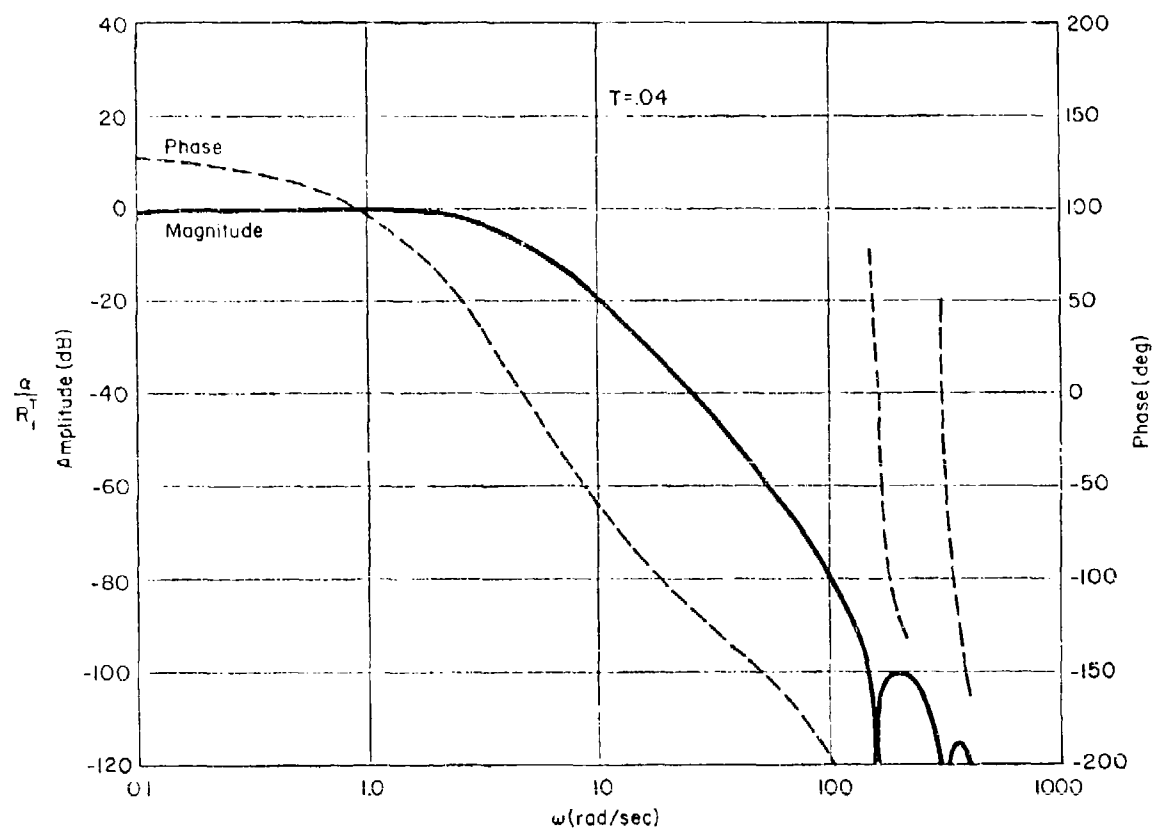


Figure 46. Bode Plot, Pseudo Differentiation Configuration

SECTION VI

SUMMARY AND CONCLUSIONS

The ability of the digital computer to perform a variety of unusual operations on input data lends credence to the idea of achieving closed-loop systems with unusual attributes. This is the key point of the present study where the logic of the computer is used to take a scalar continuous output signal, sample it at a relatively high rate, and then sort it out (in a particular fashion) into a vector of "pseudo" measurements.

The concept is based on using information contained in a scalar measurement, sampled at a high rate, to generate a lower rate measurement vector. This vector is likened to pseudo states since it effectively provides distinctively different information in the form of separate sampling sequences shifted in time. Vector switch decomposition techniques, which provide a mathematical model of the pseudo measurement vector, were reviewed and extended in Section II. The pseudo measurement concept was defined and illustrated with an example. The example demonstrated potential since:

- Unity steady-state gain without forward loop compensation was achieved.
- A five component multiple-order sample vector was generated from a scalar analog signal.
- Three poles were assigned using only one available analog measurement and therefore accomplished pole placement with multiple samples of a single output variable (in distinction to single samples of several output variables).

The illustrative example of Section II did not address the practicality of the approach, since the magnitude of key parameters, such as feedback gains (when plant dynamics, typical of modern aircraft, are used), was ignored. This deficiency was remedied in Section V, where a YF-16 case study example was used to compare pseudo measurement gains

against conventional YF-16 analog controller gains. The pseudo measurement gains were found to be comparable with the conventional gains, indicating the approach does not require control authority more excessive than the analog controller design.

In Sections III and IV the basic tools needed to assess the pseudo measurement concept were reviewed and/or enhanced. The concept of the frequency response of the continuous variables of single-rate digitally controlled systems was reviewed in Section III and then, in Section IV, given sufficient generality to treat multi-rate systems (including the pseudo measurement concept).

An unanticipated dividend accrued from the analytical development of Section IV. As a "byproduct," an important relationship was deduced which made it feasible to apply the switch decomposition/frequency response technique to the error analysis of simulations of continuous systems and/or discretely controlled continuous systems. An illustrative example demonstrated the significant spectral differences between a closed-loop system (employing an analog or digital controller) and an all-digital simulation of the closed-loop system. The example also treated problems encountered when simulation software is implemented on two different (independent) computers, each working in a slightly different frame time.

Thus the tools of Section IV can be profitably applied to the "error" analysis of simulations — perhaps to predict expected differences between actual flight test and man-in-the-loop moving-base simulations.

REFERENCES

1. Whitbeck, R. F., and L. G. Hofmann, Analysis of Digital Flight Control Systems with Flying Qualities Applications, AFFDL-TR-78-115, Sept. 1978.
2. Kranc, G. M., "Input-Output Analysis of Multi-Rate Feedback Systems," IRE Trans. on Automatic Control, Vol. PG AC-3, Nov. 1957, pp. 21-28.
3. Ragazzini, J. R., and G. F. Franklin, Sampled-Data Control Systems, New York, McGraw-Hill, 1958.
4. Tou, J. T., Digital and Sampled-Data Control Systems, New York, McGraw-Hill, 1959.
5. McAllister, J. D., et al., Fighter CCV Phase II Report - Detailed Design, AFFDL-TR-76-119, Oct. 1976.

APPENDIX A

FREQUENCY RESPONSE OF FAST-INPUT/SLOW-OUTPUT CLOSED-LOOP SYSTEM USING MULTI-RATE THEORY

The following solution of the closed-loop system in Fig. A-1 is based on the multi-rate theory presented in Ref. 1. This same system was treated in Section IV using vector switch decomposition modeling. The objective is to calculate the frequency response expression for the output variable $C^{T/N}$. The procedure for this example is typical for closed-loop systems employing fast-input/slow-output sampling.

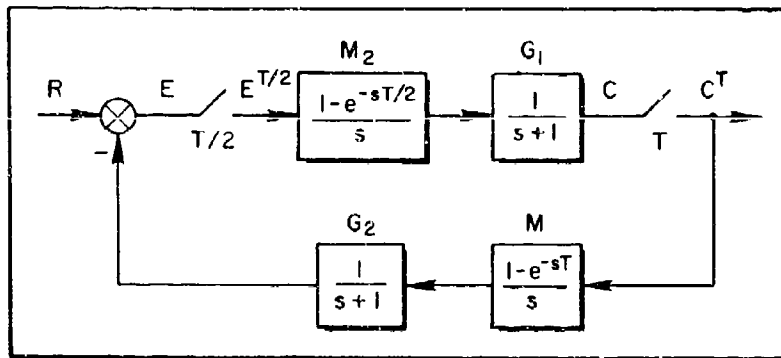


Figure A-1. Fast-Input/Slow-Output Closed-Loop System

CLOSED-LOOP MULTI-RATE CONFIGURATION

The T/N output equation for Fig. A-1 is given by

$$C^{T/N} = (G_1 M_2)^{T/N} E^{T/2} \quad (A-1)$$

First, solve for the $E^{T/2}$ signal at the input of the M_2 data hold.

$$E^{T/2} = R^{T/2} - (G_2 M)^{T/2} (G_1 M_2 E^{T/2})^T \quad (A-2)$$

Next, premultiply Eq. A-2 by $G_1 M_2$ and take the T transform of both sides of the resulting equation (or sample both sides of the equation at a T interval). The result is

$$(G_1 M_2 E^{T/2})^T = (G_1 M_2 R^{T/2})^T - [(G_1 M_2)(G_2 M)^{T/2}]^T (G_1 M_2 E^{T/2})^T \quad (A-3)$$

Rearranging Eq. A-3,

$$(G_1 M_2 E^{T/2})^T = \left\{ I + [(G_1 M_2)(G_2 M)^{T/2}]^T \right\}^{-1} (G_1 M_2 R^{T/2})^T \quad (A-4)$$

and substituting Eq. A-4 into Eq. A-2 produces Eq. A-5.

$$E^{T/2} = R^{T/2} - (G_2 M)^{T/2} \left\{ I + [(G_1 M_2)(G_2 M)^{T/2}]^T \right\}^{-1} (G_1 M_2 R^{T/2})^T \quad (A-5)$$

Finally, substituting Eq. A-5 into Eq. A-1 gives the output equation $C^{T/N}$ as a function of the input $R^{T/2}$.

$$C^{T/N} = \underbrace{(G_1 M_2)^{T/N} R^{T/2}}_1 - \underbrace{(G_1 M_2)^{T/N} (G_2 M)^{T/2} \left\{ I + [(G_1 M_2)(G_2 M)^{T/2}]^T \right\}^{-1} (G_1 M_2 R^{T/2})^T}_2 \quad (A-6)$$

Term 1 in Eq. A-6 introduces spectral components at

$$\omega_n = b + 2\pi n/(T/2), \quad n = 0, 1, 2, 3, \dots \quad (A-7)$$

and Term 2 introduces components at

$$\omega_k = b + 2\pi k/T, \quad k = 0, 1, 2, 3, \dots \quad (A-8)$$

Assume $\Gamma = -\ln(0.81)$; this gives a set of convenient numbers when Eq. A-6 is evaluated. We first evaluate the terms in the inverse expression

$$[(G_1 M_2)(G_2 M)^{T/2}]^T \quad (A-9)$$

Let $z = e^{sT/2}$, and introduce a phantom $T/2$ sampler to Eq. A-9.

$$[(G_1 M_2)(G_2 M)^{T/2}]^T = [(G_1 M_2)^{T/2}(G_2 M)^{T/2}]^T \quad (A-10)$$

This mathematical operation is depicted in Fig. A-2.

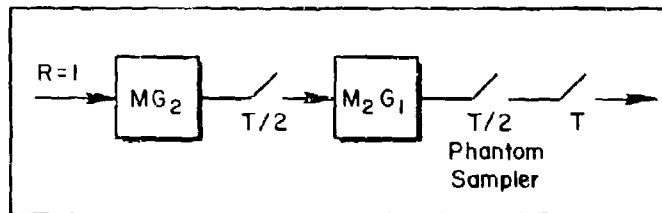


Figure A-2. Phantom Sampler Concept

This step is conceptually correct since the T output sampler simply rejects all the unwanted samples from the $T/2$ sampler. Therefore,

$$(G_1 M_2)^{T/2} = \frac{1 - e^{-T/2}}{z - e^{-T/2}} \quad , \quad (G_2 M)^{T/2} = \frac{1 - e^{-T/2}}{z - e^{-T/2}} \left(\frac{z + 1}{z} \right) \quad (A-11)$$

and

$$[(G_1 M_2)^{T/2}(G_2 M)^{T/2}]^T = \left[\frac{(1 - e^{-T/2})^2 (z + 1)}{z(z - e^{-T/2})^2} \right]^T \quad , \quad z = e^{-sT/2} \quad (A-12)$$

Equation A-12 can be solved by calculating the residues of the following expression (see Section IV):

$$\frac{1}{2\pi j} \int_{\Gamma} \frac{(1 - e^{-T/2})^2 (p + 1)z}{p(p - e^{T/2})^2(z - p^2)} \frac{dp}{p} \quad (A-13)$$

The residues for the double poles at $p = 0$ and $p = e^{-T/2}$ are:

$$\begin{aligned} \text{res}|_{p=0} &= \frac{d}{dp} \left[\frac{(p+1)z}{(p - e^{-T/2})^2(z - p^2)} \right] \Big|_{p=0} \\ &= \frac{e^{-T} + 2e^{-T/2}}{e^{-2T}} \end{aligned} \quad (\text{A-14})$$

$$\begin{aligned} \text{res}|_{p=e^{-T/2}} &= \frac{d}{dp} \left[\frac{(p+1)z}{p^2(z - p^2)} \right] \Big|_{p=e^{-T/2}} \\ &= \frac{-(e^{-T} + 2e^{-T/2})z^2 + (3e^{-2T} + 4e^{-3T/2})z}{e^{-2T}(z - e^{-T})^2} \end{aligned} \quad (\text{A-15})$$

Combining Eqs. A-14 and A-15 gives the T transform required in Eq. A-12.

$$(1 - e^{-T/2})^2 \left[\text{res}|_{p=0} + \text{res}|_{p=e^{-T/2}} \right] = \frac{(1 - e^{-T/2})^2 [z + (e^{-T} + 2e^{-T/2})]}{(z - e^{-T})^2} \quad (\text{A-16})$$

$$z = e^{sT}$$

Substituting Eq. A-16 into the inverse expression in Eq. A-6 and solving for the inverse results in

$$\left\{ I + [(G_1 M_2)(G_2 M)^{T/2}]^T \right\}^{-1} = \frac{(z - e^{-T})^2}{z^2 + [-2e^{-T} + (1 - e^{-T/2})^2]z + [2e^{-2T} - 3e^{-T} + 2e^{-T/2}]} \quad (\text{A-17})$$

For $T = -\ln(0.81) = 0.210721031$ sec, Eq. A-17 becomes

$$\left\{ I + [(G_1 M_2)(G_2 M)^{T/2}]^T \right\}^{-1} = \frac{(z - 0.81)^2}{z^2 - 1.61z + 0.6822}, \quad z = e^{sT} \quad (A-18)$$

Next, calculate the forcing function

$$[(G_1 M_2) R^{T/2}]^T = [(G_1 M_2)^{T/2} R^{T/2}]^T \quad (A-19)$$

Equation A-19 can also be solved using the residue method employed on Eq. A-12. However, a second method (Ref. 1) is to use partial fraction expansion on the $T/2$ z -transform product ($z = e^{sT/2}$) in Eq. A-19; take the inverse of each term back into the continuous time domain; and then resample back to the z -domain for a T sampling interval ($z = e^{sT}$). In practice, the intermediate step of computing the generating time function is merely a convenient conceptual step and can be skipped. Then, for $r = 1 \sin bt$,

$$[(G_1 M_2)^{T/2} R^{T/2}]^T = \left\{ \frac{(1 - e^{-T/2})}{(z - e^{-T/2})} \frac{(z \sin bT/2)}{[(z - \cos bT/2)^2 + (\sin bT/2)^2]} \right\}^T \quad (A-20)$$

Expanding in partial fractions, Eq. A-20 becomes

$$\left\{ \frac{(1 - e^{-T/2})}{(z - e^{-T/2})} \frac{(z \sin bT/2)}{[(z - \cos bT/2)^2 + (\sin bT/2)^2]} \right\}^T = \left\{ \frac{K_1 z \sin bT/2}{[(z - \cos bT/2)^2 + (\sin bT/2)^2]} + \frac{K_2 z(z - \cos bT/2)}{[(z - \cos bT/2)^2 + (\sin bT/2)^2]} + \frac{K_3 z}{(z - e^{-T/2})} \right\}^T \quad (A-21)$$

Solving for K_1 , K_2 , and K_3 in Eq. A-21 gives Eq. A-22 ($z = e^{sT/2}$).

$$\left\{ \frac{(1 - e^{-T/2})}{(z - e^{-T/2})} \frac{(z \sin bT/2)}{[(z - \cos bT/2)^2 + (\sin bT/2)^2]} \right\}^T =$$

$$\left\{ \frac{(1 - e^{-T/2})}{[(e^{-T/2} - \cos bT/2)^2 + (\sin bT/2)^2]} \right.$$

$$\times \frac{(\cos bT/2 - e^{-T/2})z \sin bT/2}{[(z - \cos bT/2)^2 + (\sin bT/2)^2]}$$

$$\left. - \frac{(\sin bT/2)z(z - \cos bT/2)}{[(z - \cos bT/2)^2 + (\sin bT/2)^2]} + \frac{(\sin bT/2)z}{(z - e^{-T/2})} \right\}^T \quad (A-22)$$

Since we are concerned with steady-state frequency response, only the sine and cosine terms need to be considered. Therefore, resampling at a T frame time results in ($z = e^{sT}$):

$$\left\{ \frac{(1 - e^{-T/2})}{(z - e^{-T/2})} \frac{(z \sin bT/2)}{[(z - \cos bT/2)^2 + (\sin bT/2)^2]} \right\}^T = \frac{K_1 z \sin bT + K_2 z(z - \cos bT)}{[(z - \cos bT)^2 + (\sin bT)^2]} \quad (A-23)$$

where

$$K_1 = \frac{(\cos bT/2 - e^{-T/2})(1 - e^{-T/2})}{(e^{-T/2} - \cos bT/2)^2 + (\sin bT/2)^2} \quad (A-24)$$

and

$$K_2 = \frac{(1 - e^{-T/2})(\sin bT/2)}{(e^{-T/2} - \cos bT/2)^2 + (\sin bT/2)^2} \quad (A-25)$$

It is now apparent that the $[(G_1 M_2)R^{T/2}]^T$ term represents a sinusoidal forcing function for Eq. A-6. In Ref. 1, Appendix E, it is shown that Eq. A-23 reduces to a complex multiplication factor in the frequency response expression. That is, the complete frequency response expression for Eq. A-6 is given by

$$A_n + jB_n = \left. \frac{G_1 M_2}{T/2} \right|_{s=j\omega_n} - \left. \frac{G_1 M_2}{T} \right|_{s=j\omega_k} (G_2 M)^{T/2} \left. \frac{z^{\Delta} e^{sT/2}}{z-1} \right|_{z=1} \omega_k (T/2) \left\{ 1 + [(G_1 M_2)(G_2 M)^{T/2}]^T \right\}^{-1} \left. \frac{z^{\Delta} e^{sT}}{z-1} \right|_{z=1} \omega_k T [K_1 + jK_2] \quad (A-26)$$

where

$$\begin{aligned} \omega_n &= b + \frac{2\pi n}{T/2}, & n &= 0, 1, 2, \dots \\ \omega_k &= b + \frac{2\pi k}{T}, & k &= 0, 1, 2, \dots \end{aligned} \quad (A-27)$$

The complex multiplication factor $[K_1 + jK_2]$ is defined in Eqs. A-24 and A-25. The remaining frequency response factors were written directly from inspection of the $C^{T/N}$ output equation (Eq. A-6) using the frequency response identities presented in Section IV, Subsection D.

Notice that K_1 and K_2 are functions of the input frequency b and not $\omega_k = b + 2\pi k/T$. In addition, both K_1 and K_2 are periodic functions at $b = 2\pi/(T/2)$, the input sampling frequency. As discussed in Section IV, the result of this singular dependence on the input excitation frequency b and the periodic nature of the K_1 and K_2 functions is multiple Bode plots.

Substituting the previously calculated terms into Eq. A-26 results in Eq. A-28:

$$\begin{aligned} A_n + jB_n &= \left. \frac{(1-e^{-sT/2})}{T/2s(s+1)} \right|_{s=j\omega_n} - \left. \frac{(1-e^{-sT/2})}{Ts(s+1)} \right|_{s=j\omega_k} \frac{(1-e^{-T/2})}{(z-e^{-T/2})} \frac{z+1}{z} \left. \frac{z^{\Delta} e^{sT/2}}{z-1} \right|_{z=1} \omega_k (T/2) \\ &\times \frac{(z - 0.81)^2}{z^2 - 1.61z + 0.6822} \left. \frac{z^{\Delta} e^{sT}}{z-1} \right|_{z=1} \omega_k T [K_1 + jK_2] \end{aligned} \quad (A-28)$$

This equation gives exactly the same results as Eqs. 159 or 175 in Section IV.

FREQUENCY RESPONSE TERM $[GR^{T/2}]^T$

It is possible to derive a general frequency response identity factor for the $[(G_1 M_2) R^{T/2}]^T$ term in Eq. A-6. Consider the more general expression in Eq. A-29 with $r = 1 \sin bt$.

$$[GR^{T/M}]^T = [G^{T/M} R^{T/M}]^T \quad (A-29)$$

The T/M transform for the sinusoidal input is expressed as

$$R^{T/M} = \frac{z \sin bT/M}{z^2 - (\cos bT/M)z + 1}, \quad z = e^{sT/M} \quad (A-30)$$

Substituting Eq. A-30 into Eq. A-29 and expanding the T/M transform product into partial fractions gives

$$G^{T/M} \left[\frac{z \sin bT/M}{z^2 - (\cos bT/M)z + 1} \right]^T = \left[\frac{K_1 z \sin bT/M + K_2 z(z - \cos bT/M)}{z^2 - (\cos bT/M)z + 1} \right]^T + \left[\begin{array}{l} \text{Terms due to} \\ \text{modes of } G^{T/M} \end{array} \right]^T \quad (A-31)$$

Since we are concerned with the steady-state frequency response, the partial fraction expansion terms due to the modes of $G^{T/M}$ can be dropped. Therefore, multiply both sides of Eq. A-31 by $z^2 + (\cos bT/M)z + 1$ and evaluate at $z = \cos bT/M + j \sin bT/M$. The result is

$$\left[G^{T/M} z \sin bT/M \right]_{z=14b(T/M)}^T = \left[K_1 z \sin bT/M + K_2 z(z - \cos bT/M) \right]_{z=14b(T/M)}^T \quad (A-32)$$

and

$$\left[G^{T/M} z \sin bT/M \right]_{z=14b(T/M)}^T = \left[K_1 \sin bT/M + K_2 j \sin bT/M \right]^T \quad (A-33)$$

Then

$$G^{T/M}(z) \left[\frac{z^{\Delta} e^{sT/M}}{z=14b(T/M)} \right] = K_1 + jK_2 \quad (A-34)$$

Substituting Eq. A-34 into Eq. A-26 produces

$$A_n + jB_n = \frac{G_1 M_2}{T/2} \left[\frac{z^{\Delta} e^{sT/M}}{s=j\omega_n} \right] - \frac{G_1 M_2}{T} \left[\frac{z^{\Delta} e^{sT/2}}{s=j\omega_k} \right] \left(G_2 M \right)^{T/2} \left[\frac{z^{\Delta} e^{sT/2}}{z=14\omega_k(T/2)} \right] \left\{ I + \left[(G_1 M_2) (G_2 M)^{T/2} \right]^T \right\}^{-1} \left[\frac{z^{\Delta} e^{sT}}{z=14\omega_k T} \right] \\ \times (G_1 M_2)^{T/2} \left[\frac{z^{\Delta} e^{sT/2}}{z=14\omega_k(T/2)} \right] \quad (A-35)$$

The following general frequency response identity can then be applied to Eq. A-6 to directly write Eq. A-35.

$$\left[G R^{T/M} \right]^T = \left[G^{T/M} R^{T/M} \right]^T \Rightarrow G^{T/M} \left[\frac{z^{\Delta} e^{sT/M}}{z=14b(T/M)} \right] \quad (A-36)$$

A complete set of frequency response identities is listed in Section IV, Subsection D.

APPENDIX B

COMPUTATION OF $(W_3 \star M_2 W_2)^T$ AND $(W_2 \star M_3 W_3)^T$

As noted in Section IV, the computation of terms such as $(W_3 \star M_2 W_2)^T$ and $(W_2 \star M_3 W_3)^T$ is straightforward. First, evaluate $(W_3 \star M_2 W_2)^T$ using Eq. 210:

$$(W_3 \star M_2 W_2)^T = \left\{ \begin{bmatrix} 1 \\ e^{sT/3} \\ e^{s2T/3} \end{bmatrix} \left(\frac{1 - e^{-sT/2}}{s} \right) \begin{bmatrix} 1 & e^{-sT/2} \end{bmatrix} \right\}^T = \left\{ \frac{1 - e^{-sT/2}}{s} \begin{bmatrix} 1 & e^{-sT/2} \\ e^{sT/3} & e^{-sT/6} \\ e^{s2T/3} & e^{sT/6} \end{bmatrix} \right\}^T \quad (B-1)$$

$$\begin{bmatrix} \frac{1}{s} - \frac{e^{-sT} e^{sT/2}}{s} & \frac{e^{-sT} (e^{sT/2} - 1)}{s} \\ \frac{e^{sT/3}}{s} - \frac{e^{-sT} e^{s5T/6}}{s} & e^{-sT} \left[\frac{e^{s5T/6}}{s} - \frac{e^{sT/3}}{s} \right] \\ \frac{e^{s2T/3}}{s} - \frac{e^{sT/6}}{s} & \frac{e^{sT/6}}{s} - \frac{e^{-sT} e^{s2T/3}}{s} \end{bmatrix}^T = \begin{bmatrix} 1 & 0 \\ 1 & 0 \\ 0 & 1 \end{bmatrix} \quad (B-2)$$

Next, evaluate $(W_2 \star M_3 W_3)^T$:

$$(W_2 \star M_3 W_3)^T = \left\{ \begin{bmatrix} 1 \\ e^{sT/2} \end{bmatrix} \left(\frac{1 - e^{-sT/3}}{s} \right) \begin{bmatrix} 1 & e^{-sT/3} & e^{-s2T/3} \end{bmatrix} \right\}^T \\ = \left(\frac{1 - e^{-sT/3}}{s} \begin{bmatrix} 1 & e^{-sT/3} & e^{-s2T/3} \\ e^{sT/2} & e^{sT/6} & e^{-sT/6} \end{bmatrix} \right)^T \quad (B-3)$$

Clearing through and writing Eq. B-3 in terms of the advanced z-transform for $1/s$:

$$(W_2 * M_3 W_3)^T = \begin{bmatrix} \frac{1}{s} - \frac{e^{-sT} e^{s2T/3}}{s} & \frac{e^{-sT} e^{s2T/3}}{s} - \frac{e^{-sT} e^{sT/3}}{s} & \frac{e^{-sT} e^{sT/3}}{s} - \frac{e^{-sT}}{s} \\ \frac{e^{sT/2}}{s} - \frac{e^{sT/6}}{s} & \frac{e^{sT/6}}{s} - \frac{e^{-sT} e^{s5T/6}}{s} & \frac{e^{sT} e^{s5T/6}}{s} - \frac{e^{-sT} e^{sT/2}}{s} \end{bmatrix}^T$$

$$= \begin{bmatrix} 1 & 0 & 0 \\ 0 & 1 & 0 \end{bmatrix} \quad (B-34)$$

Equations B-2 and B-4 justify the assignments made in Eq. 211 of Section IV.

APPENDIX C

NUMERICAL DETAILS FOR AN ILLUSTRATIVE EXAMPLE

Equation 223 of Section IV stated

$$\begin{aligned}
 C^{T/3} &= \frac{1}{2\pi j} \int \frac{p^3 z}{(p - e^{-T/3})(p - e^{-T/6})(p^2 + e^{-T/6} p + e^{-2T/6})(z - p^2)} dp \\
 &= \frac{z^2(z^2 + e^{-5T/6})}{(z - e^{-2T/3})(z - e^{-T/3})(z^2 + e^{-T/3} z + e^{-2T/3})}, \quad z = e^{sT/3}
 \end{aligned}
 \tag{C-1}$$

There are four residues required:

$$\text{res}_1 = \text{res} \Big|_{p=e^{-T/3}} = \frac{p^3 z}{(e^{-T} - e^{-T/3})(z - e^{-2T/3})}
 \tag{C-2}$$

$$\text{res}_2 = \text{res} \Big|_{p=e^{-T/6}} = \frac{e^{-T/2} z}{(e^{-T/3} - e^{-T/3})(3e^{-T/3})(z - e^{-T/3})}
 \tag{C-3}$$

$$\begin{aligned}
 \text{res}_3 &= \text{res} \Big|_{p=-(e^{-T/6}/2) + (j\sqrt{3}/2)e^{-T/6}} \\
 &= \frac{\left(\frac{-e^{-T/6}}{2} + \frac{j\sqrt{3}}{2} e^{-T/6}\right)^3 z}{\left(\frac{-e^{-T/6}}{2} + \frac{j\sqrt{3}}{2} e^{-T/6} - e^{-T/3}\right)\left(\frac{-e^{-T/6}}{2} + \frac{j\sqrt{3}}{2} e^{-T/6} - e^{-T/6}\right)\left(j\sqrt{3} e^{-T/6}\right)\left[z - \left(\frac{e^{-T/6}}{2} + \frac{j\sqrt{3}}{2} e^{-T/6}\right)^2\right]}
 \end{aligned}
 \tag{C-4}$$

Switch decomposition can be used as an alternative (refer to Fig. C-1).

$$\begin{aligned}
 C^{T/3} &= W_3 \left(W_{3*} \frac{1}{s+2} W_2 \right)^T (W_{2*} R)^T \\
 &= W_3 \left\{ \begin{bmatrix} 1 \\ e^{sT/3} \\ e^{s2T/3} \end{bmatrix} \frac{1}{s+2} \begin{bmatrix} 1 & | & e^{-sT/2} \end{bmatrix} \right\}^T \begin{bmatrix} R^T \\ (e^{sT/2} R)^T \end{bmatrix} \quad (C-5)
 \end{aligned}$$

$$\begin{aligned}
 &= W_3 \frac{\begin{bmatrix} z & e^{-T} \\ ze^{-2T/3} & e^{-5T/3} \\ ze^{-4T/3} & ze^{-T/3} \end{bmatrix}}{z - e^{-2T}} \begin{bmatrix} \frac{z}{z - e^{-T}} \\ \frac{ze^{-T/2}}{z - e^{-T}} \end{bmatrix} = W_3 \frac{\begin{bmatrix} z^2 + e^{-3T/2} z \\ e^{-2T/3} z^2 + e^{-13T/16} \\ z^2 (e^{-4T/3} + e^{-5T/6}) \end{bmatrix}}{(z - e^{-2T})(z - e^{-T})} \quad (C-6)
 \end{aligned}$$

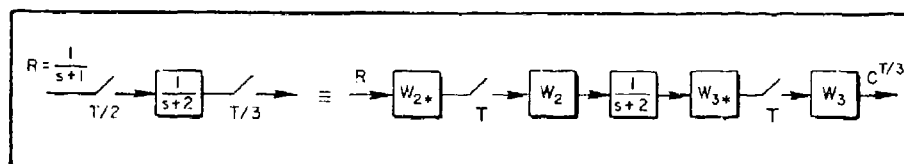


Figure C-1. Switch Decomposition of T/2, T/3 Example

Next, define $z = e^{sT/3}$ and clear through by W_3 :

$$C^{T/3} = \begin{bmatrix} 1 & z^{-1} & z^{-2} \end{bmatrix} \frac{\begin{bmatrix} z^6 + e^{-3T/2} z^3 \\ z^6 (e^{-2T/3}) + e^{-13T/16} z^3 \\ z^6 (e^{-4T/3} + e^{-5T/3}) \end{bmatrix}}{(z^3 - e^{-2T})(z^3 - e^{-T})} \quad (C-7)$$

Expand Eq. C-6 and cancel the pole/zero pair $z^2 + e^{-2T/3} + e^{-4T/3}$:

$$C^{T/3} = \frac{z^6 + e^{-2T/3}z^5 + (e^{-4T/3} + e^{-5T/6})z^4 + e^{-3T/2}z^3 + e^{-13T/16}z^2}{(z - e^{-2T/2})(z^2 + e^{-2T/3}z + e^{-4T/3})(z - e^{-T/3})(z^2 + e^{-T/3}z + e^{-2T/3})} \quad (C-8)$$

$$= \frac{z^2(z^2 + e^{-5T/6})}{(z - e^{-2T/3})(z - e^{-T/3})(z^2 + e^{-T/3}z + e^{-2T/3})} \quad (C-9)$$

APPENDIX D

LISTING OF TRANSFER FUNCTIONS

The s- and w' transfer functions are listed for a T = 0.04 seconds (25 Hz). The actuator model, $20/(s + 20)$, is included. The w' transfer functions presume a ZOH and were calculated using the DISCRET computer program presented in Volume II.

Also listed are the advanced w'-transfer functions for α needed for the analyses of Section V. The denominator, which is the same regardless of the amount of time advance, is listed only once. The numerators are listed for advances from 0.0 to 0.9.

For ease of presentation, the variable s has been used in all of the tables. The particular data heading makes clear whether s or w' is intended.

s- AND w'-PLANE TRANSFER FUNCTIONS

α/δ_e , s-Plane

$$AK = (ANK/ADK) = -1.449$$

ATF(S) NUMERATOR

I	ANPOLY(I)	AZERO(I)
1	(-1.449)S** 3	(-.8003E-02) + J(-.7455E-01)
2	(-147.6)S** 2	(-.8003E-02) + J(.7455E-01)
3	(-2.370)S** 1	(-101.9) + J(0.)
4	(-.8295)	ANK= -1.449

ATF(S) DENOMINATOR

I	ADPOLY(I)	APOLE(I)
1	(1.000)S** 5	(1.137) + J(0.)
2	(20.95)S** 4	(-.9345E-02) + J(.7705E-01)
3	(16.71)S** 3	(-.9345E-02) + J(-.7705E-01)
4	(-46.66)S** 2	(-2.071) + J(0.)
5	(-.7820)S** 1	(-20.00) + J(0.)
6	(-.2837)	ADK= 1.000

α/δ_e , w'-Plane

$$RK = (RNK/RDK) = -.2926E-03$$

RTF(S) NUMERATOR

I	RNPOLY(I)		RZERO(I)
1	(-.2926E-03) S** 5	(-.8003E-02) + J(.7455E-01)	
2	(.4986E-01) S** 4	(-.8003E-02) + J(-.7455E-01)	
3	(1.040) S** 3	(50.00) + J(.1707E-10)	
4	(-140.0) S** 2	(-54.67) + J(0.)	
5	(-2.236) S** 1	(175.1) + J(0.)	
6	(-.7873)		

RTF(S) DENOMINATOR

I	RDPOLY(I)		RPOLE(I)
1	(1.000) S** 5	(1.137) + J(0.)	
2	(19.95) S** 4	(-.9345E-02) + J(.7705E-01)	
3	(15.74) S** 3	(-.9345E-02) + J(-.7705E-01)	
4	(-44.29) S** 2	(2.070) + J(0.)	
5	(-.7430) S** 1	(-19.00) + J(0.)	
6	(-.2693)		

q/δ_e , s-Plane

$$BK = (BNK/BDK) = -147.6$$

BTF(S) NUMERATOR

I	BNPOLY(I)		BZERO(I)
1	(-147.6) S** 3	(0.) + J(0.)	
2	(-79.39) S** 2	(-.8816E-02) + J(0.)	
3	(-.6884) S** 1	(-.5292) + J(0.)	
4	(0.)		

BNK = -147.6

BTF(S) DENOMINATOR

I	BDPOLY(I)		BPOLE(I)
1	(1.000) S** 5	(1.137) + J(0.)	
2	(20.95) S** 4	(-.9345E-02) + J(.7705E-01)	
3	(16.71) S** 3	(-.9345E-02) + J(-.7705E-01)	
4	(-46.66) S** 2	(-2.071) + J(0.)	
5	(-.7820) S** 1	(-20.00) + J(0.)	
6	(-.2837)		

BDK = 1.000

q/δ_e , w'-Plane

$$BK = (SNK/SDK) = .7546E-02$$

STF(S) NUMERATOR

I	SNPOLY(I)	SZERO(I)
1	(.7546E-02)S** 5 (-.8816E-02) + J(0.)	
2	(2.428)S** 4 (-.5292) + J(0.)	
3	(-138.8)S** 3 (50.00) + J(-.1717E-11)	
4	(-75.34)S** 2 (-371.2) + J(0.)	
5	(-.6534)S** 1 (0.) + J(0.)	
6	(0.)	

STF(S) DENOMINATOR

I	SDFOLY(I)	SPOLE(I)
1	(1.000)S** 5 (1.137) + J(0.)	
2	(19.95)S** 4 (-.9345E-02) + J(.7705E-01)	
3	(15.74)S** 3 (-.9345E-02) + J(-.7705E-01)	
4	(-44.29)S** 2 (-2.070) + J(0.)	
5	(-.7430)S** 1 (-19.00) + J(0.)	
6	(-.2693)	

A_n/δ_e , s-Plane

$$CK = (CNK/CDK) = -.5315$$

CTF(S) NUMERATOR

I	CNPOLY(I)	CZERO(I)
1	(-.5315)S** 4 (0.) + J(0.)	
2	(-.5314)S** 3 (.1831E-02) + J(0.)	
3	(-24.95)S** 2 (-.5009) + J(-6.833)	
4	(.4567E-01)S** 1 (-.5009) + J(6.833)	
5	(0.)	CNK= -.5315

CTF(S) DENOMINATOR

I	CDPOLY(I)	CPOLE(I)
1	(1.000)S** 5 (1.137) + J(0.)	
2	(20.95)S** 4 (-.9345E-02) + J(.7705E-01)	
3	(16.71)S** 3 (-.9345E-02) + J(-.7705E-01)	
4	(-46.66)S** 2 (-2.071) + J(0.)	
5	(-.7820)S** 1 (-20.00) + J(0.)	
6	(-.2837)	CDK= 1.000

A_n/δ_e , w'-Plane

$$TK = (TNK/TDK) = .1003E-01$$

TTF(S) NUMERATOR

I	TNPOLY(I)		TZERO(I)
1	(.1003E-01) S** 5	(.1830E-02) + J(0.)	
2	(-.4902) S** 4	(-.5721) + J(6.847)	
3	(-.9944E-01) S** 3	(-.5721) + J(-6.847)	
4	(-23.68) S** 2	(50.00) + J(-.2797E-11)	
5	(.4333E-01) S** 1	(0.) + J(0.)	
6	(0.)		

TTF(S) DENOMINATOR

I	TDPOLY(I)		TPOLE(I)
1	(1.000) S** 5	(1.137) + J(0.)	
2	(19.95) S** 4	(-.9345E-02) + J(.7705E-01)	
3	(15.74) S** 3	(-.9345E-02) + J(-.7705E-01)	
4	(-44.29) S** 2	(-2.070) + J(0.)	
5	(-.7430) S** 1	(-19.00) + J(0.)	
6	(-.2693)		

α TIME ADVANCED TRANSFER FUNCTIONS (w')

DENOMINATOR

I	DPOLY(I)		POLE(I)
1	(1.000) S** 5	(1.137) + J(0.)	
2	(19.95) S** 4	(-.9345E-02) + J(.7705E-01)	
3	(15.74) S** 3	(-.9345E-02) + J(-.7705E-01)	
4	(-44.29) S** 2	(-2.070) + J(0.)	
5	(-.7430) S** 1	(-19.00) + J(0.)	
6	(-.2693)		

$$\Delta = 0 \text{ (0.00 seconds)}$$

NUMERATOR

I	NPOLY(I)		ZERO(I)
1	(-.2926E-03) S** 5	(-.8003E-02) + J(.7455E-01)	
2	(.4986E-01) S** 4	(-.8003E-02) + J(-.7455E-01)	
3	(1.040) S** 3	(50.00) + J(.1707E-10)	
4	(-140.0) S** 2	(-54.67) + J(0.)	
5	(-2.236) S** 1	(175.1) + J(0.)	
6	(-.7873)		

$\Delta = .1$ (.001 seconds)

NUMERATOR

I	NPOLY(I)		ZERO(I)
1	(-.1474E-03)S** 5	(-.8003E-02) + J(.7455E-01)
2	(.5291E-01)S** 4	(-.8003E-02) + J(-.7455E-01)
3	(.4797)S** 3	(50.48) + J(0.)
4	(-140.0)S** 2	(-52.18) + J(0.)
5	(-2.239)S** 1	(360.7) + J(0.)
6	(-.7873)		

$\Delta = .2$ (.008 seconds)

NUMERATOR

I	NPOLY(I)		ZERO(I)
1	(.8525E-07)S** 5	(-.8003E-02) + J(-.7455E-01)
2	(.5372E-01)S** 4	(-.8003E-02) + J(.7455E-01)
3	(-.8056E-01)S** 3	(51.82) + J(0.)
4	(-140.1)S** 2	(-50.31) + J(0.)
5	(-2.242)S** 1	(-.6301E+06) + J(0.)
6	(-.7873)		

$\Delta = .3$ (.012 seconds)

NUMERATOR

I	NPOLY(I)		ZERO(I)
1	(.1406E-03)S** 5	(-.8003E-02) + J(.7455E-01)
2	(.5228E-01)S** 4	(-.8003E-02) + J(-.7455E-01)
3	(-.6408)S** 3	(-48.93) + J(0.)
4	(-140.1)S** 2	(54.02) + J(0.)
5	(-2.245)S** 1	(-376.9) + J(0.)
	(-.7873)		

$\Delta = .4$ (.016 seconds)

I	POLY(I)		ZERO(I)
1	(.2656E-03)S** 5	(-.8003E-02) + J(.7455E-01)
2	(.4859E-01)S** 4	(-.8003E-02) + J(-.7455E-01)
3	(-1.201)S** 3	(-47.95) + J(0.)
4	(-140.1)S** 2	(57.22) + J(0.)
5	(-2.249)S** 1	(-192.2) + J(0.)
6	(-.7873)		

$$\Delta = .5 (.02 \text{ seconds})$$

NUMERATOR

I	NPOLY(I)		ZERO(I)
1	(.3672E-03) S** 5	(-.8003E-02) + J(.7455E-01)	
2	(.4266E-01) S** 4	(-.8003E-02) + J(-.7455E-01)	
3	(-1.761) S** 3	(-47.34) + J(0.)	
4	(-140.1) S** 2	(61.72) + J(0.)	
5	(-2.252) S** 1	(-130.5) + J(0.)	
6	(-.7873)		

$$\Delta = .6 (.024 \text{ seconds})$$

NUMERATOR

I	NPOLY(I)		ZERO(I)
1	(.4383E-03) S** 5	(-.8003E-02) + J(.7455E-01)	
2	(.3448E-01) S** 4	(-.8003E-02) + J(-.7455E-01)	
3	(-2.322) S** 3	(-47.10) + J(0.)	
4	(-140.1) S** 2	(68.09) + J(0.)	
5	(-2.255) S** 1	(-99.64) + J(0.)	
6	(-.7873)		

$$\Delta = .7 (.028 \text{ seconds})$$

NUMERATOR

I	NPOLY(I)		ZERO(I)
1	(.4722E-03) S** 5	(-.8003E-02) + J(.7455E-01)	
2	(.2407E-01) S** 4	(-.8003E-02) + J(-.7455E-01)	
3	(-2.882) S** 3	(-47.23) + J(0.)	
4	(-140.1) S** 2	(77.41) + J(0.)	
5	(-2.258) S** 1	(-81.13) + J(0.)	
6	(-.7873)		

$$\Delta = .8 (.032 \text{ seconds})$$

NUMERATOR

I	NPOLY(I)		ZERO(I)
1	(.4629E-03) S** 5	(-.8003E-02) + J(.7455E-01)	
2	(.1141E-01) S** 4	(-.8003E-02) + J(-.7455E-01)	
3	(-3.442) S** 3	(-47.79) + J(0.)	
4	(-140.1) S** 2	(-68.83) + J(0.)	
5	(-2.261) S** 1	(91.98) + J(0.)	
6	(-.7873)		

$$\Delta = .9 (.036 \text{ seconds})$$

NUMERATOR

I	NPOLY(I)	ZERO(I)
1	(.4047E-03)S** 5	(-.8003E-02) + J(.7455E-01)
2	(-.3481E-02)S** 4	(-.8003E-02) + J(-.7455E-01)
3	(-4.003)S** 3	(-48.87) + J(0.)
4	(-140.1)S** 2	(-60.19) + J(0.)
5	(-2.264)S** 1	(117.7) + J(0.)
6	(-.7873)	